TECHNISCHE UNIVERSITÄT WIEN

ILSB

VIENNA UNIVERSITY OF TECHNOLOGY

Master Thesis

Nanomechanical-testing of individual collagen fibrils from an osteogenesis imperfecta mouse model

Carried out for the purpose of obtaining the degree of Dipl.-Ing submitted at TU Wien, Faculty of Mechanical and Industrial Engineering in the Bioengineering Research Group Institute of Lightweight Design and Structural Biomechanics, by

Jakob Scherübl BSc.
Mat.Nr.: 1025318

Under the supervision of
Univ. Prof. Dipl. -Ing. Dr. sc. nat. Thurner P.J
Andriotis O. PhD

June 18, 2018

Affidavit

I declare in lieu of oath, that I wrote this thesis and performed the associated research myself, using only literature cited in this volume. If text passages from sources are used, they are marked as such.

I conform that this work is original and has not been submitted elsewhere for any examination, nor is it currently under consideration for a thesis elsewhere.

I confirm, that going to press of this thesis needs the conformation of the examination committee.

Jakob Scherübl

Vienna, June, 2018

Acknowledgements

The first page of the thesis I want to dedicate to all the people who supported and helped me along my studies. First of all, I would like to thank my parents Wilhelm and Andrea for making my studies possible. They always had a friendly ear to listen to my troubles during study and life. I'm very thankful for there unconditional support and encouragement to achieve my goals.

Further I want to thank my brother for spending time with me to clear my mind, either with coffee and nice talks or cycling around Vienna. During my studies I met many interesting and fascinating people and I call myself lucky to became friends with some of them. Especially, I would like to thank Julia for going through this together with me.

I sincerely want to thank Prof. Philipp J. Thurner for making this master thesis possible. I'm very thankful for the opportunity to work at the ILSB institute, where I could follow my interests to conduct biomechanical research.
Last but not least, I want to thank Dr. Orestis Andriotis for his patience, support and help during the project. Dr. Orestis Andriotis always helped at the right time and motivated me to reach my goal.

Abstract

Collagen is one of the most abundant proteins and constitutes 25% of the total protein mass of the human body. In general, collagen is the building block of most, if not all, biological tissues and contributes to a large extend to the mechanical properties of these tissues. Bone, skin, tendon, ligaments, blood vessels or the cornea of the eye consist mainly of collagen and thereby credit their mechanical properties to collagen. The versatility of the mechanical properties of the different connective tissues is attributed by their hierarchical architecture and the composition of the basic building blocks. Each tissue adapts to their demand.
This is achieved through the combination of collagen with different elements. For example, in bone, collagen is combined with minerals which results in increased fracture resistance. In tendons, collagen is assembled with elastin and thereby a high resilience and toughness is achieved. Due to the fact that collagen provides the structural stability, collagen is one of the most interesting and important macromolecules within the human body. Collageneous tissues, for example tendons and ligaments, possess a hierarchical architecture. At the lowest length scale level, collagen molecules consist of three α-polypeptide chains. In tendons, collagen molecules assemble into fibrils which further assemble into fibres, the fibres create fascicles which then constitute the tendon. Mechanical tests of these tissues have been the focus of a number of studies. However, only a few studies generated data on the length scale of fibril, which can be accomplished via atomic force microscopy indentation and tensile tests.
This project focuses on mechanical tests of individual collagen fibrils. Two types of mechanical tests were performed; nano-indentation and nano-tensile tests. Both tests were established with an atomic force microscope (AFM). The main aim of this thesis was to improve and optimize an existing protocol for tensile testing, which enabled fracture tests of individual collagen fibrils. The sample preparation for tensile testing was also optimized, resulting in shorter preparation times. In the next step the improved tests where applied to individual collagen fibrils.
The second part of the thesis was to employ these tests and examine the influence of structural alterations at the molecular level of collagen on the mechanical properties at the collagen fibril level, by examining two different collagen types. Collagen fibrils from mice with osteogenesis imperfecta (OI) and wild type (WT) mice. OI originates from mutations within the collagen coding genes and results in an alteration of the collagen molecule. To study the effects of OI a osteogenesis imperfecta mouse (OIM) model was used. The collagen fibrils were obtained from mouse-tail tendons of two different, one OIM and one WT, five month old female mice.
During this thesis two different tensile tests were performed. The first test engaged with elongations in the physiological strain range up to 10 %, whereas in the second test the fibrils were elongated until fracture. Nano-scale indentation tests gave information about the radial mechanical properties of the fibrils. Through the combination of the tests different parameters where obtained, such as the radial and longitudinal elastic modulus, ultimate strength, ultimate strain and the energy dissipation. All the values were statistically analysed and the results are visualized in section 7. Further comparisons between the generated values and literature were performed.

Contents

1 Introduction

1.1 Background

Biological tissues essentialy are nano-composite materials, with hierarchical architecture spanning from nanometer up to macrometer (tissue) level. For the field of Biomedical Engineering it is of great interest to describe the mechanical properties of biological tissues. Observing the impact of external loading to these tissues at different length scales lead to a better understanding of the working mechanism within the tissues. The structures and the architecture within every length scale have an influence on the mechanical properties at the tissue level. To get a better understanding of the mechanical behaviour of biological tissues, it is important to get information about how the lowest hierarchical level reacts to external loading.

For example, tendons consist of collagen, elastin, cells, proteoglycans and water. The hierarchical structure and the mechanical properties of tendons are based on collagen molecules, which constitute with 75-85% of the dry weight[1, p.412] the main part in the composition of tendons. Collagen is a fibrous protein which assembles into fibrils at the nanoscale level and thereby provides rigidity and structure to the tissue [1, p.32]. Collagen not only takes a major role in tendons, it also is one of the most important proteins in multicellular organisms. Collagen has a significant function in human and animal bodies, it is the most abundant protein constituting up to 25% of the total protein mass of mammal tissue [2, p.1184]. Tendons, ligaments, bones, cartilage, blood vessels, trachea and bronchial tubes consist to a large part of collagen[3]. Through being present in every connective tissue collagen defines primarily the mechanical properties of these tissues.

The collagen molecule is a helical structure consisting of three polypeptide α-chains. In the next hierarchical level the collagen molecule assembles into fibrils and these into fibres. These fibrils and fibres can be understood as nano and micro-ropes. Similar to ropes, both structures show a preferred loading case along the longitudinal direction. To obtain the mechanical properties, tensile tests may be applied. Collagen fibres can be tested with small scale tensile test systems, measuring the changes in length with optical methods. However, tests on individual fibrils are more complex since their diameters are in the range of 10s-100s of nm and thereby at the limit of optical resolution. Through an elaborated protocol and with the use of an atomic force microscope (AFM) nano-tensile tests can be performed. By analysing force-displacement curves statements about the mechanical behaviour in general, such as the energy dissipation as well as the elastic behaviour can be obtained.

Under the use of the AFM also the radial mechanical properties are recorded via nano-indentation test. The outstanding mechanical porperties are related to the structure as well as the hierarchical architecture of collagen based tissues. This can be shown by comparing healthy tissues with tissues affected by gene mutations encoding collagen. Since collagen is present in nearly every connective tissue, mutations in the collagen genes can cause severe phenotypes with multiple effects on individuals. These mutations cause pathogen diseases like Ehlers–Danlos syndrome [4], Alport syndrome [5] or osteogenesis imperfecta (OI) [6].

Through these genetic mutations of the collagen genes major changes may occur within the connective tissues of these patients, with OI showing the most severe phenotypes. Within OI, or brittle bone diseases, different phenotypes exist, for this reason a clinical classification system was defined ranging from a mild pathology to lethal.

The main clinical features are low bone mass and reduced bone material strength, which results in brittle bones, bone deformity and growth deficiency. OI is directly linked to changes of the collagen type I molecule. There exist two forms of OI the autosomal dominant and the autosomal recessive. The autosomal dominant mutation changes the amino acid sequence of the collagen protein and thereby the protein structure by itself. Whereby the autosomal recessive mutation results in a lack of proteins needed for post-translational processing and folding of the collagen protein[7].

To observe the effects of OI on biological tissue different mouse models exist resembling the different phenotypes of OI [8]. To simulate the moderate/severe phenotype of OI the homozygous mutated mouse (OIM) is chosen. For this project Collagen type I is extracted from mouse-tail-tendons of WT and OIM individuals and the mechanical properties where compared. Further two types of tensile tests are performed, tensile tests in the physiological strain-region with different strain rates and fracture tests.

1.2 Motivation

On the macroscopic level the mechanical properties of connective tissues, like bone and tendon, have been the subject of many studies [9, 10] . Also the effects of OI on these tissues at the macro-level have been an aspect of interest in different studies [11, 12, 13]. However, on the hierarchical level of individual collagen fibrils and below, the structural and mechanical changes through OI are partially unknown. To generate data on the mechanical properties of individual collagen fibrils, existing mechanical tests need to be improved and optimized. There exist two types of mechanical tests on collagen fibrils, nano-indentation tests and nano-scale tensile tests. With the current method tensile tests have only been performed in the elastic strain region up to 8 % strain. During this study, the tensile tests should be advanced to conduct fracture tests on individual collagen fibrils. Further, improvements on the preparation protocol of samples for tensile testing is of large interest. The time needed for preparation should be reduced to enable higher sample rates. This would generate more data on fibril mechanics in general and on the influences of OI on the fibrillar level.

By comparing OI with WT collagen fibrils the differences of mechanical structural properties at the fibril level may be obtained. The tests on the control group (WT) are not only performed for comparison reasons. The test results from WT fibrils are also of interest by themselves, since only a few research groups engaged with the material properties of WT at the fibrillar level. The information obtained during this study should lead to a clarification of the mechanisms within the fibrillar structures of collagen and help to determine on which level the brittleness of OI emerges. Comparing these two types of collagen fibrils the putative alteration of mechanical properties and structure through the mutation is expected to be uncovered. Information about the behaviour of collagen fibrils is not only gained from mechanical tests also the swelling of the fibrils is observed. The swelling ratios help with assumptions about the non-structural bound water within the fibril. Structural bound and non-structural bound water is thought of to be an influencing factor on the mechanical properties and thereby the information about the swelling is expected to clarify the measured properties resembling stiffness. Until now, it is not fully understood if the effects of OI present on the macroscopic level evolve from the primary changes within the molecule or secondary due to changes in intermolecular forces. Another possibility would be that the alteration of the mechanical properties develop through changes in the architecture within higher hierarchical levels.

1.3 Thesis goal

The goal of the thesis is to improve current protocols and techniques to investigate the mechanical properties of individual collagen fibrils. To gain more information and thereby a better understanding, more and also different kinds of mechanical tests are needed. For this reason the topic of research for this thesis are tensile and indentation tests on individual collagen fibrils. Therefore the procedure and the sample preparation of tensile testing individual collagen fibrils need to be optimize. With the optimized tensile tests values for the mechanical properties of individual collagen fibrils should be determined, to describe the mechanical behaviour of individual collagen fibrils. Comparing WT with OI fibrils may lead to insight in the effects of the genetic mutation on the properties of the fibrils.
The alteration of the OI properties on the fibrillar level can lead to a clarification of the clinical symptoms present on individuals effected by OI. The mechanical behaviour under external load might help with assumption about the influence of the structural changes due to OI.
Since single collagen fibrils show a transversely isotropic behaviour the mechanical properties differ along the fibre direction. The goal is to obtain the radial as well as the longitudinal material properties. By observing the diameter change of the fibrils during hydration a statement about the unbound water within the fibril can be made. The structural water could be an influencing factor in the energie dissipation during extension and retraction and thereby giving an explanation of the generated data. With the air-dried diameter of fibrils, single collagen molecule forces can be approximated according to a paper published by Hulmes et al. [14]
This states the goals of this thesis:

1. Optimization of the preparation protocol for tensile test specimens
2. Improve the tensile test to enable fracture tests of individual collagen fibrils
3. The creation of AFM images of individual collagen fibrils in dried and hydrated state.
4. To conduct AFM cantilever based nano-indentation tests on single collagen fibrils.
5. To implement tensile tests on single collagen fibrils in hydrated state.
   (a) In a physiological strain-range with changes in strain rate
   (b) Fracture tests

2 Mechanics and Structure of Collagen

2.1 The Collagen Super-Family

The family of collagen molecules is a very wide group. It consist of many different types of collagen molecules. The property which unites all of these molecules is their composition. Collagens are composed of three α-polypeptide chains. Each of these α-polypeptide chains features one or more regions with a well defined repetitive amino acid sequence of Glycine-X-Y, where X and Y can be any amino acid [15, p.15].
The α-polypeptide chains are composed of about 1050 amino acids with a distribution of 33% glycine, 25% proline, 25% hydroxyproline and lysine appearing frequently. [16, p.63] This defined order of amino acids leads to the formation of a triple helical structure consisting of three α-chains through self-assembling. The helical structure is formed by the fact that Proline is present in the polypeptide chains. The residue of Proline is a ring structure which leads to kinks within the α-chain.
Glycine is responsible for the tight packing of the α-chain into a triple helix, since the Glycine residues are small and hydrophobic. Glycine is thereby essential for the development of the helical structure. The third important amino acid for the formation is Hydroxyproline. Hydroxyproline maximizes the possibility of interchain hydrogen bonds which leads to a higher stability of collagen [16]. The orientation of the amino acids results in glycine located in the center of the triple helix and the residuals of the X and Y amino acids are presented on the surface of the structure. This self-assembly creates the procollagen molecule which consist of two non-helicale domains, anterior and posterior, and the helical domain in the middle. Through proteinases the two non-helical domains are partially cut off the procollagen, leaving short telopeptides of around 20 amino-acids at the N- and C-terminal of the protein. After this cleavage the protein is called collagen.
According to the current knowledge the family of collagen molecules present in humans consist of 27 different collagen types, each type is numbered by Roman notation. The 27 collagen molecules show different features and are thereby subdivided into the following classes:

- fibrillar collagens (types I*, II, III,V*, XI*, XXIV and XXVII)
- basement membrane collagens (type IV*)
- FACIT collagens (types IX*, XII, XIV,XVI, XIX, XX and XXI)
- short chain collagens (types VIII* and X)

- anchoring fibril collagen (type VII)
- multiplexins (types XV and XVIII)
- MACIT collagens (types XIII, XVII, XXIII, and XXV)
- collagen type VI*

The collagen types marked with a star consist of two or three different α-chains and are so called heterotrimer. The field of biomechanics and tissue engineering directs the attention to the fibril forming subgroup of collagen molecules. The outstanding mechanical properties of the collagen fibrils and the large quantity present in connective tissue thereby defines the mechanical properties of these tissues to a large part. For this reason, the focus during the thesis is on fibril forming collagens and in particular on fibres consisting predominantly of collagen type I.

2.2 Fibril forming collagens

From the subgroup of fibril forming collagens the most common one in humans and generally in mammals are collagen type I molecules. Collagen type I is a hetero trimer molecule assembled from two identical α1-chains and one α2-chain. This composition can also be noted by $[\alpha 1(I)]_2\ \alpha 2(I)$.[15]
The collagen type I molecule has impressive mechanical properties. The properties are passed from the molecule level up to tissue and thereby defining the tissue properties. This leads to collagen type I being present in nearly every connective tissue exposed to mechanical stress. As one of the main components of tendons and ligaments, the molecule defines the mechanical properties of these connective tissues to a large degree.
However, collagen type I not only appears in soft tissue, it also plays an import role in bone formation. In general bone is a nano-composite material, having minerals and collagen and non-collagenous proteins as its main parts. The mineral part consists of calcium-phosphate crystals and provides the bone with stiffness. The other main part, collagen, determines the flexibility and strength of bone [17, p. 39]. The non collagenous proteins (NCPs) play an important role in the fracture mechanisms within the bone. NCP's connected the minerals with the mineralized fibrils within the bone and thereby act as predetermined breaking points.
Another abundant fibril forming collagen is collagen type II. It occurs in soft tissues, mainly in cartilage. Collagen type II is a homotrimeric molecule and consists of three

identical $\alpha 1(II)$-chains. Collagen has a variety of features, for example the well defined order of collagen fibrils within the cornea of the eye create a transparent nevertheless mechanical stable tissue [18, p.198].
In the fibril forming group of collagen the collagen molecules form microfibrils which then form fibers in the higher hierarchical level as can be seen in Fig.1. Further Fig.1 shows that the assembling in each length scale occurs in a well organized order. The structures created by this order exhibits cross-striations every 67 nm. These stripes are described by the 2-dimensional Hodge-Petruska model or by the 3-dimensional Orgel model. The

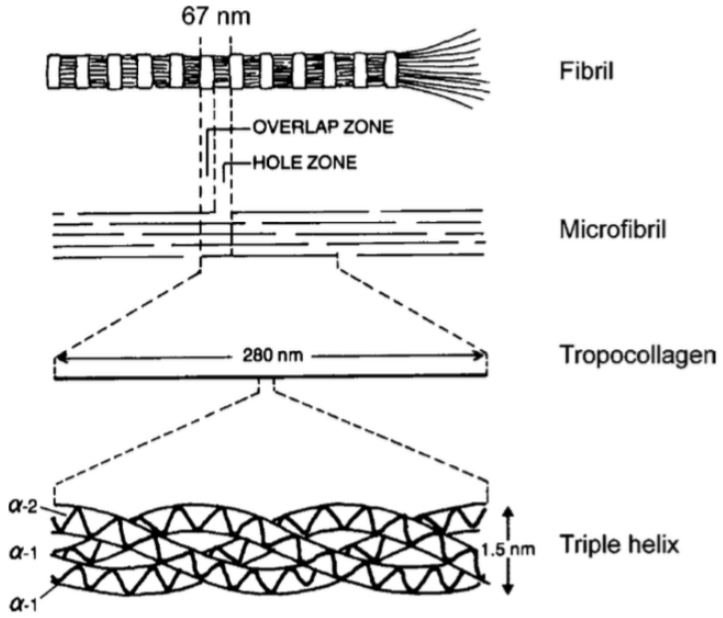

Figure 1: Hierarchical structure of collagen type I [1]

resulting stripes are called D-banding. The darker lines are areas where the collagen molecules overlap and the lighter areas mark the gap regions. The diameter of single collagen fibrils lies in the range of 40-300 nm [2, p.1188].
In this project the collagen fibrils were obtained from mouse-tail tendons. By that mainly collagen type I was observed since 90-99% of the collagen types in tendons are of type I [19]. The strength of single collagen molecules was obtained via x-ray diffraction. Since collagen molecules assembly into larger structures (the fibrils) the interactions between the molecules define the mechanical properties of the fibrils. The intermolecular connections can be formed by non-covalent bonds like hydrogen-bonds, Van der Waals forces and hydrophobic interactions or covalent bonds forming between the residuals of the amino acids called cross-links.

2.3 Collagen cross-linking

Intermolecular cross-links between collagen-molecules within collagenous tissues could play a role in defining the mechanical properties. Tissues primarily consist of different types of collagens, however all the different types are connected via the same mechanism. Although the cross-link profile depends on the tissue and further on which mechanical stress the tissue experiences [20].
There are two pathways of cross-link formation, the enzymatic formation and the non-enzymatic formation.

2.3.1 Enzymatic cross-linking

The enzymatic cross-linking processes are the first which appear during collagen fibril formation. Lysyl-oxidase deaminates the ϵ-amino group of lysine or hydroxylysine in the telopeptide ends of a collagen molecule. The formed aldehyde reacts with a lysine or hydroxylysine in the helical domain of another collagen molecule. This leads to the connection of two neighbouring molecules, firstly immature, divalent cross links are formed and with age and by different chemical reactions trivalent cross links develop. [21]

2.3.2 Non-Enzymatic cross-linking

This cross-links establish during ageing and to a greater extent in individuals with diabetes mellitus. The formation involves reactions with glucose found in tissue. From this reactions between the glucose and lysine, furosine and pyridosine can be determined. These molecules form cross-links which are called advanced glycation end-products (AGEs) [21]. Glucosepane are AGEs formed between lysine and arginin under non-oxidative conditions. The glucosepane are likely to be the only AGEs which might have a significant influence on the mechanical properties of collagen structures [20]. These AGEs link two helical domains of neighbouring collagen molecules together.

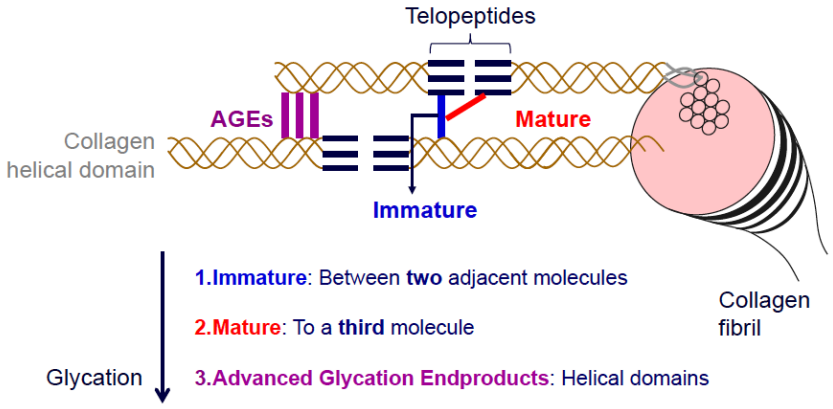

Figure 2: Cross-linking during maturation[19]

2.4 Mechanical properties of collagen

Biological tissues evolved over millions of years and each molecule plays a special and individual role in a living organism. Through this evolution, molecules are shaped in a manner which perfectly fits the functional requirements of the tissue.

2.4.1 Collagen-rich tissue

Since collagen molecules are present in every connective tissue, previous studies engaged with tensile testing on different length scales ranging from the tissue level down the fibril level. As mentioned before most tissues are composed of different compounds. This variation in composition results in different mechanical behaviour. For example, comparing bone and tendons, both materials are composed to a large quantity of collagen, mainly type I. Nevertheless, there are severe differences in the mechanical properties due to the architecture of the components present in these tissues.
Bone is composed of water, collagen,hydroxyapatite minerals and to a small quantity of proteoglycans and noncollagenous proteins (NCP's) [17, p. 39]. Compared to this, tendons consist of water, collagen, elastin and also to a small quantity of proteoglycans and other proteins. The main difference in composition is that in bone minerals occur and in tendons a protein called elastin. To see how these elements and the arrangement of these elements within the tissue effect the mechanical behaviour in general, we engage with the composite structures in the following, beginning with bone.

As represented in Fig.3 the lowest hierarchical level in bone is composed of mineralized collagen-fibrils. Based on the current model the mineralization occurs within the fibril and more specific within the periodic gap-regions in between the collagen molecules.(Fig.

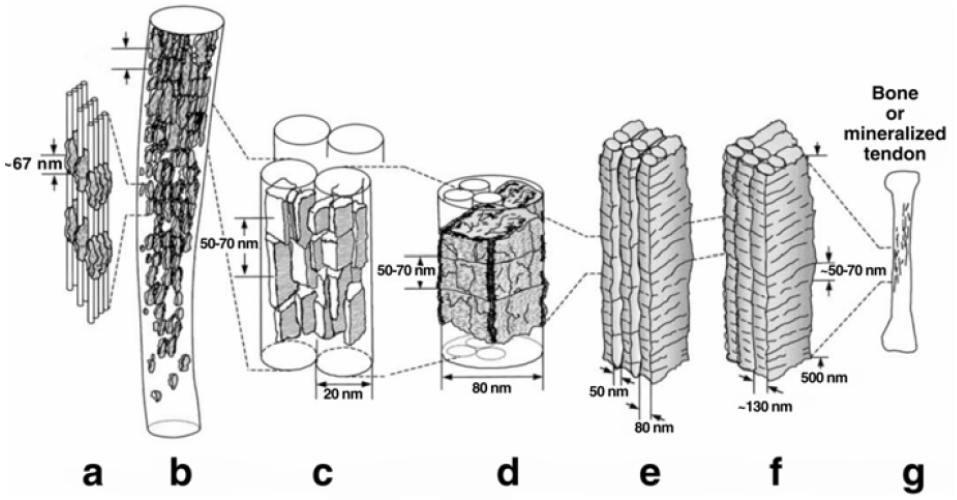

Figure 3: Mineralization within the bone [22, p. 344]

1 (a)) In this gap regions the crystal platelets form, which grow in length and width through the channel or gap spaces as it can be seen in Fig. 1 (b). Since collagen-molecules assemble into fibrils also the crystals form larger and thicker plates. However, the periodicity and parallel nature of the plates is preserved Fig. 1 (c) and in this stage also interfibrillar plates develop. At the level of collagen fibres Fig. 1 (d), the crystal plates evolve in all directions. In the next level of tissue hierarchy, Fig. 1 (e) the fibres accomplish parallel plates. Some plates may display the inter-fibrillar connections formed earlier. In the beginning there is a space between the plates, this space decreases gradually with progressing mineral deposition Fig. 1 (f). Finally there plates become lamellar in shape Fig. 1 (g), the lamellar build up either osteons in cortical bone or trabecular packets in cancellous bone. Further mineralization occurs not only in the gap regions, there also exists surface mineralization of the collagen structures from b-f [22, p. 344]. The example of bone mineralization shows that bone is a complex composite material with properties evolving over time and length-scale generating a strong but also flexible material. When now compared tendons with bone it can be seen that although the basic elements are present in both tissues the small differences, such as the missing of minerals and NCPs lead to complete different tissues with different mechanical properties. The lack of hydroxyapatite in tendons results in a non mineralized structure. More exact a small part of the tendon at the junction between the tendon and the bone is mineralized too, whereby a strong linkage between bone and tendon is achieved. This mineralized tendons are neglected for the comparison.

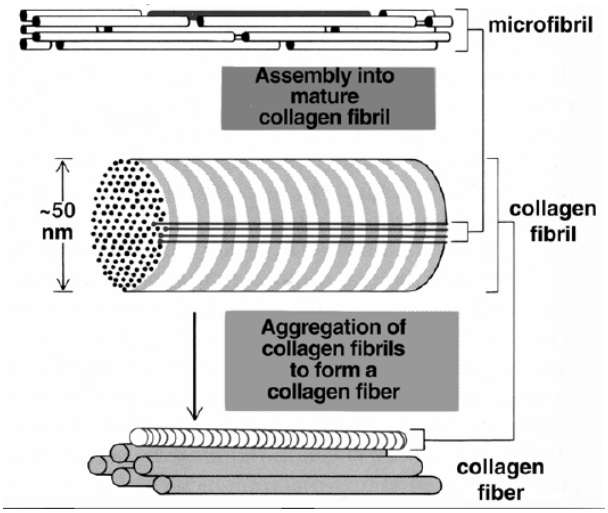

Figure 4: Detailed assembly of collagen molecules to microfibril then fibril and further to a fiber[23]

The basic unit of tendons is the collagen type I molecule. The arrangement within the collagen fibril is highly defined which results in a periodic cross striation of the fibril called D-banding, with a width of 67 nm in tendons (64nm in ligaments).
Under the use of the microfibril model this cross-striation can be explained. Five collagen strands assemble into a helical structure due to electrostatic forces. This structural model of five molecules is called micro-fibril. However, the collagen molecules assemble with an offset which results in defined gaps between the ends of the molecules.
The microfibrils further assemble by wounding around each other into larger helical structure called fibrils with a diameter ranging from 40 to around 300 nm. The force responsible for this aggregation are hydrogen-bonds and Van der Waals-forces. Further covalent intermolecular bonds (cross-links) are thought to stabilize the fibrillar structure. One hierarchical level higher the collagen fibrils form collagen fibres, this fibers are enveloped by the endotenon containing the cells (fibroblasts). Going further up the length scale the fibres form fascicle, this structure is again enveloped by a membrane called epitendinium. By observing this fascicles and also fibres under light microscope a crimp pattern can be recognized. When the tendon is under tension the fibres align and the crimp pattern vanishes. It is unclear if the crimp pattern is present within the body, since tendons are throughout under tension.
The effect of the difference in architecture and composition between the tissues can be visualized by comparing stress-strain curves of bone and tendon as can be seen in Fig.6. Bone is much stiffer which is represented by a higher elastic modulus and visual through a steeper stress-strain curve. Therefore, tendons show larger energy expense until fracture, represented by the area underneath the stress-strain curve. As can be seen this is mainly

due the fact that bone is mineralized, which results in a stiffer and less elastic material. The higher stiffness gained through mineralization results in a lower toughness of bone [15, p.9].

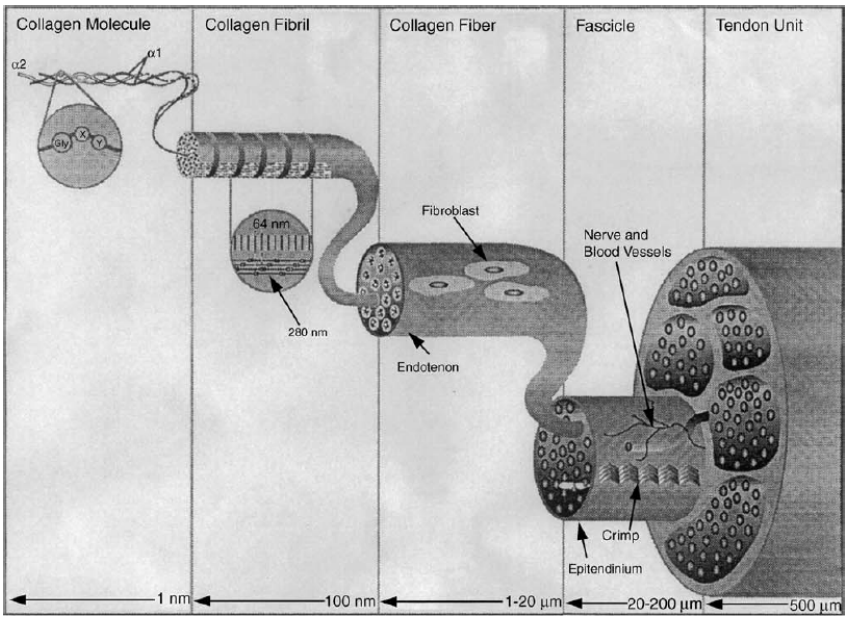

Figure 5: Hierarchical structure of tendons[23]

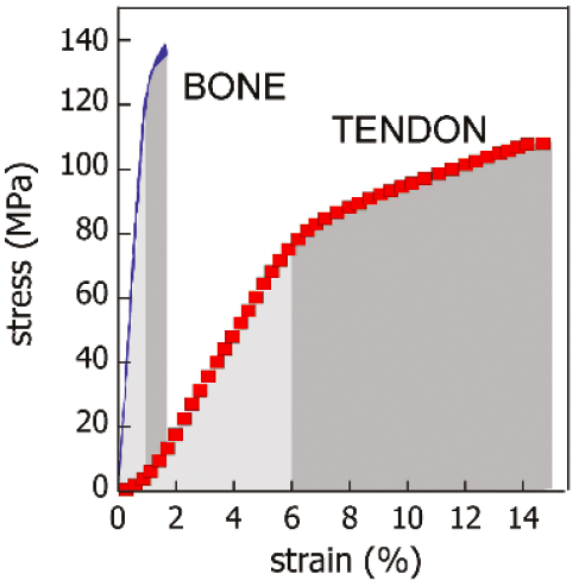

Figure 6: Stress-Strain diagramm for mouse tail tendon and for parallel fibered bone [15]

2.4.2 Tendon

When looking at the basic elements of a connective tissue it can be seen that collagen is the most important and also mechanically defining element. This shows how important it is to obtain information about this protein.
Mammal tendons consist to a large quantity of collagen type I (90-99%) which makes this tissue ideal to extract individual fibrils. However, the mechanical properties are not only defined by the collagen molecule also the arrangement within the fibrils/fibres especially the cross-linking and also the quantity of constituents contributes.

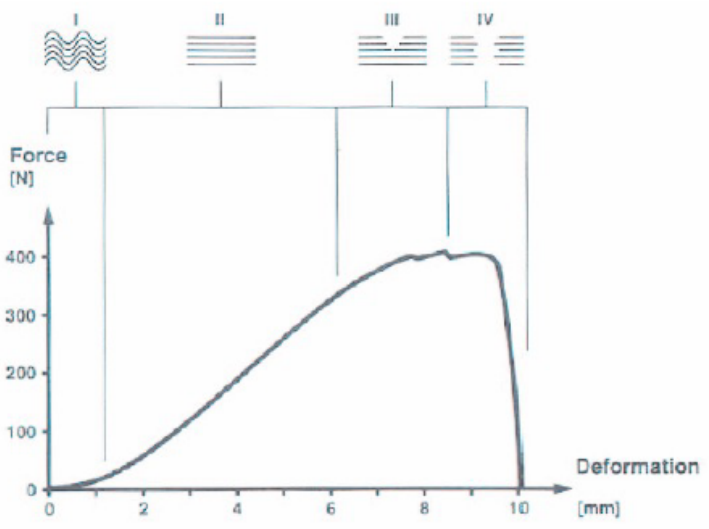

Figure 7: Load-elongation diagramm of a tendon tested until fracture [19]

In Fig. 7 the load-elongation curve of a rabbit tendon is shown as an example. Four distinguishable regions can be seen within this diagram:

1. Toe-region
2. Linear-region
3. Sliding/Micro-damage and micro-failure
4. Rupture

In the toe region only small forces are required for elongating the sample. This reflects the crimp straightening of the collagen fibrils. When further elongated the tendon reaches the second stage. The linear region, more collagen fibres are recruited which results in an uniformly increasing stiffness until a strain of approximately 4-5%.

In living organisms it is unclear if the toe-region is present since the tendons are always under tension. When the muscle then is activated the deformation of the tendon is in the linear region under physiological conditions. The elongations in this two regions is recoverable. When the elongation passes the linear region micro-damage (3) occurs within the tendons which results in softening of the material and permanent damage. The micro-damage is characterised through the breaking of covalent intermolecular bonds between the collagen fibrils (see Section 2.3). Resulting in collagen fibrils sliding and thereby an elongating of the tissue [10]. In region 4 all fibres fail and the tendon ruptures.
During tensile testing not only fracture tests are operated, also important knowledge is gained from observing the elongation and retraction within the elastic region. Most of the biological tissues show viscoelastic behaviour, which is represented by a difference in the elongation and retraction curve. Information on the degree of viscoelasticity within the structures can be gained from tensile tests in the linear region.
Tendons play an important role in force transmission connecting muscles with bones. The energy dissipation during loading and unloading describes the efficiency during locomotion. The viscoelastic properties are tested by cyclic loading. When tendons are tested in tensile direction the energy dissipation can directly be evaluated. As it is represented by the difference in area of the elongation and retraction curve of the material. Tendons return about 90-95% of the stored-strain energy. The viscoelastic behaviour is not clarified in total until now. Papers suggest that the spring behaviour is created by the elongation of the collagen molecules and the viscous behaviour appears through water flow. For this reason the mechanical properties of the lower length-scales are of great importance [15] and therefore the mechanics of individual collagen fibrils are the topic of ongoing research.

2.4.3 Collagen Fibril

On the hierarchical level of collagen fibrils viscoelastic behaviour can be observed similar to the higher length-scales. In fibrils the change in inter-molecular bonds like Van der Waals, hydrogen-bonds, intra- and intermolecular crosslinks are assumed to be influencing factors of this behaviour [10].
Further, water molecules play an important role for determining viscoelastic behaviour. There exist two types of interactions of fibrils with water moleces, the structural bound water molecules and unbound water molecules. During dehydration the unbound water molecules evaporate and the bound water molecules remain in the collagen fibril. In the physiological hydrated state the unbound water influences the mechanical behaviour of collagen fibrils. Shen et. al. [24] stated that the viscoelastic behaviour of individual

collagen fibrils is created by the rearrangements of collagen molecules in the fibril and by movements of the unbound water molecules across the fibril. As already mentioned the collagen fibril defines the material properties of connective tissue to a large part. However, due to the structure and shape of collagen molecules, fibrils and fibres show a single preferred loading direction. This preferred direction is along the longitudinal axis of the molecule, fibril and fibre. The behaviour orthogonal to the longitudinal direction, the radial direction, displays also constant but weaker mechanical properties.
Materials which behave in this manner are called transversely isotropic with respect to the preferred direction [25, p.266]. In our case the preferred direction is the longitudinal axis, the directions orthogonal to this axis act isotropic.
The goal of this thesis is to achieve data on the mechanical behaviour of single collagen fibrils. Along the longitudinal direction, this is achieved by tensile tests on nanoscopic level. In the radial direction, the properties are evaluated through nano-indentation tests. Through this tests more information about the reaction of individual collagen fibrils to external mechanical stress may be obtained.

Only a few research groups engaged with tensile tests on individual collagen fibrils. Until now there exist three different approaches to evaluate the mechanical properties of individual collagen fibrils. This 3 approaches differ in the used device:

1. Microelectromechanical systems (MEMS) liu2015
2. Micro-manipulators [26]
3. Atomic force microscope (AFM) [27, 28, 29, 30, 31, 24, 32, 33]

From this listing can be seen that the AFM, amongst other techniques such as MEMS and micromanipulators, has been the most commonly used device to perform tensile tests on individual collagen fibrils. In section 3.4 the individual methods are explained in greater detail.
The main comparable mechanical parameters gained from tensile tests on individual fibrils are the longitudinal elastic modulus, the rupture strain and the ultimate strength. The following values for these parameters were all obtained from hydrated fibrils. For the tensile elastic modulus of individual collagen fibrils literature values range from 326 MPa ±112 MPa [33] up to 2.2 GPa ±0.9 GPa [28].
Fibrils achieved values from 16% ± 4% [28] up to 63% ± 21% [33] for the rupture strain and for the ultimate strength values from 71 MPa ±23 MPa [33] up to 200 MPa ±110 MPa [28] are reported. The difference within the values could arise from multiple factors,

beginning with collagen obtained from different tissues, the osmotic pressure, the age of the animals or the storage of the samples.

The tensile measurements on individual collagen fibrils are time consuming with a maximum output of 3 tensile fracture tests per week. A faster method to evaluate the mechanical properties of individual collagen fibrils are nano-indentation tests. The obtained parameter is the radial elastic modulus of the collagen fibril. The radial elastic modulus is physiologically not as relevant as the longitudinal elastic modulus, since the collagen fibril is mostly loaded along the longitudinal axis within tissues[15].
However, nano-indentation test are not considered as uniaxial loading tests. Therefore the obtain indentation modulus during nano-indentation-tests is a compound of the radial as well as the longitudinal elastic modulus [34]. However, the radial elastic modulus mainly defines the indentation-modulus and therefore the indentation-modulus is called radial elastic modulus during this thesis.
Existing studies [35, 36, 37, 34, 38] of indentation-tests on individual collagen fibrils commonly are performed with AFMs. In literature values for radial elastic moduli of hydrated fibrils range between 1- 10 MPa [34, 38]. Early studies [35, 36, 37] performed nano-indentation tests on dried-collagen fibrils and thereby values for the radial elastic modulus of 1-10 GPa were measured. In human bodies collagen fibrils are surrounded by water and different ions, the indentation test in hydrated state are therefore more adequate to the physiological situation. However, the fibril is composed of collagen molecules and therefore the lowest hierarchical level of collagenous tissue is the collagen molecule. The mechanical properties of this molecules have been researched in the past and are researched until now.

2.4.4 Collagen-molecules

During the last thirty years studies evaluated the axial elastic modulus of single collagen molecules with different methods obtaining values for the elastic modulus ranging from 3 to 9 GPa [22]. The difference in the values of the elastic modulus can originate from the fact that different tissues were used. Another reason could be the difference in the testing method, dynamic or static. Static and dynamic tests produce different values for the mechanical properties. Since collagen molecules are thought off as viscoelastic structures. One reason for the viscoelasticity could be the breaking and reconnecting of the hydrogen bonds within the molecule. Another reason could be the liquid flow during deformation, similar to larger structures. When collagen is stressed in a cyclic manner the bonds do not have enough time to reform or the water molecules can not penetrate back into the molecules fast enough. However, these are just assumptions and are the topic of

ongoing research. The influence of the viscoelasticity on the mechanical properties can be studied during cyclic tests.

Tissue from which the collagen was obtained	State	Nature of the test procedure	Young's modulus (GPa)	Source
Bovine Achilles tendon	Solid state in 0.15 M NaCl solution	Static X-ray diffraction	2.9 ± 0.1	Sasaki & Odajima (1996a)
Rat tail tendon	Solid state in 0.15 M NaCl solution	Brillouin scattering	9.0	Harley et al. (1977)
Rat tail tendon	Solid state in 0.15 M NaCl solution	Brillouin scattering	5.1	Cusack & Miller (1979)
Lathyritic rat skin	Acetate/NaCl/glycerol solution	Dynamic measurement of persistence length	4.1	Nestler et al. (1983)
Dermatosparaxic calf skin	0.05 M acetic acid glycerol solution	Static measurement of persistence length	5.1–3.0	Hofmann et al. (1984)

Table 1: Different Experiments to obtain the Young's modulus of collagen molecules [22]

2.4.5 Physiological strain

Non-invasive in vivo measurements in humans based on ultrasound imaging showed that during physiological movements the strain of tendons ranges from 2.5% up to 8% depending on the activity [15]. The achilles tendon showed 2.5% strain during walking [39], 5% while jumping [40], 5.5% during running [41] and for isometric maximum voluntary contractions up to 8%[42]. This shows that the physiological non-traumatic strain range in humans is up to 8% although it depends on the observed tendon. Since all biological tissues adapt perfectly to their requirements, there exist differences within the body. For example a finger tendon shows different properties than the achilles tendon. The impressive mechanical properties which allow human locomotion in general can be altered by diseases. For example osteogenesis imperfecta, a genetic mutation influencing nearly every connective tissue of the effected individual.

2.5 Osteogenesis imperfecta

Gene mutations of the collagen genes can affect the amino acid sequence and thereby create pathological conditions within individuals. One of the most severe diseases is osteogenesis imperfecta (OI) also known as brittle bone diseases. OI is a relatively rare genetic disorder which concerns one individual within 15-20.000 [6]. The classical genetic mutation for OI occurs in one of the two genes coding for collagen type I, either the COL1A1 or COL1A2 gene, which causes defects in structure and quantity of collagen type I proteins [6].
The disease manifests in weak bones, skeletal fragility and substantial growth deficiency which leads to fracture of bones at very mild trauma. However, OI not only effects the bone, as collagen is very frequent in nearly every connective tissue. The genetic mutation also leads to blue sclerae, dentinogenesis imperfecta, hearing loss, cardiopulmonary abnormalities, easy bruisability, excessive sweating and loose joint[43].
In 1979 a classification system was developed by Sillence et al. under the use of genotype, phenotype and radiographic data. The affected individuals were divided into four classes. This classification described the classical osteogenesis imperfecta which occurs autosomal dominant and is connected to gene mutations in the collagen type I genes.
New developments have shown that osteogenesis imperfecta also appears autosomal recessive with mutations in genes coding for proteins necessary for posttranslational modifications of collagen type I. Two other forms of OI have been discovered under the use of bone histology, although the molecular defect remains unknown.[44]
This circumstances lead to an update of the Sillence classification by Marini et al. in 2007, with the result of eight classes instead of four. [43]

	Type	Inheritance[a]	Phenotype	Defect
Sillence Types	I	AD	Mild	Null α1(I) allele; Some glycine substitutions
	II	AD	Lethal	Structural defects in Type I collagen
	III	AD	Progressive deforming	Structural defects in Type I collagen
	IV	AD	Moderate	Structural defects in Type I collagen
New Types	V	AD	Hypertrophic callus; dense metaphyseal band; distinctive histology	Unknown
	VI	?	Mineralization defect "Fish-scale" lamellae	Unknown
	VII	AR	Severe to lethal	Mutations in *CRTAP*
	VIII	AR	Severe to lethal	Mutations in *LEPRE1*

[a] *Abbreviations:* AD, autosomal dominant; AR, autosomal recessive.

Table 2: Classification of ostegenesis imperfecta [43]

Until now more than 1500 gene mutations of the collagen type I genes have been identified, over 800 of them lead to glycine substitution in the helical domain of the protein. Substitution of glycine with another bulkier amino acid can lead to misfolding in the

collagen molecule. The worst and also lethal case is if the helical formation is inhibited in total. Other mutations create exon splicing defects and a small number of mutations also results in nonglycine changes [6]. Osteogenesis imperfecta is a very difficult disease to characterize, since it is multi factorial. In the past an osteogenesis imperfecta murine(OIM)-model had been developed, this model shows a well defined genetic mutation which simulates the situation of the severe phenotype in humans in an accurate way[1].
The OIM-model produces only $\alpha 1$-chains, which results in an abnormal homo trimeric $[\alpha 1(I)]_3$ collagen type I molecule rather than an heterotrimeric $[\alpha 1(I)]_2$ $\alpha 2(I)$ molecule. These $[\alpha 1(I)]_3$ collagen type I molecule forms helical structures which show decreased mechanical properties compared to the heterotrimeric molecules of the wildtype[45]. The decreased mechanical properties model the situation in humans properly and for that reason this OIM-model was chosen for this study. The goal of the thesis is to study the influence of osteogenesis imperfecta on the tissue properties and thereby on individual collagen fibrils. The diameter of individual collagen fibrils is in the range of 40-300 nm, this limits the devices with which these structure can be observed. The maximum resolution of light microscopes is in the range of 200 nm, this makes observations on individual fibrils impossible and therefore another technique is needed. There are two solution to gain a higher resolution in microscopy either change the wavelength of the observing beam, e.g. electron-beam, or resolve the structures with mechanical methods. Due to the fact that the collagen fibrils are observed in aqueous environment only the mechanical method can be used. This method is called atomic force microscope and is described in the following chapter.

3 Atomic Force Microscopy

3.1 Scanning Probe microscopes

Scanning Probe Microscopes are devices which use mechanical principles to resolve structures and surfaces. Atomic force microscopes(AFM) belong to this family of microscopes. The main part of an AFM is the cantilever with a tip on the front part, the tip interacts with the surface of the observed material. Through deflection of the cantilever statements about the topography and mechanical properties of the sample can be made. The deflection of the cantilever is detected either with an electrical method or an optical detection system.
The movement of the tip is achieved by piezoelectric transducers in a three dimensional

manner. By moving the tip row-wise over the sample and recording the lateral and vertical deflection of the cantilever the topography of the sample can be visualized. The resolution of the produced image depends on the cantilever tip, the positioning accuracy of the cantilever and the investigated material. When the parameters are chosen right the AFM can reach atomic resolution [46].
Additionally, to the high resolution imaging the AFM is also the device of choice for sensitive force measurements. To measure forces with an AFM a calibration of the cantilever is performed, this task is described in detail in section 3.1.4 and 3.1.5. Under the use of the calibrated cantilever precise tensile tests and circumferential indentation tests on single collagen fibrils are possible. These tests help to define the mechanical properties of single collagen fibrils. All of the processes and measurements can be performed in hydrated state which simulates the biological environment. One of the most important parts of the AFM is the tip of the cantilever, since this part of the device is in direct contact with the sample.

3.1.1 Tip

The tip is positioned at the front end of the cantilever and is in contact with the sample. Either direct by touching the sample or indirect by force interactions with the atoms of the sample surface.
In the early days of atomic force microscopy the cantilever consisted from a thin gold foil and the tip was a diamond glued on the front-end of the foil. Since this process is very complex the method of producing cantilevers from silicon or silicon nitride enforced. The cantilever including the tip is thereby produced from silicon or silicon nitride, depending on the shape of the tip different etching methods are used [47]. This materials are choosen as they show a good uniformity of characteristics and allow a circuit fabrication with a high reproducibility of the wanted parameters [48]. The essential parameters of the tip are the sharpness of the apex, defined by the radius of the curvature and the aspect ratio of the tip. [48]

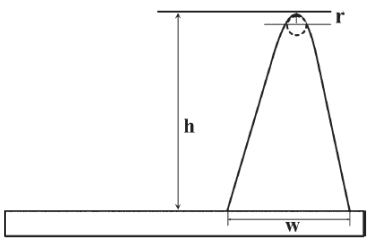

Figure 8: Essential parameters of the cantilever tip, r the radius of the curvature and the aspect ratio (h/w)[48]

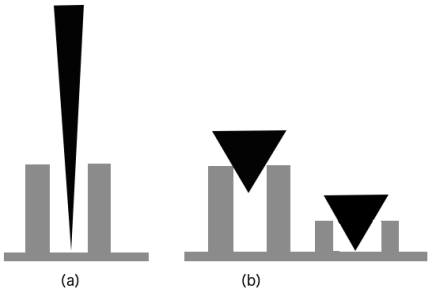

Figure 9: Influence of the aspect ratio on imaging sharp structures. Fhe figure shows (a) high aspect ratio and (b) low aspect ratio[49]

The tip radius and the opening angle can affect the quality of the image and lead to artifacts within the image. If the structures of the sample are sharp, as can be seen in figure 9 (b) , the image does not resemble the real shape of the surface. This, results in the shape of the tip limiting the image depth. As long as the tip is sharper than the observed feature the image will resemble the real height. Depending on the width and the height of the observed structure, the sharpness of the tip and the angle of the side-wall will become relevant. Generally, the measured height of the object is not affected by the shape of the tip, these artifacts are called probe-broadening [49] and appear on the lateral direction of the objects. Particularly when there are steep edges as can be seen in Fig. 10.

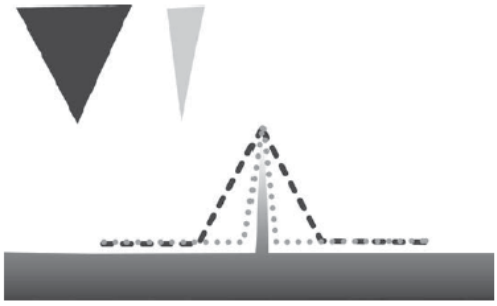

Figure 10: Broadening of the observed structure caused by the tip geometry[48]

For this reason different tip shapes are commercially available and one can choose the best fitting tip for the wanted purpose. There exist three main types of cantilever tips, the pyramidal, isotropic and 'rocket tip' [49]. These tips differ in there aspect ratio with the rocket tip showing the highest aspect ratio than the isotropic an the pyramidal with the lowest ratio. The aspect ratio of the tip defines the opening angle of the side-walls of the tip, the steeper the tip the lower the probe-broadening. It is important to mention that the opening angle of the tip has nothing to do with the sharpness of the apex as the sharpness of the apex is defined by radius of the curvature at the peak of the tip. Which

means a rocket tip can be as sharp as a pyramidal tip.
However, the phenomenon of probe-broadening is also used to determine the shape of the tip. To gain the shape a well defined surface equipped with sharp cones similar to the cantilever tip is used. This calibration grating is called TGT1 (NT-MDT Spectrum instruments).When the surface is imaged, the resulting picture includes information about the exact three-dimensional profile of the cantilever-tip. This image is analysed and the projected contact area (A_c) of the tip can be defined which is needed for the indentation tests.

3.1.2 Cantilever

The tip of the AFM is on the front end of the cantilever and the cantilever deflects according to the acting forces on the tip. The deflection of the cantilever is proportional to the force and connected via the spring constant. This connection was first described by Robert Hooke in 1676 and thereby is called Hooke's law. Hooke's law describes the force needed to extent or compress a spring. For linear elastic materials the connection between the two variables is proportional and called spring constant [50].

$$F = k * s \tag{1}$$

F resembles the force [N], s the displacement [m] and k [N/m] the spring constant. In the range of deflection occuring during an AFM measurent the cantilever can be seen as a linear elastic material and thereby Hooke's law is valid [51]. In other words, the cantilever acts like a spring with the only difference being that the displacement in our case is the deflection of the cantilever. When looking at Hooke's law it shows that the spring constant describes the stiffness of the cantilever. To generate images with the AFM the cantilever with the right stiffness and thereby spring constant has to be chosen. The selection is performed according to the imaging mode and the observed structure [48]. For example, a softer cantilever is needed for either non-contact mode (see section 3.2.3) or soft tissues. Since a softer cantilever deflects to a higher magnitude when small forces act on the tip. The larger deflections resemble a high sensitivity of the cantilever and lower forces can be detected which result in a high resolution. The spring constant of cantilevers are in the range of 0.006 N/m up to 135 N/m depending on the geometry of the cantilever [51]. There are two main cantilever shapes, the triangular (or V-shape) and the single beam shape. The two shapes show different torsional motion, which was also the reason for developing the triangular shape[49]. The different spring constants are achieved by different values of the width (W), the length (L) and the thickness (T) of the cantilever.

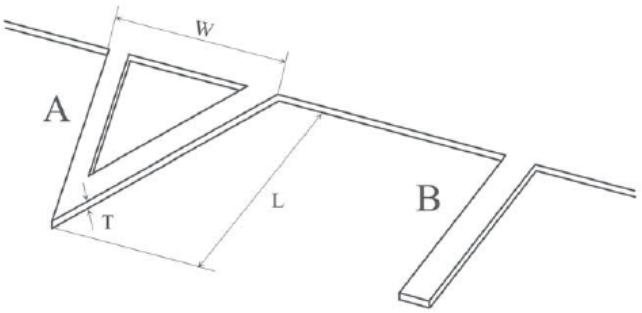

Figure 11: Triangular(A) and single-beam (B) cantilevers[48]

As mentioned before, the AFM can also be used for sensitive force measurements and by that to detect the mechanical properties of a sample. This is possible due to the fact that the AFM can record the force and the displacement at the same time. The force is detected through the deflection of the cantilever and the real deformation of the sample results from the piezoelectric-movement subtracted by the cantilever deflection. For these measurements it is important to choose a cantilever with the spring constant fitting the measured magnitude. If the spring constant is too week the force exerted on the sample will be too low which results in no deformation of the sample. If the spring constant is too large the force resisting the cantilever movement will be too low and no deformation of the cantilever will occur. However, before force measurements the cantilever is calibrated to connect the data of the detection system [V] with the real deflection [nm]. Further, the spring constant is evaluated for each cantilever. This calibration is described in detail in section 3.1.4.

3.1.3 Optical Detection System

To measure the deflection of the cantilever with picometer resolution [48] the optical lever or beam-bounce method is used. This arrangement of optical items achieves very precise result comparable to an interferometer. The device consists of a laser beam, photo detector and mirrors.The laser beam is focused on the backside of the cantilever, the surface reflects the laser beam either directly or indirect over a mirror onto the position sensitive photo detector. The photo-detector consist of four photo-diodes arranged in a square. When the cantilever is deflected the reflected beam will shift, which leads to a change of the position of the laser beam on the detector resulting in a voltage change [51]. Since the length of the cantilever is approximately 3 magnitudes smaller than the distance between the cantilever and the detector, the deflection of the cantilever is strongly magnified this results in a high sensitivity and thereby a high resolution.

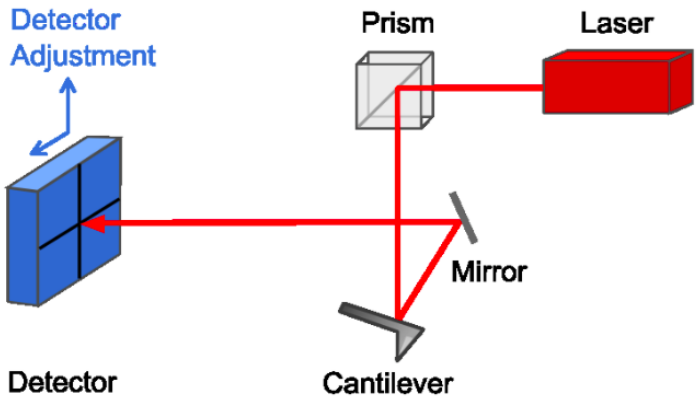

Figure 12: Principle of an Atomic force microscope [51]

Through the intermediate mirror the laser beam can be adjusted. For example, to compensate the refractive differences between air and fluid, if the sample is in aqueous conditions. To generate a connection between the voltage change on the photo-diodes and the real deflection a calibration of the cantilever is implemented. This calibration process is described in the following section.

3.1.4 Sensitivity calibration

As already mentioned in the previous sections the AFM is very versatile and the possibilities range much further than topographic measurements. Through information about the deflection and further by connecting this value with the spring constant the acting forces can be determined.
The cantilevers are produced via photolithography which shows a high accuracy for the length and width, down to the sub-micron range [49]. However, the thickness of the individual cantilevers can vary significantly which leads to wide ranges of the spring constant. For this reason each cantilever has to be calibrated when force measurements are performed.
In the first step of the calibration the optical lever (sensitivity) is evaluated. The sensitivity connects the deflection with the recorded voltage change at the detector. To gain the sensitivity a force spectroscopy is performed on an incompressible material, such as glass or mica. A force spectroscopy or in other words an indentation test can be divided into different parts, as can be seen in the following figure 13.

When the cantilever approaches the surface the tip reaches a distances where attractive forces act between the atoms of the tip and the atoms of the surface. The attractive force leads to a negative deflection of the cantilever, the so called "Jump to contact"[51]. This

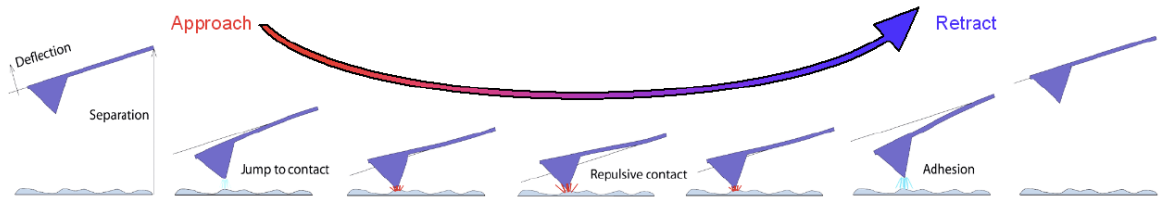

(a) Movement of the cantilever during a force spectroscopy including the acting forces on the tip

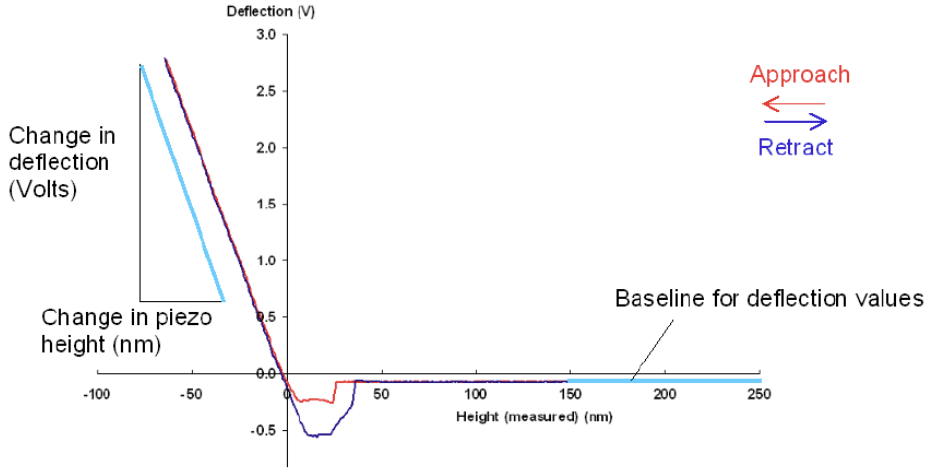

(b) Recorded data during a force spectroscopy

Figure 13: Explained properties of force spectroscopy [51]

brings the cantilever in contact with the sample surface. Depending on the imaging mode the attractive forces are utilized for visualization of the surface, this method is described in the section 3.2.3. During force spectroscopy the z-piezo extends further driving the tip into the surface. This process creates a repulsive force leading to a positive deflection of the cantilever. The z-piezo extends until a threshold value is reached, the threshold value is defined by a voltage change recorded by the photo-diodes.
In the beginning of the retraction the repulsive force minimizes until the lift off of the tip. At this point again the atomic forces between the tip and the surface lead to an attraction. The recorded data can be seen in the lower image of figure 13. As mentioned before the force spectroscopy is performed on an incompressible material. This means when the tip is in contact with the surface and the repulsive forces act on the cantilever, the tip cannot further penetrate the material[51]. At this point the deflection changes linear with the z-piezo movement. Leading to a relation between the z-piezo movement [nm] and the deflection of the cantilever [V]. Through this process the sensitivity of the cantilever is defined which transforms the deflection of the cantilever from voltage to (nano-)meters. Another offset has to be balanced, due to the initial setup or thermal drift there is an offset of the baseline. This offset is subtracted from the recorded deflection and thereby the real deflection is obtained [51].

Finally, Hooke's law is used to estimate the applied force depending on the deflection of the cantilever. For Hooke's law the spring constant of the cantilever is needed. There are multiple ways to obtain the spring constant of the cantilever. For this thesis the thermal noise method was used.

3.1.5 Thermal noise spring constant calibration

During this method of calibration the cantilever including the tip is thought of as an ideal harmonic oscillator. If the cantilever tip is far away from the sample surface there is a motion of the tip created by thermal fluctuation. Measurements of this fluctuation near the resonance frequency of the cantilever allow an estimation of the spring constant of the cantilever [52]. The energy of the natural thermal environment of the cantilever creates vibrations. The AFM records this fluctuations in deflection against time and this data can be analysed. However, the low frequency components would dominate the data over longer periods of time and therefore the frequency dependence of the fluctuations is analysed. Due this the low frequencies or specific noise sources are excluded and the analysis is focused on the resonance frequency of the cantilever [51].
The resonance peak is analysed and a harmonic oscillator fit is applied, the area underneath the fit resembles the energy in the resonance. According to the equipartition theory the energy in any free mode of a system needs to be the same as the thermal energy of the system.

$$E_{Thermal} = \frac{1}{2} k_b T \tag{2}$$

In this equation k_b resembles the Boltzmann's constant and T the temperature in Kelvin . Another way to calculate the energy is via the spring constant and the mean square value of the vertical deflection q. Through the frequency spectrum the mean square value of q is obtained and the spring constant can be calculated under the use of the following equations.

$$\frac{1}{2} k_b T = \frac{1}{2} k < q^2 > \tag{3}$$

$$k = \frac{k_b T}{< q^2 >} \tag{4}$$

This calculation assumes that the cantilever is a complete harmonic oscillator. A complete harmonic oscillator consists of a mass at the front end of a spring and the spring is mass less. In the case of the cantilever the cantilever also has a mass and not only the tip, the mass of the cantilever influences the calculation [49]. Another error occurs due to the sensitivity measurement. The sensitivity is measured for relatively large and static deflections of the cantilever. During thermal fluctuations the deflection of the cantilever is

small and thereby shows a different sensitivity than during the sensitivity measurements. The difference occurs because of the fact that the detection system mainly records the inclination and not the deflection. In 1995 Butt and Jaschke calculated a correction factor compensating this flaw [53].
Resulting in the final equation with β being the correction factor

$$k = \beta \frac{k_b T}{< q^2 >} \tag{5}$$

3.1.6 Movement of the Tip

To create images of the surface, the tip is moved raw wise over the sample. This precise movement in three dimensions is achieved by piezoelectric-elements. The elements are based on piezoelectricity, which describes a formation of an electrical potential when certain solid materials (e.g. quartz, tourmaline or topaz) are compressed, this effect is called direct piezo-effect[50].
Compression of the crystalline material lead to a polarisation of the molecules in the material, the polarisation generates a potential over the material dimensions. This potential can be used to create an electric current.
The effect also works vice versa, when a certain electrical potential is applied onto the surface, the element either extends or retracts, this is called inverse piezo effect[50, p.788].
To achieve the wanted movements within atomic resolution the inverse piezo effect is used[54]. Movements with such high resolution are only sustained over certain distances, for the used AFM (JPK Nanowizard Ultra speed, JPK, Germany) this lead to movements of 30μm in the horizontal directions (x,y) and 6μm in the vertical direction (z).The larger movements in the z-direction for approaching the surface are performed with a stepper motor.

3.2 Imaging modes in AFM

3.2.1 Lennard-Jones potential

The Lennard-Jones potential describes the interaction between two particles or atoms. This potential is present when atomic distances are reached between the cantilever tip and the surface. It includes the long range attractive Van der Waals and the short range repulsive electron shell forces of the atoms. Due to this two forces the potential can be separated into two parts. In the first part attractive forces act between the atoms. When the distance between the atoms decreases the repulsive forces get larger than the attractive forces. Thereby the second part of the potential is reached.

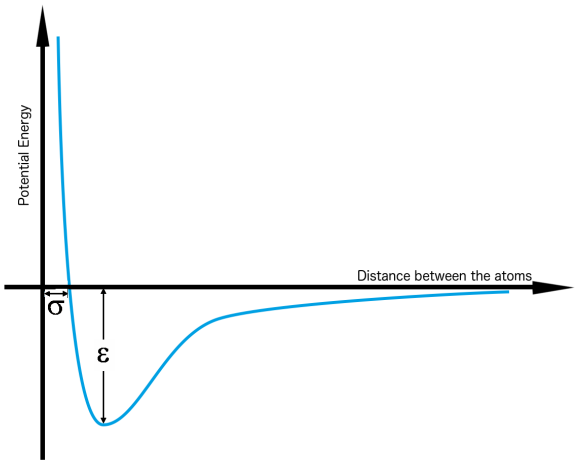

Figure 14: Potential energy between two atoms as descripted in the Lennard-Jones function

To characterise these forces we have to take a look at the variation within the potential energy of a particle, for example at the apex of the tip. Depending on the distance between the particle on the tip of the cantilever and the particle on the surface the potential energy changes. This potential is described mathematically by the Lennard-Jones function:

$$E_{pot}(r) = 4\epsilon[(\frac{\sigma}{r})^{12} - (\frac{\sigma}{r})^{6}] \tag{6}$$

ϵ and σ are constants depending on the material. In more detail σ is the distance at which the intermolecular potential between the two particles becomes zero and ϵ describes the depth of the local minimum of the potential energy [49]. The term $\frac{1}{r^{12}}$ stands for the steep increase in the potential energy when the distance of the two atoms decreases (r$< \sigma$) and thereby for the electron shell repulsive forces. The term $\frac{1}{r^{6}}$ on the other hand describes

the slower changes in the attractive behaviour at relatively large separations due to the van der Waals forces.

For topographic measurements there are two main AFM imaging modes, the DC and the AC mode. During the AC mode the tip oscillates either with constant amplitude or with constant frequency. While in the DC mode the tip is in contact with the sample surface and therefore does not oscillate. For both modes a feedback-loop is required. In DC-mode the feedback-loop generates a constant force at the sample, while in AC mode the oscillation of the tip is kept constant[48]. The AC mode subdivides into the non-contact and intermittent contact mode. The difference of the contact and non-contact mode is in the force acting between the tip and the sample. The force depends on the distance between the tip and the sample and is either attractive or repulsive. During the DC mode the tip always stays in contact with the surface which leads to repulsive forces at the tip. On the other hand in non-contact mode only attractive forces act and in intermittent contact the acting force jumps between attractive to repulsive forces.(see Fig. 15)

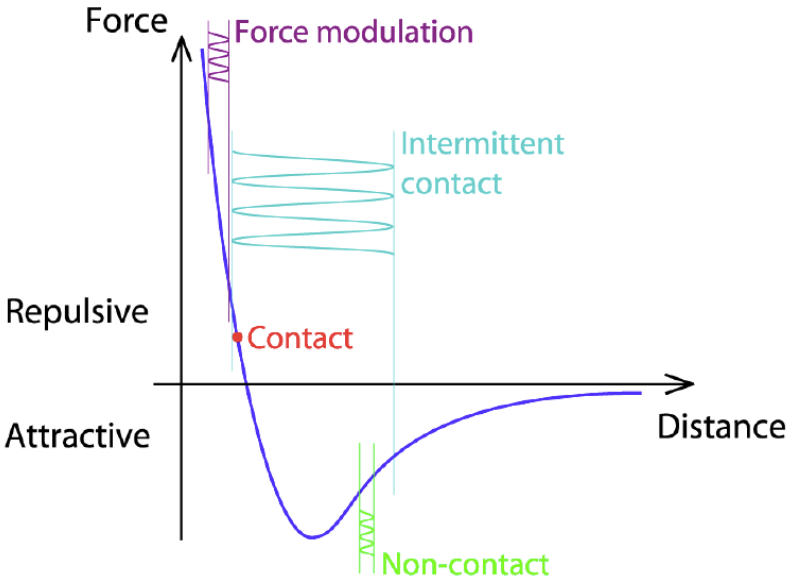

Figure 15: Diagram showing the forces acting between the tip and the surface including the different imaging modes[51]

3.2.2 Contact-mode

While imaging in the DC or contact-mode the deflection of the cantilever creates an electrical signal which is analysed by a control system. There are two ways to obtain images in contact mode. One with constant force and the other with constant height. A constant force is achieved by a feedback loop, which is applied control the z-piezo height.

During the imaging process of the sample, the z-piezo extends and retracts according to the topography to maintain a constant force. The correction of the z-piezo height thereby generates information about the topography of the surface.
The constant height method keeps the height of the Z-piezo constant during imaging. Thereby the image of the sample surface is generated through the deflection of the cantilever. The constant height method should only be used for smooth surface, otherwise the acting force can get too large and thereby destroy the sample and the tip [55].
In both methods the tip moves row wise over the observed area and creates a three dimensional image of the sample. When soft materials are imaged it is important to choose the right cantilever and constant force. If the cantilever is too stiff or the force too high it can damage the sample surface or the cantilever. Another disadvantage of the contact mode are shear forces. Shear forces are generated during the scanning process. Since the tip is always in contact with the surface. These shear-forces can cause damage on the sample or image artifacts.

3.2.3 Non-contact mode

As the non-contact mode is a dynamic-mode the tip is excited and oscillates close to the resonant frequency. By bringing the tip into close proximity of the sample surface Van der Waals attractive forces arise and create a shift within the frequency. The shift in the frequency is recognized by the feedback-loop and leads to an elevation of the tip, via the z-piezo, to maintain the frequency. The movements of the z-piezo resemble the topography of the sample[49].

3.2.4 Intermittent Contact Mode

The intermittent contact mode is similar to the non-contact mode, since the tip also oscillates. During the intermittent contact mode the tip is excited to a predefined amplitude instead of frequency. This results in tapping of the sample surface. When a variation appears on the sample surface the amplitude of the oscillation changes. This change is recognized by the feedback-loop and results in a movement of the z-piezo to maintain the predefined amplitude. The topographic image is thereby obtained through the information of the z-piezo movement.

3.3 Feedback loop

The goal of the feedback loop is to maintain a predefined threshold value. This predefined value is called setpoint. In the case of imaging, this setpoint resemble either the deflection or the oscillation of the cantilever. In constant force contact mode imaging surface irregularities result in a deflection of the cantilever. This deflection is fed-back to a control system. The control system recognizes the difference between the actual deflection and the setpoint and adjusts the cantilever height to maintain the setpoint value [51]. For this task two requirements are needed, the control system must have a high accuracy and needs to react fast to changes[49].
The on-off control is the most basic way of a feedback-loop. However, during the on-off control the setpoint value is never reached since the signal always oscillates around the setpoint [49]. The AFM is a device with high accuracy and therefore the simple on-off control does not suit the requirements. Three more precise control types are introduced which are commonly used for AFM devices. The Proportional, the Integral and the Derivative (PID) controller[49].

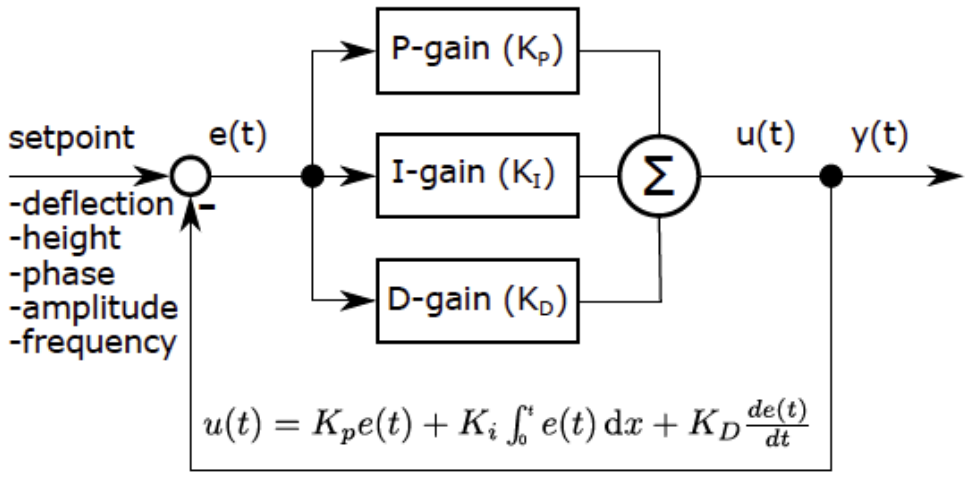

Figure 16: Blockdiagram showing the three gains, Proportional gain, Integral gain and the Differential gain [56].

The proportional control amplifies the difference between the actual value and the setpoint, to generate the required size of the correction signal. This is done by determining a proportional band which is a percentage of the total span of the controller. The width of the band defines the reaction of the controller to an error signal. For example if the proportional band is 50% then the P-gain is 2 and if it is 10% the P-gain is 10. This shows that a high gain resembles a narrow proportional band and the width defines the magnitude of response to an error signal[49].

Proportional control leads to a slightly lower or higher actual value than the setpoint, or in other words to an offset. The offset could be reduced by simply narrowing the width. However in reality this leads to an unstable, oscillating system.
By introducing the integral term to the control system the offset can be removed in a more promising way. The integral term as its name suggests integrates the difference between the value and the setpoint over a small period of time. It is important to set the time period not smaller than the reaction time of the piezo-element otherwise the integrative control starts to oscillate.
To create a steady behaviour of the feedback loop a derivative part is added, this part is proportional to the rate of change from the control signal. The derivative part results in a homogeneous signal during large deviations of the error signal. The three gains can be summarized, the proportional gain reacts quickly to changes on the sample surface, the integrative gain helps to reach an accurate setpoint and the derivative gain reduces unwanted oscillations [49].
The used AFM allowed adjustments of the P- and the I-gain, where as the D-gain is controlled automatically by the system [51].

3.4 Tensile Test

Beyond imaging the AFM has extensively been used for mechanical characterization. The AFM can apply and measure forces and displacements at nano-scale range. These properties allow nano mechanical tests such as tensile test on individual collagen fibrils. Through tensile tests statements about the mechanical properties of materials can be determined. Tensile tests produce data on the relation between stretch and sustained force of the material.The results of these tests are then processed to be independent of the sample geometry [50]. This leads to the translation of force/elongation into stress/strain. The outcome of tensile tests is thereby the stress-strain-diagram, since stress/strain are independent of geometrical parameters they qualify for comparison between different materials.
Tensile testing devices need to record the displacement and the force exerted by the material at the same time. Since biological materials are often build up hierarchically it is of importance which scale is observed. For example, tensile tests on collagen-rich tissues have been performed in multiple ways by different research groups. There exist many tensile studies on the macro-scale level of tendons or bones and also on smaller levels like osteons or fibers.[11]
Mathematical models created on the basis of these experiments show a lack of knowledge of the stress-strain relations of the substructures of these hierarchical assembled tissues.

For this reason it is important to perform mechanical tests on the substructures of collagen fibres, the single collagen fibrils. Until now only a few research groups engaged with tensile tests on the fibrillar level. There are three methods developed to perform these tests, they differ in the used device:

1. Microelectromechanical systems (MEMS) liu2015
2. Micro-manipulators [26]
3. Atomic force microscope [27, 28, 29, 30, 31, 24, 32, 33]

Microelectromechanical systems have been costumized to performe tensile tests on individual collagen fibrils. Each MEMS can be understood as a micro tensile testing instrument where a fibril is glued on and the displacement is obtained via piezoelectric transducers [33]. Through deformations within the MEMS the exerted force of the fibril is measured. These MEMS devices consist of silicon or silicon nitride and are manufactured by etching or via photo-lithography. Measurements in air as well as in hydrated state were performed.
The second method works with micro-manipulators. During this method both ends of the hydrated collagen fibril are coiled around micro-needles. For the tensile test one micro-needle then displaces and stretches the fibril. The exerted force of the collagen fibril during elongation is measured via the deflection of the steady micro-needle[26].
The last method uses the AFM for the stress-strain measurements of the individual fibrils. Since the AFM is able to measure the force and the displacement at the same time this device fits the purpose of tensile tests. During the AFM method one end of the fibril is attached to a surface and the other end is attached to the cantilever.

By moving the cantilever upwards the fibril is verticaly aligned, this arrangement is needed to generate uniaxial forces in the longitudinal direction. The cantilever is then driven away from the surface pulling the collagen fibril . Through the deflection of the cantilever the developing force is recorded. The displacement of the fibril can be calculated by subtracting the deflection of the cantilever from the piezo position in z-direction[27, 30]. Recent studies at the Institute of Lightweight Design and Structural Biomechanics of the TU Vienna engaged with this AFM method. During past studies only measurements in the low strain ranges have been performed. Generally this method is very time consuming. One goal of this thesis is to optimize the sample preparation previous to the tensile test. Further the method has to be improved, as for now only

tensile tests with small fibril elongations have been performed and the other goal of this thesis is to perform fracture tests.

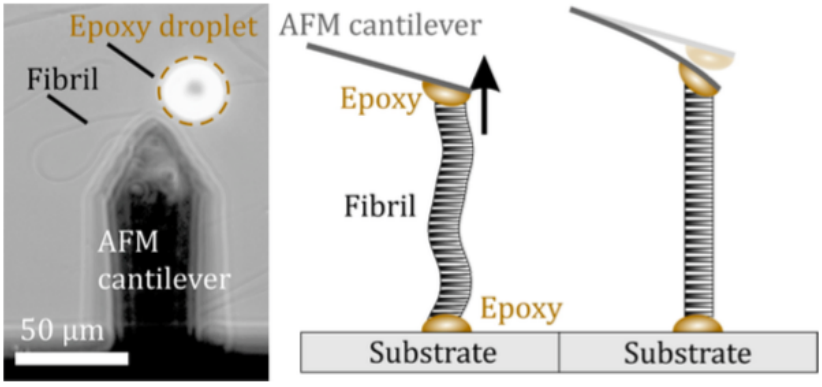

Figure 17: Tensile test setup of the AFM method [30]

3.5 Indentation Test

The AFM allows to measure the force and displacement acting on the cantilever tip at the same time. Through this feature different tests can be performed, also indentation tests on the micro-meter down to the nano-meter level . Since the radial mechanical properties of fibrils are of interest, the indentation test is a very useful tool which provides information about these properties[55].
Although, the radial elastic modulus does not reflect the physiological loading of fibrils, it presents a fast method to generate a comparable mechanical property of individual collagen fibrils. Further the radial elastic modulus may expose the degree of cross-linking in collagen fibrils. The basic principal of an macroscopic indentation test is to analyse the imprint which is created by a defined geometrical tip pressed with a predefined force into the material surface. The size of the residual imprint is measured and information about the material properties are obtained. Depending on the geometrical shape of the tip the method has different names, for example if the tip is spheric the test is called Brinell's hardness test.
Since the diameter of the fibril is in the nano-meter range, the imprint of the cantilever can not be optically determined as the resolution of the optical microscope is limited by the wavelength. Further the collagen fibril is a viscoelastic material and the indentation depth is in the elastic region of the material, therefore no indention imprint will be present.
For this reason the material properties are measured from the load vs indentation data which is generated during force-mapping of the hydrated collagen fibrils in PBS. To de-

fine the radial elastic modulus from force-maps the projected contact area A_c of the cantilever tip is needed[56]. Through the calibration of the cantilever and the evaluation of the spring constant the raw deflection vs z-piezo height data from the AFM is transformed into force vs indentation curves. The indentation-depth is calculated by subtracting the cantilever deflection from the measured z-piezo height. Two methods exist which evaluate the mechanical properties from the indentation data the Hertz [57] and the Oliver-Pharr method [58].
During the Hertz method the material is assumed to show ideal elastic deformation, therefore the loading or unloading part of the indentation curve is fitted with the Hertzian model, the fitting parameter is the elastic modulus of the material[57].
The second method for analysing the indentation curve was developed by Oliver and Pharr. Different to Hertzian method Oliver and Pharr do not assume ideal elastic behaviour along the whole loading and unloading curve of the material. For this reason Oliver and Pharr only examined the upper third of the unloading data [58]. When indentation tests on elasto-plastic material, such as collagen fibrils, are performed, then the unloading curve represents the elastic response of the material [59]. By combining this data with data of the indentation tip, the contact area at contact depth is obtained. This information leads to the elastic modulus of the observed structure [58]. The information about the tip shape is calibration grating equipped with sharp cones is imaged in contact mode. The obtained image is analysed and the projected contact area (A_c) of the tip can be defined.

4 Mechanical Aspects of Biological Tissues

4.1 Viscoelastic Behavior

The mechanical behaviour of materials is characterized by the relation between the stress σ and strain ϵ during external loading. The ratio between stress and strain is called Young's modulus E and is definded by

$$\sigma = E\epsilon \tag{7}$$

The Young's modulus describes the elasticity of elastic solid material. Depending on the material this relation can be linear or E can be a function of the strain. In generell three different behaviours are defined:

1. Elastic behaviour is defined by the stress/strain slope being the same for loading

and unloading

2. Plastic behaviour appears when the material deforms during loading, leading to permanent changes of the original shape.

3. Viscoelastic behaviour is described by a time dependency of the stress and strain. Further different stress/strain slope occur during loading and unloading. Viscoelastic materials return slower to there original shape, this slope is also called hysteresis loop.

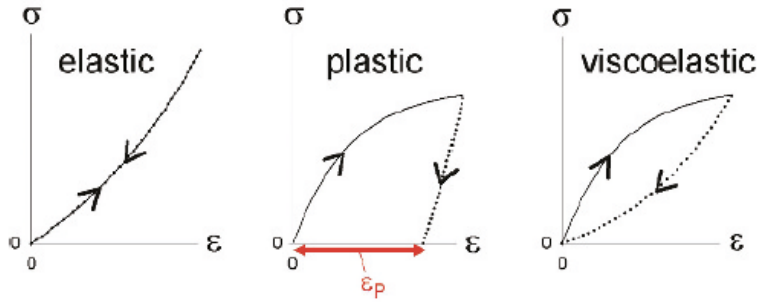

Figure 18: Stress-strain slope showing the three different material behaviours [15]

The viscoelastic behaviour is the most abundant behaviour in biological tissues including collagen. Within tissues fluids play a very important role, the interaction between the extracellular fluids and the structures of connective tissues are one reason for their mechanical viscoelastic behaviour. The fluid flows in and out of the structures during the external loading. Since the uptake of the fluid back in the structures takes time the unloading curve differs from the loading. Another reason for the viscoelastic behaviour, for example in tendon, is the interfibrillar sliding within the tissue network.[15, p. 148] A simple model to describe this behaviour is the Kelvin-Voigt model. The Kelvin-Voigt model consist of a dashpot or viscous element, which describes the fluid friction or fibril sliding and a parallel acting elastic spring. Since a dashpot is involved in the equation the material behaviour is time dependent.

$$\sigma = E\epsilon + \eta\dot{\epsilon} \tag{8}$$

When a viscoelastic material is stretched and the strain is maintained at the same level the stress within the material decreases, which is called stress relaxation. The counterpart to this behaviour is called creep, this phenomena appears when the stress is kept constant and the body continues to deform. The fact that the behaviour is time dependent results in an influence of the loading speed on the measured stress-strain curves. With other

words the strain rate (strain/time) influences the material behaviour. For ligaments, which are very similar to tendons, it has been shown that higher strain rates result in increased [60].

We examined the viscoelastic behaviour of individual collagen fibrils by loading fibrils at different strain rates. At the level of single collagen fibrils the elastic spring reflects the stretching of the helical structures within the molecule. However there might be more factors which create the viscous behaviour at the fibril level, but the mechanism are not fully understood. One factor could be the water flow during streching. Intermolecular sliding, molecular aligning and straightening of the collagen molecules within the fibril could be further factors. To study the viscoelastic behaviour of single collagen fibrils, a creep or stress relaxation test would be ideal. Unfortunately, the used setup is unable to perform such measurements. Due to the fact that the force cannot be maintained constant while the displacement is changed or vice versa, as these two parameters are linked together via the deflection of the cantilever.

5 Material and Methods

5.1 Sample preparation

To obtain information about the mechanical properties of collagen-fibrils with osteogenesis imperfecta, a mouse model was chosen. As described earlier in section 2.5 the OIM mouse model has a well defined genetic mutation. The aims of this thesis was to gain information about the mechanical properties collagen fibrils from OIM mice. To achieve this goal mouse-tail tendons (MTT's) from 5 month old female mice were used. Tendons from wild type (WT) mice and from mice with osteogenisis imperfecta (OIM) were examined. T The extraction of single fibrils from the mice-tail is performed in the following manner:

1. The skin of the mouse-tail is cut open lengthwise with a scalpel, then a tendon is taken out of the tail with tweezers
2. The tendon is placed on poly-l-lysine coated glass slides (Polysine^{TM} Microscope Adhesion Slides, Thermo Fisher, United States of America). These glass slides show a higher adhesion for collagen fibrils in hydrated state which simplifies the extraction process. Under the use of a stereomicroscope (SZX10, Olympus, Japan) the tendon is split up into the fascicles and further into fibre bundles. This is done manually with the use of two sharp tweezers or scalpels.
3. The fibre bundles are further observed with a light microscope (Imager.Z1m, Zeiss, Germany) and separated into single collagen fibrils.
4. The glass slide is rinsed with deionized water.
5. The sample is air-dried and stored.

During all the preparation steps the tendon is in a hydrated state, the hydration is assured by rinsing the sample with deionized water.

5.2 Imaging collagen fibrils in air

The diameter of individual collagen fibrils is in the range of 10-300 nm, this leads to a challenge for observing the structure with light microscopes. In light microscopy the resolution is limited to a value, which is defined by the wave length of the observing light

and by the numerical aperture of the objective.
The resolution limit is described via the following formula [61]:

$$\Delta d = 0.61 \frac{\lambda}{n \sin \alpha} = 0.61 \frac{\lambda}{NA} \tag{9}$$

n ... refractive index of the medium between cover slip and objective
α ... half angular aperture of the objective
λ ... The wavelength of the observing light
NA ... Numerical aperture of the objective
Δd ... smallest resolvable distance between two objects
By using a microscope where the observing light is produced by an halogen lamp with wavelengths in the visible light spectrum, it is clear that the structures of individual collagen fibrils cannot be observed(maximum resolution of 200 nm). This leads to the conclusion that single fibrils cannot be verified by a light microscope and further also diameters of these fibrils cannot be determined. Nevertheless fibres and fibril bundles can be observed. However, it is impossible to determine if the observed structure resembles a individual fibril or more aggregated fibrils.
For this reason a different method must be used to determine individual collagen fibrils. Atomic force microscopes (AFM) can resolve structure in the range of individual collagen fibrils and below. The used AFM within this study is an Nanowizard Ultra Speed (JPK, Germany), the setup is combined with an inverted optical microscope (Observer. D1, Zeiss, Germany). With the AFM images of the air dried collagen fibrils where obtained in contact mode as shown in Fig. 19.

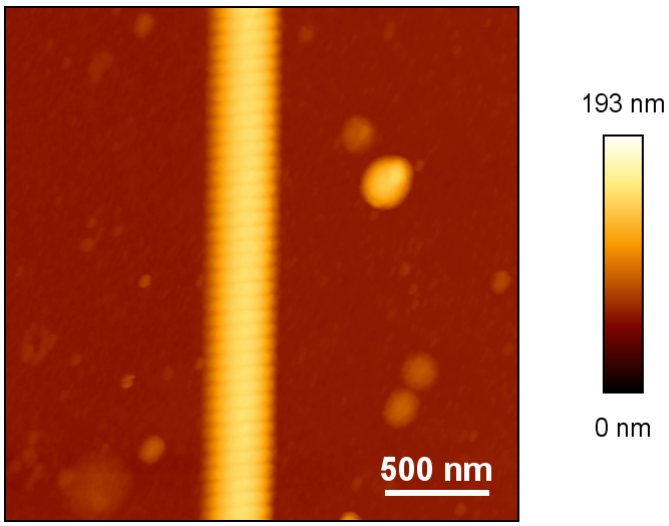

Figure 19: Image of an individual OIM collagen fibril in air

AFM imaging was conducted with the Pyrex Nitride Probe-Diving Board cantilever (PNP-DB, Nano World Innovative Technologies) equipped with a pyramidal tip and with a nominal spring constant of $k_{nom} = 0.48N/m$. The dimension of the recorded images are 2.5x2.5 μm with a resolution of 512x512 pixels and 1 Hz scanning rate. The contact-mode image determines if the observed fibril is an individual fibril and further the diameter of the individual fibril. To evaluate the diameter the raw images of the AFM are further processed, this is explained in greater detail in section 6.

5.3 Imaging and Indentation test in PBS

To create similar properties as within the organisms the fibrils are immersed in phosphate-buffered saline (PBS, 10mM, 7.4pH). The sample was immersed in PBS and the measurements where taken after 45 minutes. This time is needed for water uptake within the fibril and for the sample to reach a thermal equilibrium. Due the different collagen type I molecules in OIM and WT it is assumed that the water uptake within the fibril structure is different. This difference could originate from the tighter packing of collagen molecules within the WT fibrils [34]. By determining the swelling of the fibrils, the water uptake can be quantified. Therefore it is necessary to evaluate the diameter of the fibril in hydrated as well as in dried state.

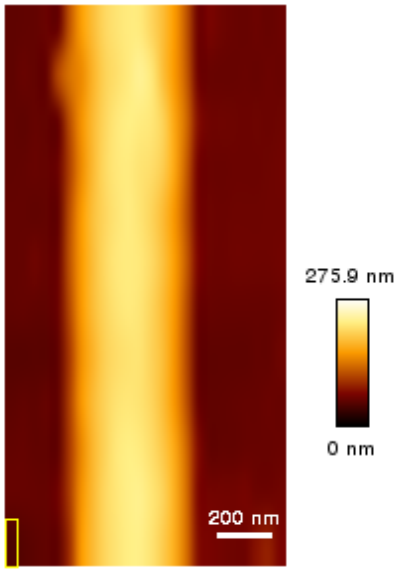

Figure 20: Force-map of a hydrated fibril immersed in PBS. the yellow box on the left side resembles one force spectroscopy

However, contact-mode imaging in liquid creates artefacts that make it difficult to measure the fibril diameter. To minimize the error within the image and to create force maps of the fibrils, force-mapping is used. Force-mapping is a method where the observed area is divided into pixels and in each pixel the tip performs a force curve, loading the sample to a certain force-threshold. In our case the threshold was set to 1 nN. The contact point of the force curve thereby determines the height of the fibril without artefacts. To create an exact correlation between the deformation of the cantilever and the recorded change on the detection system the cantilever needs to be calibrated described in section 3.1.4. AFM imaging in PBS was conducted with the same (see section 5.2) Pyrex Nitride Probe-Diving Board cantilevers (PNP-DB, Nano World Innovative Technologies) equipped with a pyramidal tip and with a nominal spring con-

stant of $k_{nom} = 0.48N/m$ which where used for the imaging in air. The force-map was adjusted to each fibril individual according to the dimensions and under the following guidelines:

- Pixel ratio of 4x1 pixels
- Minimum quantity of 10 pixels across the the fibril for each slow-scanning line
- Minimum of 2 pixels on the glass slide on each side of the fibril

This requirements are essential to obtain correct values of the fibril height when analysed in see Section 6. Within the obtained force-maps information on the mechanical properties of the fibrils is contained. While recording the force-map the cantilever tip performs an indentation test on the fibril. By analysing this data the radial elastic modulus of the fibril is generated. This process is described in section 6.5. Again, for this measuremnts the cantilever needs to be calibrated as described in section 3.1.4. As described there a correction factor is needed for the thermal noise calibration of the cantilever. As the first peak of the resonance frequency was used this value was set to $\beta = 0.817$ according to [51]. Further the exact shape of the tip must be known to analyse the indentation curves, for this reason a tip reconstruction is performed.

5.3.1 Measurement of the 3 dimensional tip shape

An AFM image is always a convolution of the topography of the sample and shape of the tip as can be seen in figure 10. This phenomenon can be used to get information about the real shape of the tip. By scanning a known reference surface the shape of the tip can be separated from the topography. Or thinking one step further, if the surface consists only of very sharp edges or peaks, then the produced image is an envelope image of the reference peaks and the AFM tip[63]. The shape of AFM tip is then obtained by applying an reconstruction algorithm as proposed by Keller et. al.[62]. Such surfaces are called "calibration gratings" and are commercially available, during this studies the TGT1 grating (NT-DMT Spectrum Instruments) was used.

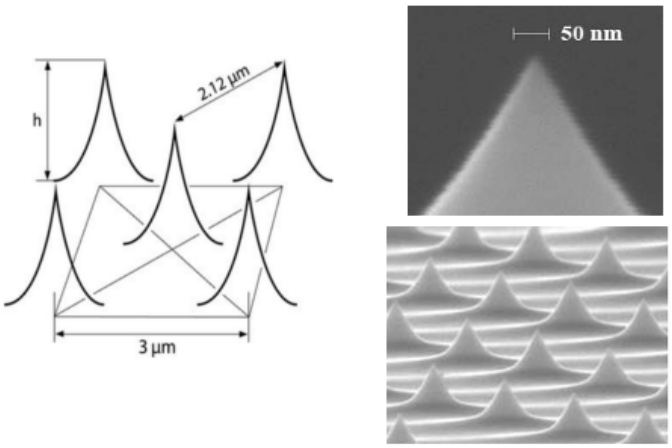

Figure 22: Image showing the TGT1 surface, courtesy Dr.John Mamin, IBM Research Division

The height of the peaks varies from 0.3 to 0.5 μm. The calibration image was obtained by approaching to the surface and creating an overview image of 5x5μm. In the next step one peak was selected and a detailed image in contact mode of the dimension 1.5x1.5μm was recorded. With the AFM imaging parameters set to 512x512 pixels and a line rate between 0.5 and 1.5 Hz. It is very important to use a low setpoint while imaging otherwise the tip or the calibration grating can be damaged. Further the P- and I-gain where optimized to create the best output. The generate images where further analysed according to [63], this process is described in section 6.5.

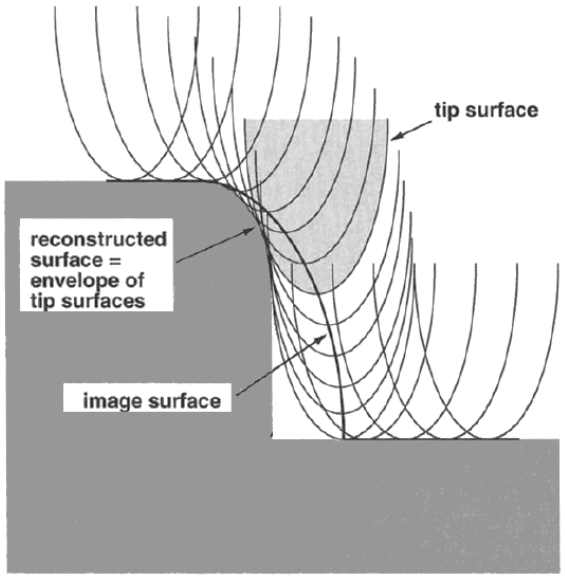

Figure 21: Example for the convolution of the topography and tip shape within an AFM contact-mode image adapted from [62]

5.4 Micro-manipulator

One aim of this thesis was to speed up the sample preparation process for nano tensile tests performed with the AFM. For the individual tensile tests, the fibril is fixed to the glass slide on one side and the other side is attached to the cantilever. To obtain this arrangement a device to manipulate the fibrils and further to glue them to the glass slide is needed. As the diameter of fibrils is in the range of 50- 300 nm a precise device with a tip in the sub micrometer range is required. When samples this magnitude are mechanically manipulated the simplest and best fitting shape is a needle tip. For this reason a needle tip with a tip radius of 0.6 μm was used.(see Section 5.4.1)
To operate this tip a mechanical device was designed. For positioning the tip and to move the fibrils on the glass slide a three dimensional movement is required. The movements where achieved with two manual stages. The stages where obtained from an TopViewOptics^{TM} (JPK, Germany) device. This topview setup included a post where the stage for the movement in the vertical direction is positioned. On this vertical stage a 90 degree mounting plate is fixed to connect the vertical stage with a 2-axis stage for the horizontal plane. In the original setup of the TopViewOptics^{TM} this 90 degree mounting plate is mounted in a way that the 2-axis stages is attached on top. For our purpose we removed the optical system and used only the mechanical stages. The directions of these mechanical stages then where changed, the 90 degree mounting plate was turned by 180 degrees and the 2-axis stage was mounted from below, as can be seen in fig. 23. This step was needed for a better access of the micro-manipulator tip to the glass slide.

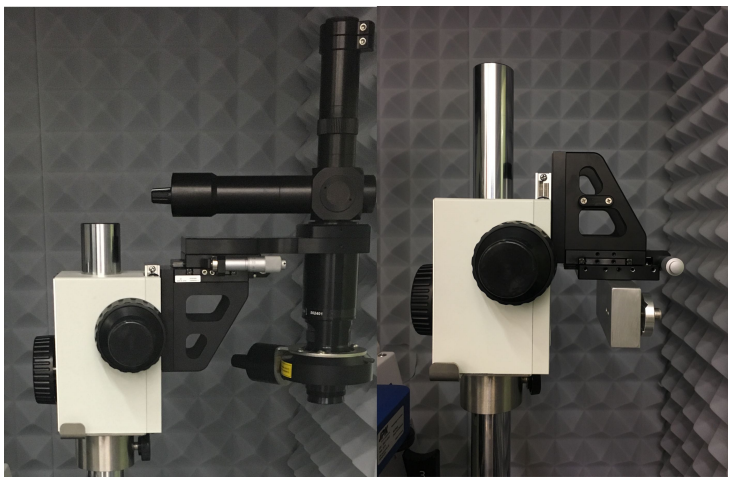

Figure 23: Adaptation of the stages from the TopViewOptics^{TM} by JPK

The setup of the stages allows a manually controlled movement in the horizontal plane and in the vertical axis. The needles were fixed in a probe holder (Micro-Tec PV5 long probe

holder, Micro to Nano, Netherlands) for round diameters in the range of 0.1-0.65mm. For the fixation of the probe holder onto the 2-axis stage no commercial product was available. This circumstance led to a self manufactured adapter between the 2-axis stage and the probe holder. The dimensions of these manufactured device where defined by the setup of the microscope.Fig. 24 shows the used micro-manipulator setup. For further details on the micromanipulator setup see [64].

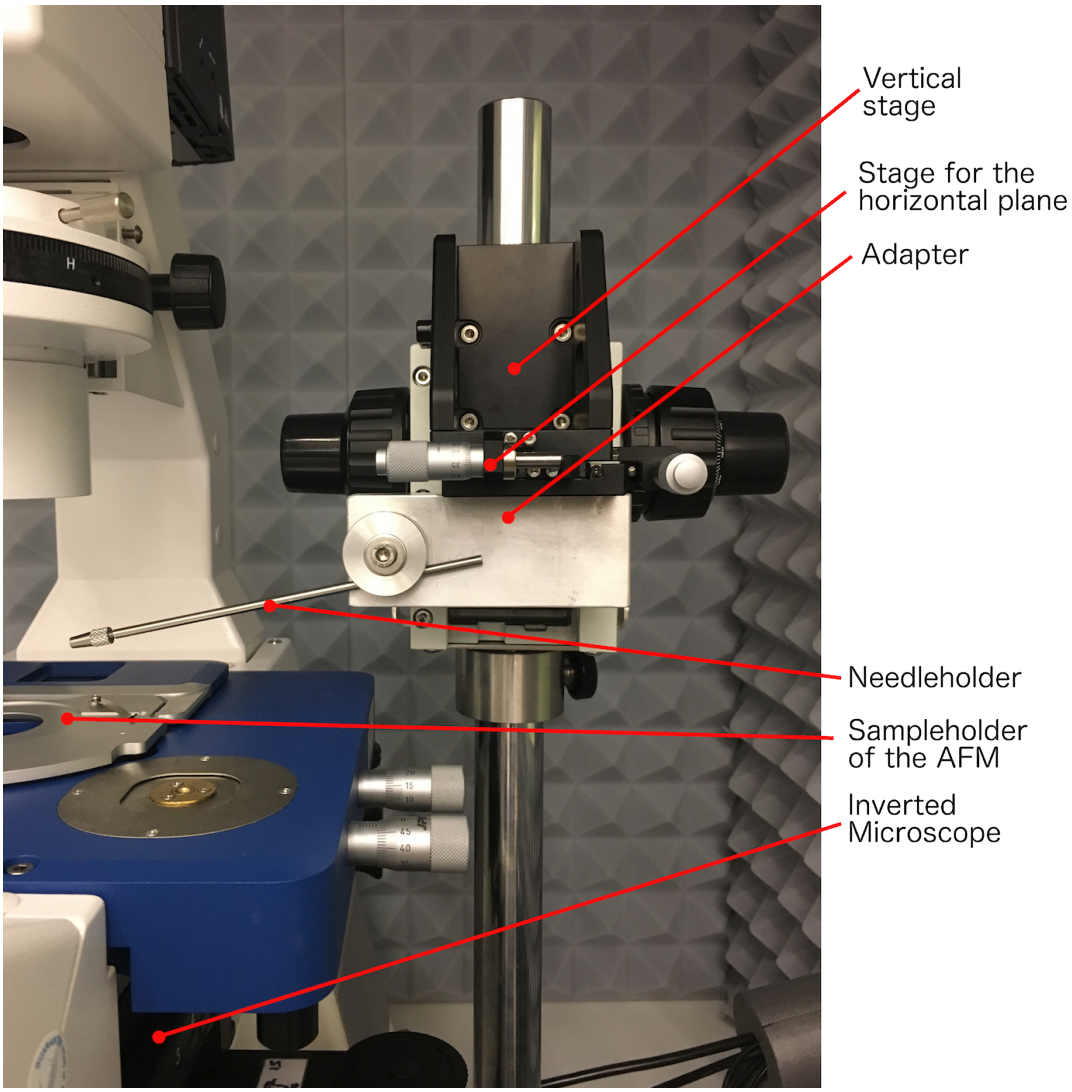

Figure 24: Micromanipulator-setup

5.4.1 Tips of the micro-manipulator

To generate the tensile test setting two types of tungsten needle tips are used, both needles derive from the same type of needle (Micro-Tec T5 straight ultra-fine tungsten needle probe $\varnothing$0.52 mm with 0.6μm tip-radius, 25 mm long, Micro to Nano, Netherlands)

:

1. very fine tungsten needle manually bend to an angle of 90 degrees
2. straight very fine tungsten needle

The first needle is used during the attachment of the collagen fibrils to the glass slide which is described in section 5.6 and the second straight needle is used for the detachment of the epoxy droplet in section 5.9.

5.5 Preparation of single fibrils for tensile tests

To achieve the setting where the tensile test can be performed a protocol for the sample preparation is executed. During sample preparation the individual collagen fibrils are placed on poly-l-lysine coated glass slides (see section5.1). The poly-l-lysine coating leads to adhesion of the individual fibrils to the glass slide. For tensile testing the adhesion is not strong enough and therefore the individual fibrils need to be attached to the glass slide with epoxy resin. Therefore a preparation protocol is performed. This protocol consists of seven steps and is described in the following:

1. Attachment of individual collagen fibrils to a glass substrate via epoxy resin.
2. Verification of single collagen fibril by AFM imaging.
3. Length measurement of the verified individual collagen fibril with an optical microscope.
4. Performing the imaging process in PBS.
5. Detachment of one epoxy droplet in PBS.
6. Loosening of the detached droplet in air.
7. Attachment of the tipless cantilever to the detached epoxy droplet by epoxy resin.

In step 1 the fibril is attached to the glass slide by two epoxy resin micro-droplets. The distance between these two droplets determines the non-deformed length of the fibril before the tensile test. After the length measurement the sample is immersed in PBS and the force-map measurements are performed as described in section 5.3. However, for

the tensile test one side of the fibril needs to be attached to the cantilever to perform the elongation of the fibril. For this reason one of the two micro-droplets is detached in PBS in step 5. This detached droplet is then fixed to the tip-less cantilever. Thereby the connection between one side of the fibril and the cantilever is obtained.
The step of attaching both ends of the fibril to the glass slide and then detaching one droplet must be performed. Otherwise, if the cantilever would be glued directly onto the fibril, epoxy would connect the cantilever with the glass slide. By an upward movement of the cantilever the adhesion between the cantilever and the glass slide would be stronger than the mechanical properties of the cantilever. This would lead to fracture of the cantilever upon retraction. To avoid this the intermediate step of attaching and then detaching one epoxy droplet is needed. In this case the epoxy layer prevents the cantilever from being glued onto the glass slide.
However, the cantilever can only be attached to the detached droplet when the sample is dried. During evaporation of the water the detached droplet attaches again to the glass slide. For this reason the droplet is detached once more in air, before the cantilever is glued on top of it.
In the following section the steps and device used to perform this protocol are described in detail.

5.6 Attachment of individual collagen fibrils to a glass substrate via epoxy resin

The prepared air-dried glass slides loaded with collagen fibrils is observed with an inverted optical microscope (Observer D.1, Zeiss, Germany) under 100x magnification. As mentioned in section 5.2 collagen fibrils can be visualized with a light microscope. However, it cannot be stated if the observed fibril is a single fibril or if two fibrils are aggregated, for this reason step two is necessary.
The attachment of the collagen fibrils is performed under the use of the micro-manipulator, which is described in section 5.4. The fixation of single collagen fibrils to the glass slide was achieved by placing drops of epoxy resin onto the fibrils. The used adhesive is a two component epoxy resin (UHU plus endfest 2-K-Epoxidharzkleber, UHU, Germany). This resin was selected by its processing behaviour and the stiff material properties when hardened.
A special protocol has to be followed to create droplets in the size of 10μm to 30μm :

1. Mixing the two components in a ratio of 1:1 of the epoxy resin for 5 minutes
2. Placing a barely seeable droplet of epoxy on the glass slide via a glass-fibre

3. Tipping the needle of the micro-manipulator fully into the glass-fibre placed droplet and leaving the needle for 5 min.
4. Retract the needle from the droplet
5. Immerse only the apex of the needle into the droplet
6. The apex is then retracted slowly from the epoxy resin
7. The tip is now loaded for one glueing procedure

The stage of the microscope then moves to the single collagen fibril and the glueing procedure is done via the movement of the micro-manipulator. One fibril is attached to the glass slide with two droplets, with a distance of 50-200 μm in between the droplets.

5.7 Verification of prepared individual collagen fibril by AFM imaging

As mentioned in section 2.2 the diameter of individual collagen fibrils is in the range of 40 to 300 nm. Observations with light microscopes cannot determined if the observed structure is an individual fibril or if it is a bulk of fibrils aggregated together. Through AFM imaging the individual collagen fibrils can be visualized and it can be verified if the observed structure is an individual fibril. This verification imaging process is performed in air and the obtained images are recorded in contact mode, according to the process of imaging in air described in section 5.2.

5.8 Length measurement of the verified individual collagen fibril by an optical microscope

One goal of this thesis is to obtain the stress-strain curves via tensile testing. The stress and strain are material properties independent of the sample geometry. To derive the stresses and strains experienced by the observed fibril, two geometrical sample parameters need to be measured. One parameter is the diameter of the individual collagen fibril , this is needed to calculate the cross sectional area which is essential for the stress. The diameter is obtained via imaging the fibril with the AFM and further analysis(see 6.1). The second necessary parameter is the original length of the fibril before tensile testing. This length is required to calculate the strain, since the strain compares the stretched length to the original length.

For the length measurement the sample was observed with the Imager.Z1m (Zeiss,Germany) microscope. Under use of the software provided by Zeiss the length of the fibril can be evaluated, by a measuring option within the analysing software. The measurements were taken by a 10x magnification objective in air.

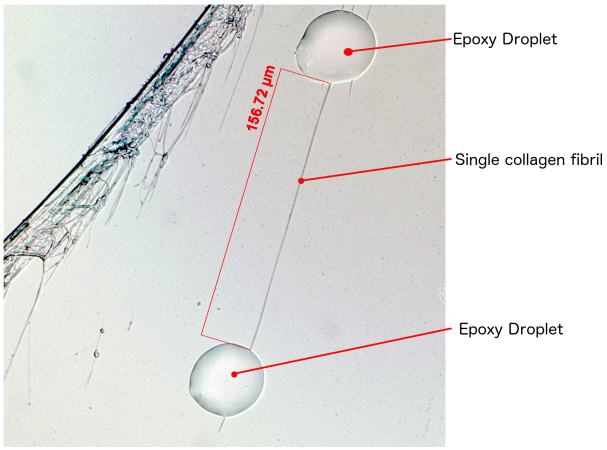

Figure 25: Measurement of the original length of the collagen fibrils before the tensile test

5.9 Detaching the epoxy droplet in PBS

After the length measurement of the fibrils and before the detachment process, force-maps of the collagen fibrils are produced, these measurement were performed as described in section 5.3.

Both steps, the force-map and the detachment process, require immersion of the sample in PBS. The epoxy droplet was separated from the glass slide by the use of the micro-manipulator. The micro-manipulator is equipped with the straight very fine tungsten needle (see 5.4.1). The goal is to detach the epoxy droplet without tearing the droplet apart. Different trials showed that the process of detachment produces the better results when performed in PBS and not in air.

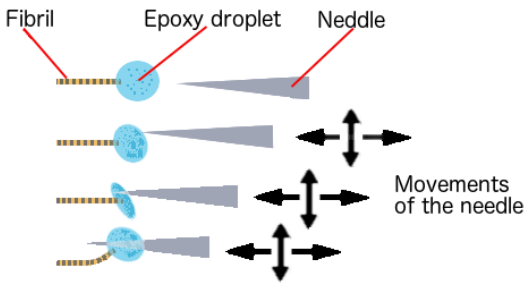

Figure 26: Guidance for detaching the epoxy droplet attached to the fibril

Figure 26 shows the process of detachment. The blue dot represents the epoxy droplet, the brown/yellow "wire" represents the collagen fibril and the grey area shows the needle tip. In the figure, the black arrows represent the movements of the needle, which are

performed with the manual stages of the micro-manipulator. During the detachment process the needle moves horizontal forward and backward and after some movements the vertical position is lowered. The movements from top to bottom are performed for several times. For each top to bottom movement the tip is moved further to the left. With each movement to the left the tip goes further underneath the droplet until the peal off of the droplet can be performed. During the last part of the detachment care has to be taken to avoid applying tension to the fibril via the needle apex. This tension can result in a flicking off of the droplet and thereby potentially fracturing the fibril. After the detachment of the epoxy droplet the sample is rinsed with deionized water to prevent crystallization of the PBS during evaporation.

5.10 Loosening of the detached droplet in air

Tests showed that when detaching the droplet only in air, without previous detachment in PBS, the droplet either tears apart or curls up. This deformation of the droplet aggravates the step of attaching the cantilever or may even render the sample unusable. For this reason the primary detachment of the droplet is performed in PBS. However, to attach the cantilever to the detached droplet dry conditions are necessary, otherwise the resin cannot establish a proper connection of the items.
During drying, the water evaporates and adhesion between the detached droplet and the glass slide emerges. Before attaching the cantilever to the droplet it is essential to loosen this connection. This step is performed via the micro-manipulator an the same tip as in step 4. Generally only a few taps with the apex of the needle in the direction of the fibril are necessary to break the connection.

5.11 Attachment of the Cantilever

The final process before the execution of the tensile test is the attachment of the cantilever onto the detached droplet. For the tensile test a gold coated tipless cantilever (TL-NCH-AuD, Nano and More GMBH, Germany) with a nominal spring constant of 42 N/m was used. The adhesion is again achieved with the same two component epoxy resin used in step 1 (UHU plus endfest 2-K-Epoxidharzkleber, UHU, Germany). The two components are mixed together and the resin is transferred to the glass slide loaded with the fibrils. To achieve the transfer of a small quantity of resin a fibreglass rod is used. This creates a "micro-drop" (diameter of approximately 0.5 mm) which is deposited aside the prepared

fibril in a distance of 1-2 mm, to not interfere with the tensile experiment.
In the next step, the cantilever is moved to the edge of the micro-drop and the apex of the cantilever is approached on the edge of the epoxy. To reduce the amount of resin present on the cantilever an approach with a setpoint of 0.3 [V] to the glass slide and a retraction afterwards is performed. After retracting the cantilever from the glass slide the size of the produced droplet can be observed with the inverted microscope. Depending on the amount of resin absorbed from the micro-drop, the size of the droplet varies. If too much resin was absorbed another approach need to be performed to reduce the epoxy on the cantilever front-end. The final diameter of the droplet produced on the glass slide via approaching should be the half of the diameter of the detached droplet. When this size is achieved the cantilever is ready to be attached to the detached droplet.
The tip loaded with the resin is positioned exactly onto the loosened droplet. It is important that no resin overflows the loosened droplet. This could result in attachment of the cantilever to the substrate. For the glueing of the cantilever to the droplet a setpoint of 0.8-1.2 V was used, this was increased by 0.2 V after half an hour past glueing. The cantilever is kept for 12 hours in the approached position. After this time the hardening of the epoxy is assured and the cantilever is attached to the droplet. The setup for the tensile test is now ready, with one end of the fibril attached to the glass slide and the other end attached to the cantilever.

5.12 Process of tensile testing

When hardening of the epoxy resin is finished after 12 hours the sample is immersed in PBS. To obtain a thermal equilibrium and to permit fluid uptake within the fibril, the sample is rested for 45 minutes. The lift off of the cantilever is performed after this time. First, the setpoint of the AFM is decreased to zero then the stage is moved carefully perpendicular to the longitudinal axis of the observed fibril. Second, a movement of the droplet and the attached cantilever is recognized through the inverted microscope. This states that the detached droplet is attached to the cantilever and the fibril is ready to lift up from the substrate. However, the AFM is designed for movements towards the sample surface. Thereby the apparatus and JPK software has an issue with retraction of the cantilever from the surface. The standard operation for retraction includes the full contraction of the z-piezo independent of the in-put value of distance. This means even when an elevation of 1 μm is the in-put value the piezo contracts first by 6 μm and then the stepper motor moves 1μm. This can lead to a detachment of the droplet or premature fracture of the fibril. To bypass this issue, a script for the AFM software was provided by the AFM manufacturer (JPK)(see 11.1 for the script).

The JPK software allows simple programming of complex experiments through the experimental planner. The provided script from JPK initiates specific movements of the stepper-motor without previous retraction of the z-piezo. With a smallest vertical step-size of 0.3 μm. This script was conducted with the experimental planner in the JPK software.

For the tensile test the two epoxy droplets, or more precise the two ends of the fibril, must be aligned horizontally above each other to create uniaxial tensile forces. This alignment process starts with to the third step, the elevation of the cantilever and the individual collagen fibril. With the provided script an elevation of 0.3 μm from the substrate surface is performed. To achieve the horizontal alignment a step wise movement in vertical direction with the provided script and in horizontal direction with microscope stage is performed. Each time the cantilever moves upwards the stage moves in direction to the fibril end attached to the glass slide, as can be seen in figure 27. During the process the movement towards the fixed epoxy droplet is greater than the upward movement which is necessary to avoid pre-stretching of the fibril before tensile testing.

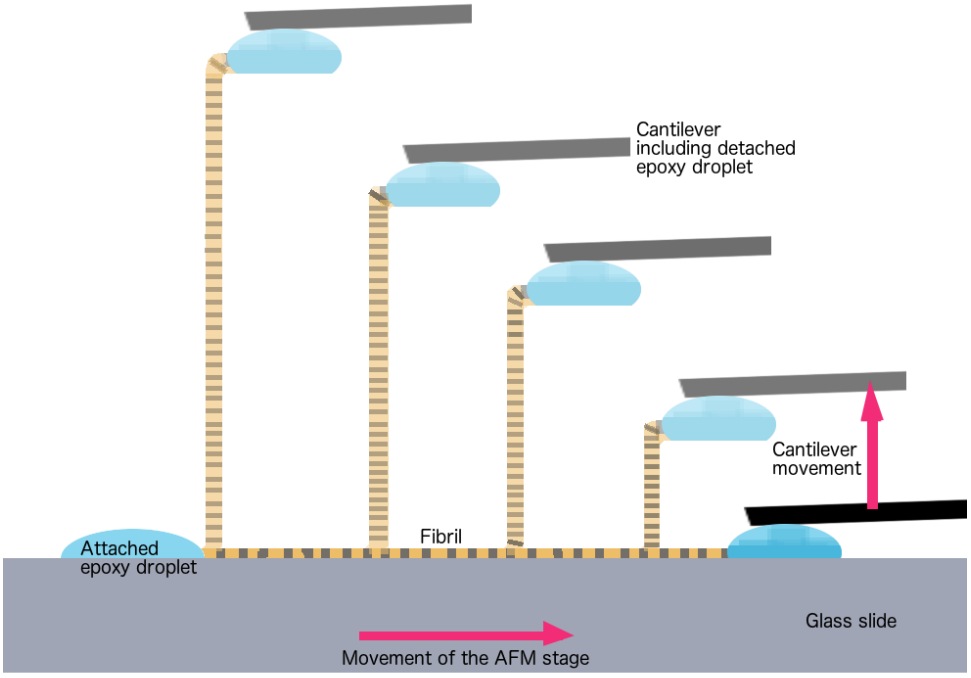

Figure 27: Aligning process of the fibril previous to tensile testing

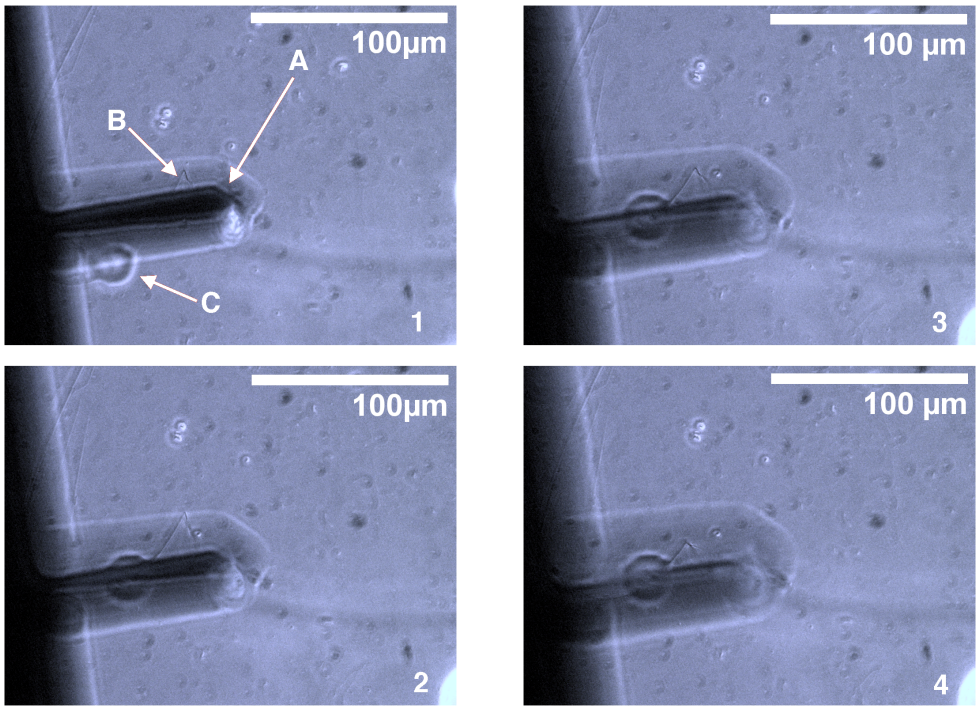

Figure 28: Images of the detaching process. (A) Cantilever tip attached to the detached epoxy droplet and thereby to the fibril (B) Fibril (C) Epoxy droplet fixing the fibril to the glass slide. The height of the cantilever increases from image 1 to 4

The length of the tested fibrils ranges between 50 to 200 μm. It was not possible to focus the inverted microscope on both ends at the same time, if the fibril stands in upright position. To level both fibril ends exactly, a marker tool within the JPK-Software was used. At first, the end attached to the glass slide is focused and marked, in the next step the fibril end on the cantilever is set in focus. Via the AFM-stage, the marked lower fibril end, and the focused upper fibril end are aligned. If the fibril is aligned accordingly only vertical forces act on the fibril during the tensile test.
In the next step the zero strain height of the cantilever is evaluated. Through the measurement within the sample preparation the length of the fibril is known. (Section 5.8) The stepper motor is moved up to a height of the original length minus 10 μm, this movement is performed with steps of 3 μm the vertical step size can be defined in the provided script (see section 11.1). In the proximity of the fibril length the step size are reduced to 0.3 μm and performed until a vertical deflection of -0.1 V of the cantilever is identified.
To assure the vertical alignment and thereby the uniaxial tensile test, the cantilever is moved in the horizontal plane and the deflection is observed. By observing the cantilever deflection while performing the movements the minimum deflection of the cantilever is

found. This position resembles the exact vertical alignment of the fibril. To obtain information about the mechanical properties of the individual collagen fibrils two different tensile test were performed. The first test series were focused on strain-values within the physiological region of fibril elongation. These tests are conducted with different speeds to obtain information about the viscoelastic behaviour of the individual collagen fibrils. After the physiological test the fibril was pulled till fracture.

5.12.1 Physiological tensile tests with different speeds

As mentioned in the chapter 2 in section 2.4.5 the physiological strain-range at the hierarchical level of tendon is up to 8%. The length change possible during one tensile cycle is limited by the z-piezo movement to 5.5 μm. This limits the strain, depending on the length of the fibril. (formula 6.2.1) The tensile test consists of an force curve consisting of two parts: An retraction of the z-piezo by 5.5μm followed by an extension of 5.5 μm. This sequence was implemented with the Force Ramp Designer in the JPK Software.

With the following Force RampDesigner settings:

- Advanced Spectroscopy Control

  Settings preferences: Sample Rate

  Z movement: Constant Speeds

  Settings after spectroscopy stopped: Return to starting mode

- Ramp Settings

  Adjust Baseline: 1

  Z Start Option: Continue from previous

  Height 1μm

  Velocity 2 μm/s

- Retraction-Z

  Z-length 5.5 μm

  Z-speed 1(2, 4, 8, 16, 32) μm/s

- Extend-Z

  Z-length 5.5 μm

  Z-speed 1(2, 4, 8, 16, 32) μm/s

Retraction Z and Extend Z keeps the z-piezo displacement constat to 5.5 μm. The test was performed with 6 different speeds ranging 1,2,4,8,16, 32 μm/s and 12 repetitions per fibril and speed.

5.12.2 Fracture-test

Literature data of individual collagen fibril fracture tests reported that single collagen fibrils fracture at strain levels of 20-50% [33, 27, 30, 26]. The lengths of the observed fibrils were in the range of 50-200 μm, with this value a displacement of the cantilever of up to 100 μm or even more would be needed. However, the range of the z-piezo is limited to 6 μm. The deflection versus height of the cantilever can only be recorded during movements with the z-piezo element and not while movements performed by the stepper-motor. This led to a stepwise fracture test each step consisting of one recorded force curve. Again each force curve existing of two parts an retraction and extend of 5.5 μm via the z-piezo. These force curve was generated with the same ForceRamp Designer settings as described in section 5.12.1 with a Speed of 4μm/s.
After one force curve was recorded a movement/step with the stepper-motor was performed previous to the next spectroscopy. The movement of the stepper motor was set smaller than the distance of the previous elongation. Through this procedure the whole force-displacement curve of the fibril could be recorded due to overlapping regions in the individual force curves.
Procedure of fracture test of individual collagen fibrils:

- Position cantilever at zero strain height
- Record first Force Spectroscopy (ForceRamp Designer settings see section 5.12.1) with 4μm/s
- Perform stepper motor movement through Experimental planner an customized script (see section 5.12)
- Record second Force Spectroscopy
- Perform stepper motor movement through Experimental planner
- Record third Force Spectroscopy
- this steps are further repeated until fracture of the collagen fibril

Since collagen fibrils can resist very high forces stiff cantilevers(TL-NCH-AuD, Nano and More GMBH, Germany see section 5.11) are needed to perform the test. Although the stiffest commercially available cantilevers were used, the deflection reached a level larger then the size of the photo-detector of the AFM. This resulted in an adjustment of the laser beam during the tensile fracture test. The fact that the stepper-motor movement, in between the force spectroscopies, is smaller than the z-piezo movement during force spectroscopy resulted in an overlapping region of the obtained force curves.
Through these regions the force curves were merged together during data analysis. The z-piezo movement was set to 5.5 μm for all fibrils. However, the step size of the stepper-motor in between the measurements were improved during the thesis. Beginning with step size of 4 μm and resulting at a step size of 2.5μm. The step size of 2.5 μm made it easier to merge the force curves and thereby a smoother overall fracture curve was generated. This measurement process allowed the recording of the whole fracture curve including the point of fracture.

6 Data Analysis

The data obtained from the AFM was analysed with costumized Matlab (Version: R2015b) scripts. For analysing the height, from the images taken in air as well as in PBS a programm provided by Dr. Orestis Andriotis (Institute of Lightweight Design and Structural Biomechanics (ILSB), Technical University Vienna) was used. Further the scripts for the indentation test were provided by Dr. Andriotis. The scripts for tensile testing where developed during this thesis.

6.1 Height measurement

From the images obtained in air and PBS the diameter of the fibrils was evaluated. By looking at the raw images of the fibrils it can be seen that the background, the glass slide, is shifted and not levelled. Which is a common artefact in AFM images. For the analyses this error is eliminated and the correct height of the fibril is obtained. During this correction the fibril is masked creating an image consisting of the background, e.g. the glass slide. A linear least-square fit is applied for each row of the masked image. The linear fits are then subtracted from the raw image data per line. Each row of the AFM-image is then analysed for the highest point which resembles the height of the fibril. If errors occured during within the images a median filter is applied to obtain a more homogeneous image. The maximum values of each row are obtained and the median, standard deviation and the standard error are calculated. Figure 29 shows a collagen fibril with the observed maximum point per row and a boxplot of the maximum values.

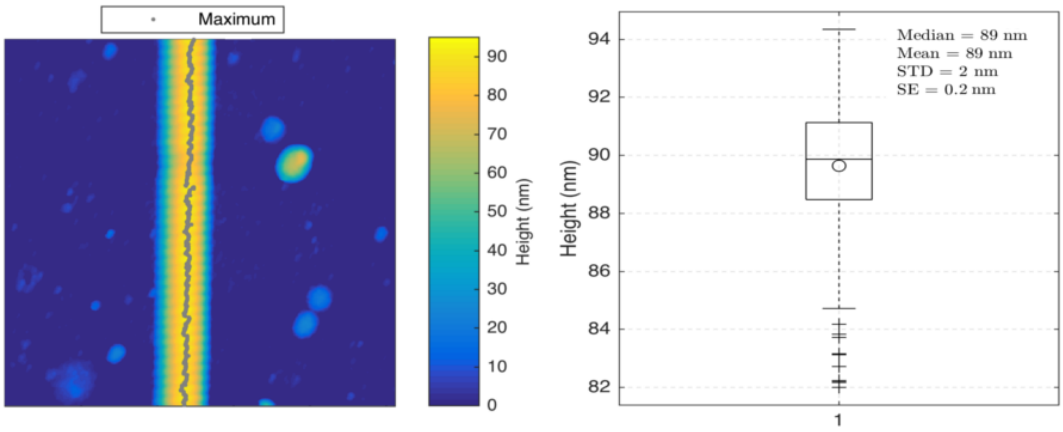

Figure 29: (left) Linewise plane fitted image with maximum points (right) values for the maximum height per raw

The analysis is performed for both images of the fibril, the dried and the hydrated. The

main difference is that the accuracy in the air-image is higher due the fact that more data-lines exist, and thereby more maximum points for the calculation of the diameter are present. The same correction processes were applied to the force-map recorded in PBS resulting in values for the hydrated diameter of the fibril.

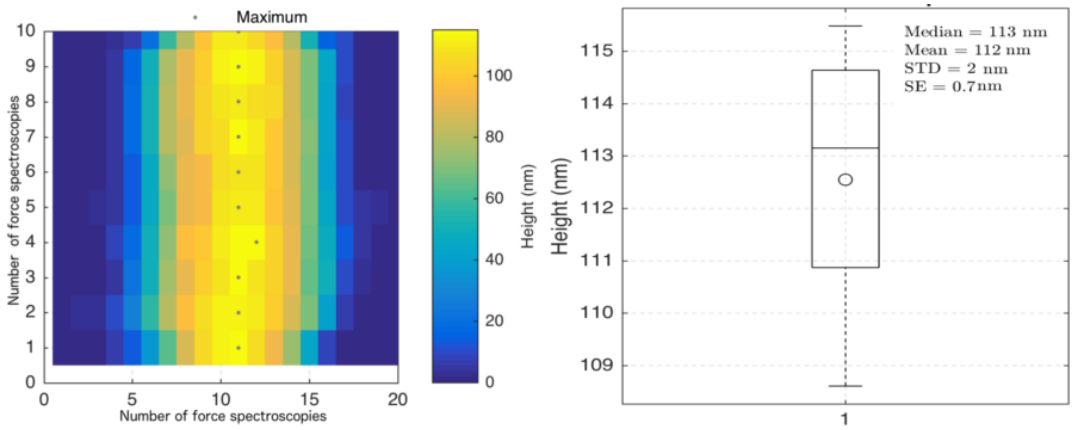

Figure 30: (left) Linewise plane fitted force-map with maximum points (right) values for the maximum height per raw

6.1.1 Swelling

With the two parameters obtained in the previous section, the hydrated and the dried diameter of the fibril, statements about the hydration behaviour can be made. The water uptake within the fibril is of interest for this thesis, therefore the swelling ratio of the fibrils was calculated. During hydration it has been observed that the fibril dillates in radial direction. The fold change in fibril diameter, i.e. the swelling, is calculated with mean fibril diameter gained through the height analysis.

$$Swellingratio = \frac{diameter_{PBS}}{diameter_{air}} \tag{10}$$

6.2 Stress-Strain analysis

The force-spectroscopy data obtained from tensile tests is imported into Matlab. A script is needed to read out the data from the JPK file, since the JPK software saves the data gained during one measurement in one zipped file. This zip-file includes data about the cantilever in general, such as the z-piezo height, the vertical as well as the lateral deflection of the cantilever. The custom script unzips the JPK-file and saves the data within a Matlab structure.

6.2.1 Stress-Strain curve

In the first step, the force-displacement curves are generated from the recorded data. To obtain the force values the vertical deflection of the cantilever is translated into force via the calibrated spring constant. The force and the deflection of the cantilever show a linear relation via the spring constant, k. The spring constant is obtained via previous calibrations as explained in section 3.1.4.
The AFM records two parameters during force spectroscopy measurements. The deflection of the cantilever and the z-piezo height. This two parameters are saved via the previously described script (6.2) in a Matlab structure. However, this data needs to be modified for the analysis. Due to the settings of the AFM the deflection created by the resisting force of the fibril is defined as negative and for this reason the deflection sign is changed. Further the baseline of the recorded deflection-height curves show slight inclines and a baseline offset. This effects are induced by thermal noise or an already existing deflection of the cantilever due to the attached fibril. For this reason two corrections of the data are performed; an angular shift and a displacement of the baseline to zero.
The corrections are implemented by fitting a straight line along the base-line of the recorded data. By manually selecting one point in the beginning of the data-points and a second point before the rise of the curve. A line is fitted between these two points. The fitted line is then subtracted from the recorded data leading to a tilt and offset correction of the data.

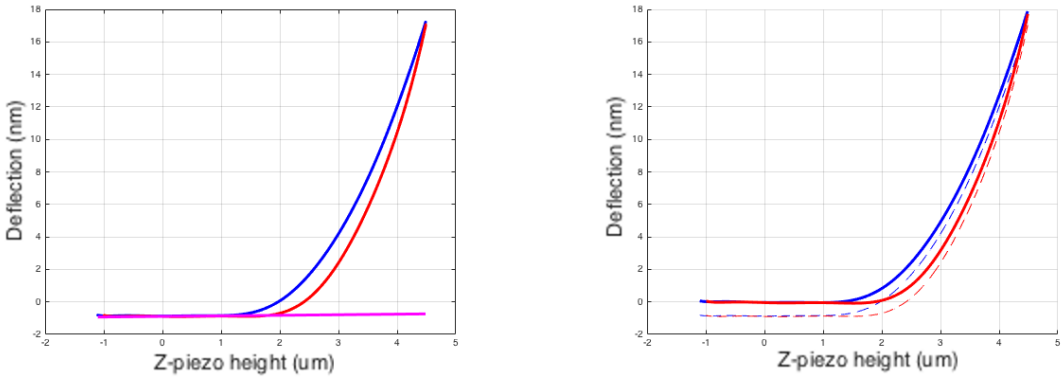

(a) Raw data including the fitted base-line (b) Tilted and off-set corrected data

Figure 31: The blue line resembles the elongation of the fibril and the red line is records the retraction

The starting point of the tensile test needs to be determined. At this point no deflection of the cantilever is present and the length of the fibril corresponds to the original length measured in section 5.8. Past this point the deflection-height curve starts to rise. There-

fore this point is called contact point. After the contact point the fibril starts to elongate and a force is induced. To obtain correct results a horizontal shift of the deflection-height data must be performed, to relocate the contact point to zero.
To obtain the contact point the first derivative of the height, i.e. the slope was observed. The derivative describes the incline of the slope. Since the shown curve consists of data points and is not a function, the difference between each point is analysed.

$$Difference_n = deflection_n - deflection_{n-1} \tag{11}$$

This difference is calculated along the data set. The values show a high noise which made the difference-slope impossible to analyse. However, when looking at the function a kink at the contact point was clearly visible. For this reason a polynomial 10^{th} grade function was fitted into the difference-data. The maximum value of the fitted function resembles the maximum difference between two data-points of the corrected data. The contact point was defined as the point where the value reaches 2% of the maximum value of the function.
The data-point of this value was evaluated and subtracted from the height data. This resulted in an shift of the curve along the x-axis and set the contact-point to zero.

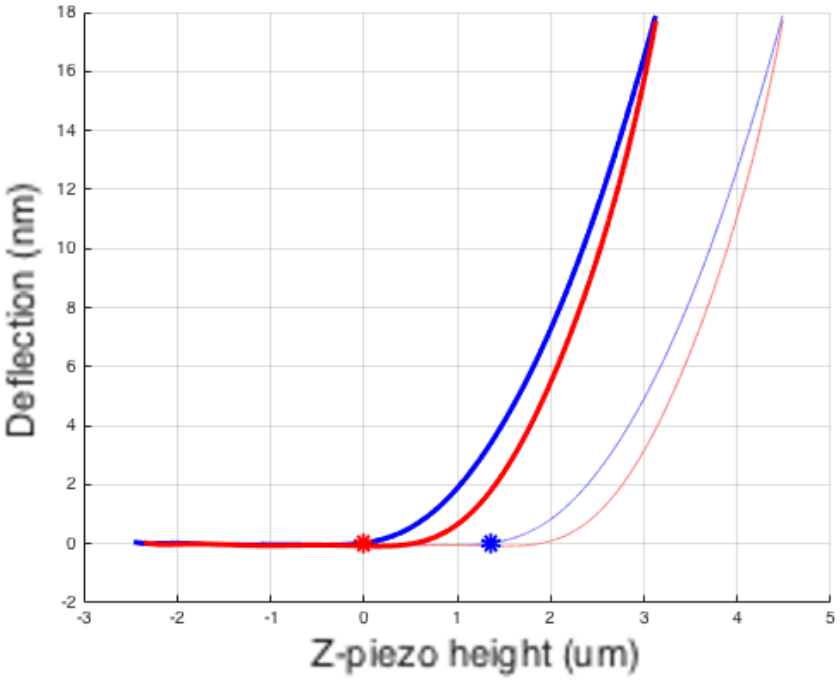

Figure 32: Shift of the deflection-displacment curve according to the contact-point

In the next step, the x-axis is transformed from the piezo height into the fibril displace-

ment, by subtracting the deflection from the z-piezo height. Under the use of Hooke's law and with the spring constant of the cantilever, which is obtained through the calibration process of the cantilever, the deflection is translated into the force. Thereby the force-displacement curve is generated. For a better comparability the force-displacement curve is further translated into stress-strain curves. Whereby stress (σ) and strain(ϵ) are defined in the following manner.

$$\sigma_{eng} = \frac{F}{A} = \frac{F * 4}{\pi * D^2} \tag{12}$$

$$\epsilon_{eng} = \frac{L - L_0}{L} = \frac{\Delta L}{L} \tag{13}$$

$$\epsilon_{GL} = \frac{1}{2}((\frac{L - L_0}{L} + 1)^2 - 1) \tag{14}$$

σ_{eng} ... stress
F ... tensile force
A ... cross-sectional area
D ... fibril diameter in hydrated state
ϵ_{eng} ... Engineering strain
ϵ_{GL} ... Green-Lagrange strain
L ... current length
L_0 ... original length
ΔL length change

The cross-section area of the fibril is calculated using the hydrated diameter observed in PBS and assuming a circular cross-section. The Green-Lagrange strain is applied for large displacements and for this reason ϵ_{GL} is used for the analysis of the fracture curve. However, during the physiological tensile tests the strain of the fibrils is in smaller then 8% and therefore the engineering strain is applied. The original length of the sample is gained in section 5.8 and ΔL resembles the fibril displacement. With these two parameters both strains can be evaluated.

6.2.2 Longitudinal elastic modulus

The relation between the stress and strain resembles the slope of the curve. The value for the incline is denoted as the elastic modulus; which is a material property. The definition of the elastic modulus is :

$$\sigma = E\epsilon \tag{15}$$

E ... elastic modulus [Pa]
However, the collagen fibrils show a non-linear behaviour under tension. This led to an approximation of the elastic modulus over the stress-strain curve: The recorded curve is divided into 20 segments each containing the same amount of data-points. The first and the last point is taken and a straight line is fitted through all points within one segment. The incline of each of these 20 segments resembles the respective elastic modulus.
In the visualization of the elastic modulus along the strain every elastic modulus is assigned to the centre of the segment.

$$\epsilon_{segment} = \frac{\epsilon_{first} + \epsilon_{last}}{2} \tag{16}$$

6.2.3 Energy dissipation

To calculate the energy dissipation during the elongation/retraction process within the tensile test in the physiological range, the areas underneath the curves are calculated. By calculating the area of the force-displacement curves from the extension the energy needed to extend the fibril is obtained. The area from the retraction resembles the energy released. When the stress-strain curve is used instead of the force-displacement, then the energies are referred to one volume element and thereby the energy is independent of the sample geometry and her the units $[\frac{J}{m^3}]$. The energy dissipated is the difference of the area under the extension and retraction curve. By subtracting the area of the retraction from the extension curve the energy dissipation can be calculated.
The fibrils were extended and retracted at different loading speeds which results in different strain rates[%/s]. The influence of the strain rate on the energy dissipation can also be examined. The change of the energy dissipation due to different strain rates indicates viscoelastic behaviour of the material. However, due to the different lengths of the fibrils the different speeds resemble different strain rates. By creating a slope of the strain over time, the strain rate for each individual test could be evaluated. The energy dissipation can hence be visualized for the different strain rates applied to the fibrils.

For better comparison also the energy dissipation in [%] is calculated by dividing the Energy dissipation, the blue area, through the energy needed for extension, blue and green area in figure 33.

$$Energy_{dissipation}[\%] = \frac{Energy_{dissipation}}{Energy_{extension}} * 100 \tag{17}$$

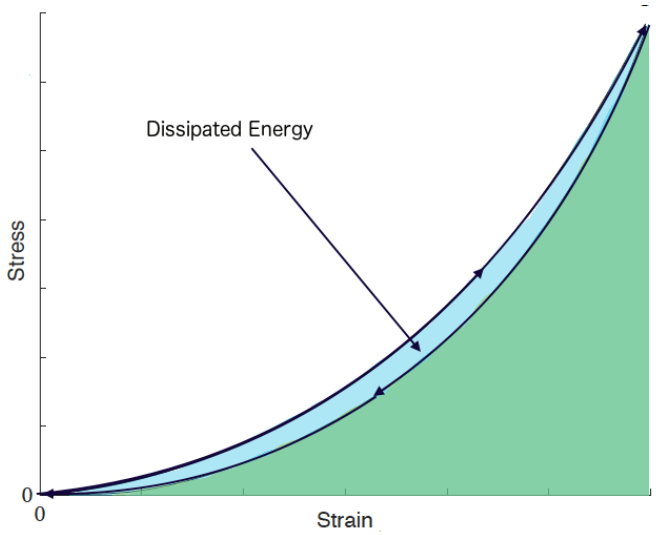

Figure 33: Explanation of the Dissipated Energy in [%]

6.3 Single-molecule forces

A paper published in 1995 by David J. S. Hulmes states a value for the cross-sectional area claimed by one collagen molecule within dried collagen fibrils. The collagen molecules orient in a highly ordered manner, aligned along the longitudinal direction of collagen fibrils. Hulmes et. al [14] stated that the molecular packing in the radial direction is organized concentrically around the fibril core.
Further a concentric ring model for the assembly within fibrils stated to be the most accurate description. According to this model one molecule corresponds to an area of $10.079[nm^2]$ in dried collagen fibrils[14].
This value allows an approximation of single collagen molecule forces during the tensile tests. The single molecule forces are transformed to estimated stress and strain per molecule. The values are generated by calculating the stress, according to the formula 6.2.1, with the air dried diameter evaluated during the analysis in section 6.1 and then

dividing this stress through the number of molecules present in the fibril.

$$\sigma_{dried} = \frac{F}{A_{dried}} = \frac{F * 4}{\pi * D_{dried}^2} \tag{18}$$

$$\sigma_{molecule} = \frac{\sigma_{dried}}{Numberofmolecules} = \frac{\sigma_{dried}}{A_{dried}} A_{molecule} \tag{19}$$

6.4 Fracture-test

As mentioned in 5.12.2 the AFM used limits the elongation of the fibrils during one measurement. For this reason the fracture test had to be performed in a stepwise fashion. The generated data per fracture curve consists of multiple deflection-height curves per fibril. Through the construction of the test, adjacent curves contain overlapping regions allowing an assembly to one total fracture curve.
Since the movement of the stepper motor is constant and known during the fracture test, the point where the force curves overlap are known. The starting point along the x-axis of the following curve is calculated by adding the step width of the stepper motor to the starting point of the previous curve.

$$Position_n = Position_{n-1} + d_{stepper} \tag{20}$$

Where $Position_n$ resembles the height of the current force curve starting and $Positon_{n-1}$ the height of the starting point of the previous curve. $d_{stepper}$ represents the step width of the stepper motor after each force spectroscopy.
As can be seen in Fig. 34 (a) the last three curves are shifted downwards, this is due the realignment of the photo-detector. The realignment is needed to record the force throughout the whole fracture test. During the test the deflection of the cantilever would reach a level where the laser is deflected to a point outside of the photo-detector. Previous to this point it is necessary to realign the laser-beam, otherwise the force would not be properly recorded. Due to the realignment of the laser beam an alignment of the y-values of the recorded curves must be performed. However, this task is simple since the corresponding y-value (deflection) of the previous curve is saved in the same line as the x-value, obtained along the correction of the x-axis, within the Matlab structure (figure 31). Through this scheme the starting point of the following curve is determined and all force-spectroscopy curves are merged. The overlapping region of the previous curves are omitted and one smooth fracture curve is obtained. Figure 35(a) shows the combined fracture curve. Each color resembles one force curve from the fracture test. This merged data then is combined into one single curve 35(b).

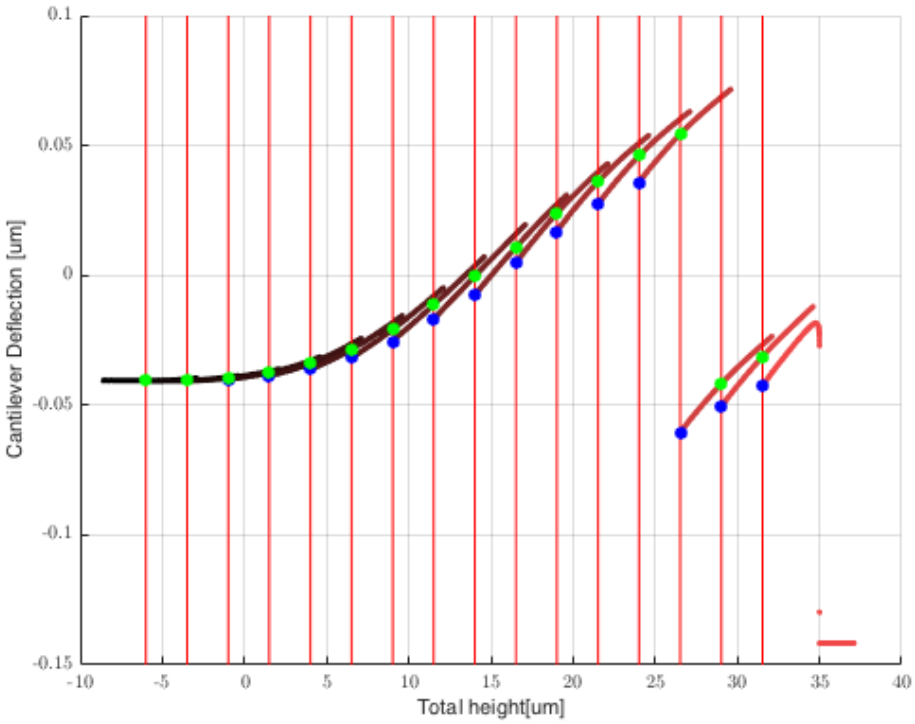

(a) AFM data including the displacment performed with the stepper motor

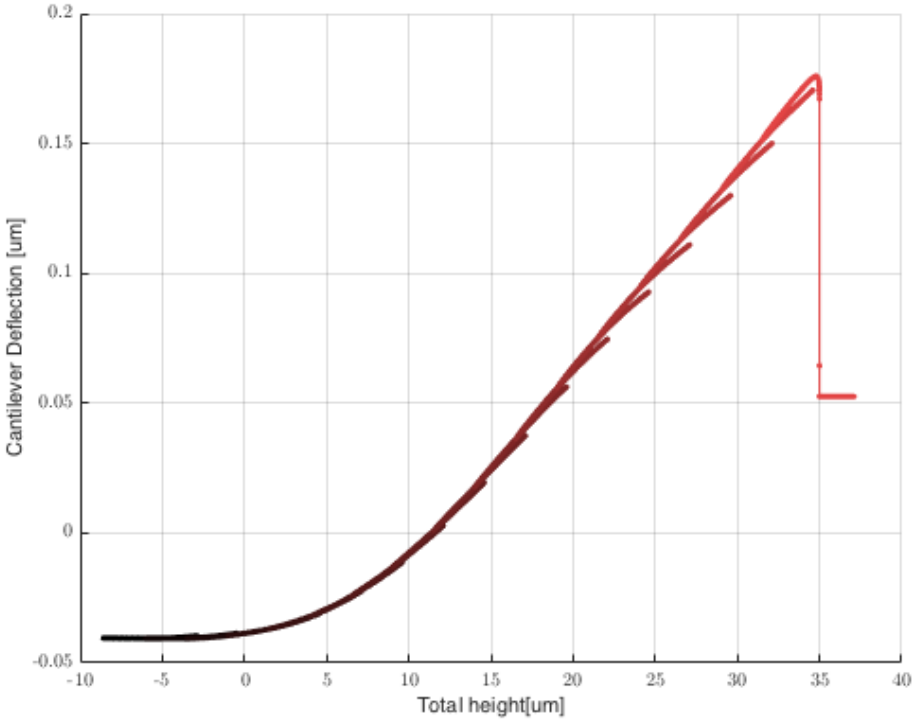

(b) Aligned data

Figure 34: Alignement of the data obtained from the fracture test

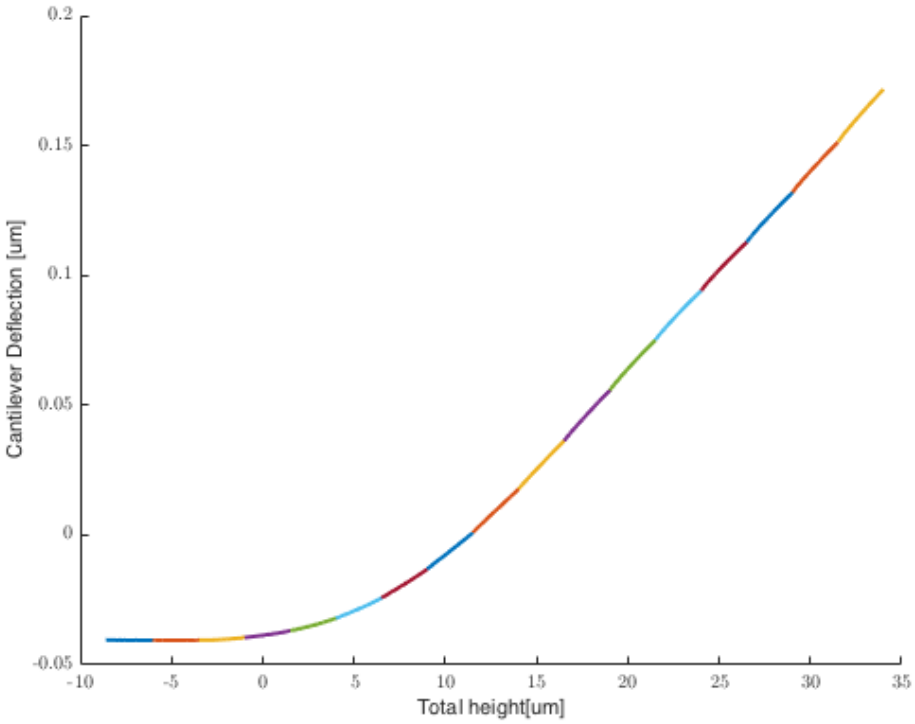

(a) Aligned curves with omitted overlapping regions, each color represents one force spectroscopy

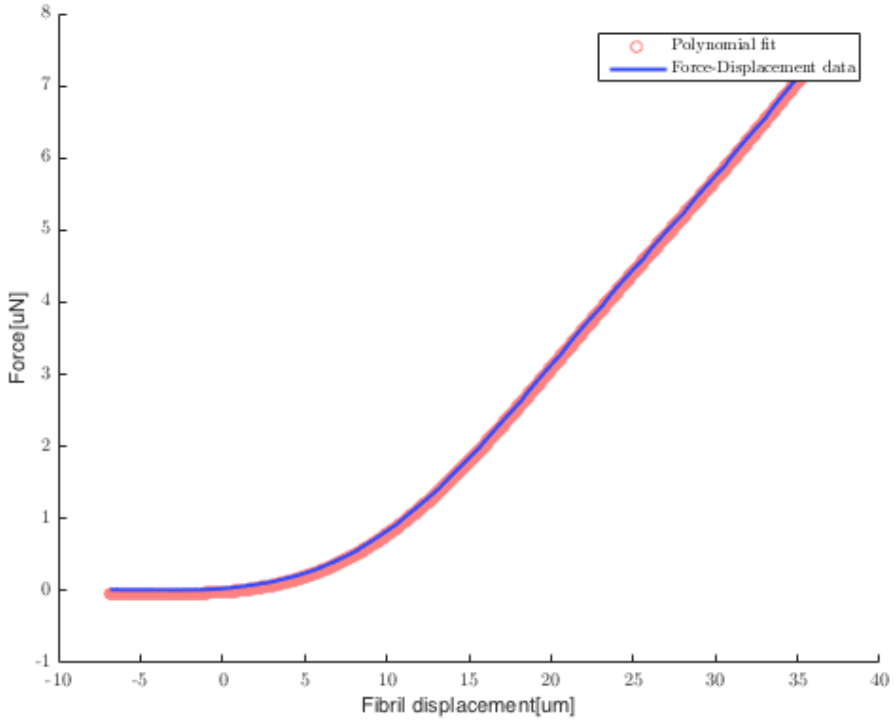

(b) Shift of the Force-displacement curve according to the contact-point including the 10^{th} grade polynomial fit

Figure 35: Resulting fracture Force-displacement curves

In the next step the starting point is defined manually and the merged curve is shifted along the x-axis to match the contact-point to zero force and displacement. The deflection/displacement then is transformed in force/fibril-displacement and fitted with a polynomial 10^{th} grade function. Further the force-displacement curves are translated into stress-strain curves as described in 6.2.1.
To generate with the literature comparable data , several parameters are extracted from the stress-strain curves of the fracture test. According to a paper published in 2013 by Svensson et al.[28] most fracture curves of fibrils show a typical behaviour. For the analysis of the fracture curves comparable parameters need to be defined. The first part of the elastic modulus versus strain curve is described by a steep incline, by reaching the second part the curve flattens to a plateau and ending again with a rise of the slope in the third part. For rat tail tendons Svensson stated that the first elastic modulus(E_1) is larger then the second elastic modulus (E_2).
For this the first local maximum or saddle points and the maximum elastic modulus in region III of the elastic modulus versus strain curve need to be determined. Due the fact that the elastic modulus is calculated by separating the curve into 20 segments (see 6.2.2) this two elastic (E_1 and E_2) moduli where manually determined for each curve.

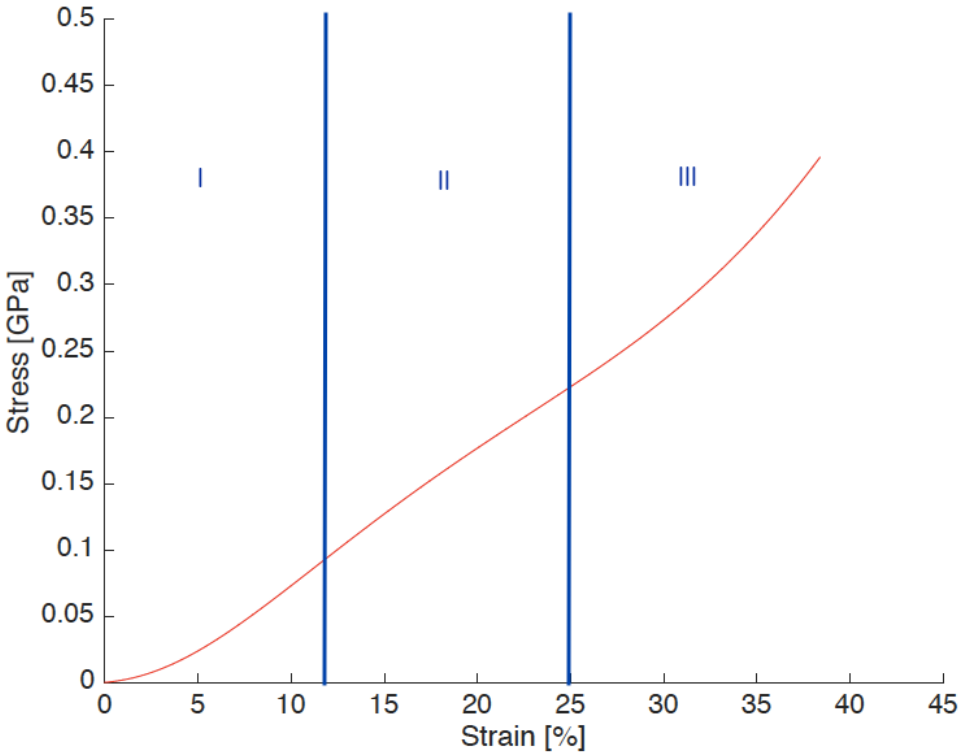

(a) Stress-Strain Diagramm

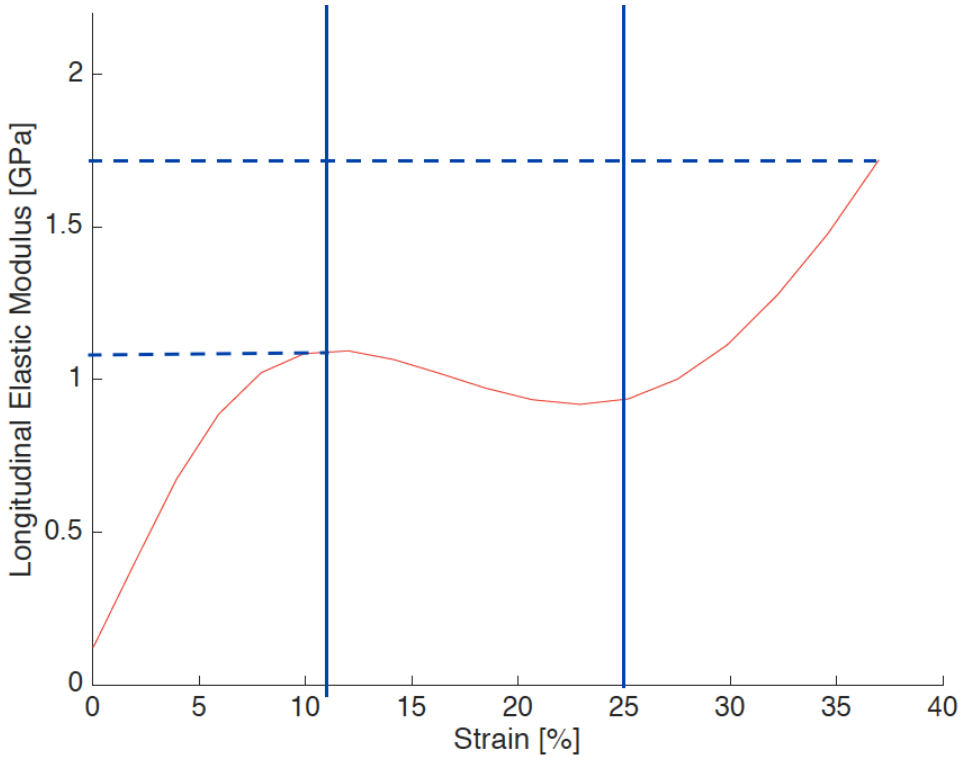

(b) Elastic modulus versus strain

Figure 36: The three defined regions according to Svensson et. al.

6.5 Indentation analysis

The indentation analysis script was provided by Dr. Andriotis (ILSB, TU Vienna). In the first step of the script, the shape of the cantilever tip which is used to perform the indentation-test is analysed. With this data the indentations performed during the force-map recording are analysed.

6.5.1 Tip analysis

The 1.5x1.5μm image taken from the TGT1 calibration grating described in 5.3.1 is analysed. In the same manner as described in section 6.1 a line wise plane fitting was applied to the recorded image of the tip. A polygon mask is manually applied to the image to separate the tip from the background. Then the height data of the background image is line-wise linearly least-square-fitted and in the next step the fit is subtracted from the image data.
This process evens the image out. However, the image still does not resemble only the shape of the cantilever tip. As the image still is a conjunction of the TGT1 spikes and the cantilever tip. For this reason a deconvolution of the image is performed. This task can be performed by simulating the peaks of the TGT1 as perfect cones with an opening angle of 50 degrees (as can be seen in the grating description of the manufacturer, http://www.ntmdt-tips.com/products/view/tgt1). The tip deconvolution has been described by Keller and Franke [62]. According to the procedure of Keller and Franke the tip deconvolution is performed during this thesis [63]. Keller and Frankl performed the tip deconvolution by defining the s(x,y) as the surface of the reference sample and $z(x', y')$ as the image surface at a point (x', y') thereby the inverted tip surface,-t(x,y), is given through: the minimum of the functions $w(x, y, x', y') = z(x', y') - s(x - x', y - y')$ so that: $-$t(x,y)= the minimum of the set $\{z(x', y') - s(x - x', y - y')$ all $(x', y') \in R\}$ [62]. For the reconstruction the TGT1 spikes are assumed to be cones with an opening angle of 50 degrees and a tip radius of 5 nm as provided by the manufacturer (NT-DMT Spectrum Instruments)[63].
In the next analysing step the projected area function of the tip is defined , the area changes with the height of the tip $A_c(h_c)$. For this reason the 3-dimensional image of the tip is layered along the vertical axis and for each layer the area of the tip is calculated via the pixels. Through the definition of 1.5x1.5μm with a resolution of 512x512 pixels the pixel size is known and can be used for the area calculation.

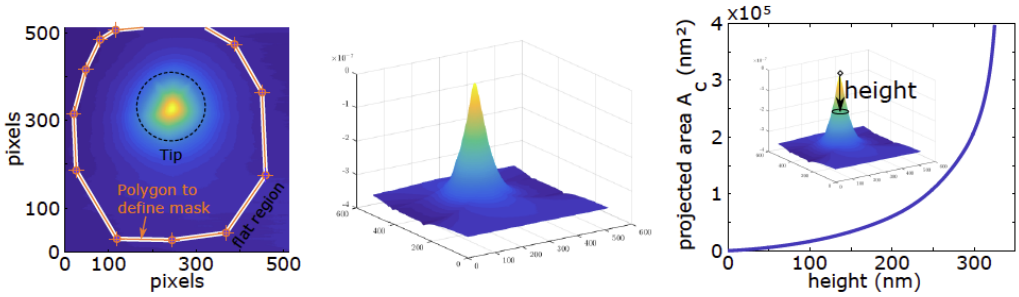

Figure 37: Analyse of the tip (a) creating the mask (b) deconvoluted height profile (c) Project area along the height [56]

With the known tip shape the force-maps can then be analysed. During this thesis the method of Oliver and Pharr was chosen for the analyses of the elastic circumferential modulus according to [63].

6.5.2 Oliver-Pharr method

The indentation analysis developed by Oliver and Pharr [58] was introduced in section 3.5, during this chapter the analysing method will be described in greater detail.
According the a paper published in 2014 by Andriotis et al. [63] the indentation test was analysed.

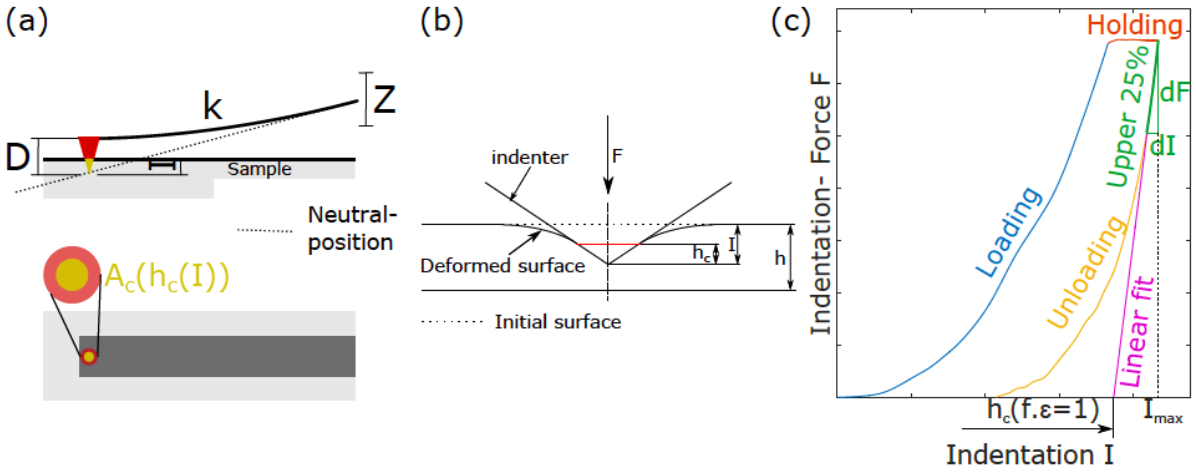

Figure 38: (a)AFM tip during indentation. The displacement D is gained through substraction of the cantilever deflection from the Z-piezo height (b) Illustration from the tip penetration in the collagen fibril visualizing the different parameters (c) Example of force vs indentation curve with an holding period in extended position [56]

The indentation curves generated along this project did not have a holding part. However, this is indifferent for the calculation of the indentation modulus. During an indentation test the sample as well as the indentation-tip experience stress and deformation. Therefore the relation between the reduced elastic modulus E_r is defined through equation: [58]

$$\frac{1}{E_r} = \frac{1-\nu^2}{E} + \frac{1-\nu_i^2}{E_i} \tag{21}$$

In this equation E and ν are Young's modulus and Poisson's ratio of the sample and E_i and ν_i are the same parameters of the cantilever tip[58]. According to [63] the indentation modulus of collagen fibrils is in the range of 10 MPa and the elastic modulus of the cantilever tip (silicon nitride) is in the range of 100 MPa. For this case of $E_i >> E$ equation 21 is reduces to [35]:

$$\frac{1}{E_r} = \frac{1-\nu^2}{E} \tag{22}$$

The sample stiffness resembles the slope of the upper 25% of the unloading force-indentation curve. Through the projected Area function A_c of the tip, obtained in section 6.5, and the reduced elastic modulus E_r the sample stiffness can be calculated with following equation [35]:

$$S = \frac{dF}{dI} = \beta E_r \sqrt{A_c} \frac{2}{\sqrt{\pi}} \tag{23}$$

Within equation 23 a correction factor β is introduced, this correction factor takes the nonaxisymmetry of the indenter and large strains into account [35]. During this analysis β was set to a value of 1. By merging the two equations 21 and 23 the elastic modulus of the sample can be calculated according to the following equation.

$$E = \frac{\sqrt{\pi}}{2\beta}(1-\nu^2)\frac{S}{Ac} \tag{24}$$

During the indentation the sample surface does not follow the shape of the indenter fully, leading to the result that contact depth h_c is different to the maximum indentation depth I. Oliver and Pharr provide a equation which takes this difference into account [65] connecting the contact depth h_c, the stiffness S, the maximum indentation I and the maximum indentation force F_{max}. Within the following equation another correction factor ϵ is introduced, this correction depends on the geometry of the indenter. For the used cantilever during this thesis the value for ϵ was set to 0.73 according to [58].

$$h_c = I - \epsilon \frac{F_{max}}{S} \tag{25}$$

6.6 Statistical analysis

The statistical analysis was performed with the software SPSS (IBM,USA). Due to the low sample number a non parametric test (Mann-Whitney-U-Test) was used in most cases. For the energy dissipation in percent more data points where generated during the measurements. This allowed a test for normal distribution, due to the fact that the values where not normal distributed also a Mann-Whitney-U-Test was executed. For the indentation test more fibrils where observed resulting in more data to analyse. Again a normal distribution analysis was performed, which confirmed the normal-distribution of the values. Therefore an equality of variances test(levene's test) was performed and afterwards a analyses of the variances was implemented via an ANOVA test. During the data-analysis box-plots are generated for visualization, therefore the different arrangements and the meaning of the lines and boxes within the plots are show in figure 39.

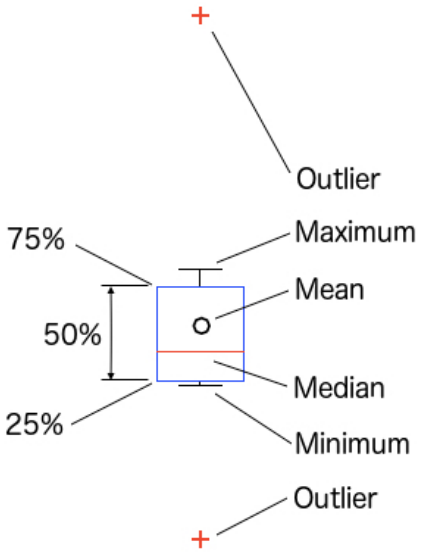

Figure 39: Example box-plot with notations

7 Results

7.1 Optimization of the sample preparation-protocol

The basis of the sample preparation for the tensile test where established by Desissaire in 2016 [30] based on the work of Svensson et al. [28, 27] . According to this protocol the AFM is used for most of the sample preparation steps. In the following these steps are shown, the steps performed with the AFM are indicated by *.

1. Attachment of individual collagen fibrils to a glass substrate via epoxy resin.*
2. Verification of single collagen fibril by AFM imaging.*
3. Length measurement of the verified individual collagen fibril with an optical microscope.
4. Performing the imaging process in PBS.*
5. Detachment of one epoxy droplet in air.*
6. Attachment of the tipless cantilever to the detached epoxy droplet by epoxy resin.*

By substituting the AFM with the micromanipulator in step 1 and 5 the optimization was achieved. When the attachment process of the fibril (step 1) is performed with the AFM the epoxy resin present on the cantilever tip need to be downscaled previous to the glueing process. By using the micro-manipulator and the introduced protocol(see section 5.6) the size of the epoxy droplet fits directly. Further the manipulation of the micro-manipulator is faster compared to the AFM. This allows more fibrils to be attached to the glass slide in a shorter period of time. Another advantage of the attachment process with the micromanipulator is that during one session a high amount of fibrils can be attached to the glass slide (20-30 fibrils per hour).
However, the largest improvement was gained by performing the detachment of the epoxy droplet with the micromanipulator. In the previous protocoll, Desissaire [30] performed this step with the AFM, by scraping the epoxy droplet off using the tip of the cantilever. This step took around 4 hours per droplet. Through the substitution of the AFM with the micro-manipulator, equipped with a needle tip (see section 5.4), the time of the detachment is reduced to 10 minutes per droplet (see section 5.9). Although, the process need to be repeated in air. Thereby the needed time to perform this step is reduced from 4 hours to 10 min. The only time consuming step left during the improved protocol is the

attachment of the tipless cantilever to the loosened epoxy droplet. This process is performed with an epoxy resin (UHU plus endfest 2-K-Epoxidharzkleber, UHU, Germany) with 12 hours hardening time. Different epoxy resins, with shorter hardening times were observed during previous studies [64]. However, the 12 hour epoxy resin showed the best behaviour during sample preparation and tensile testing. For this reason no other epoxy resin could be used. Thereby the hardening time determines the time needed for sample preparation.

Prior to the described improvements, one sample could be analysed per week. With the optimized protocol this number increased to 4-5 samples per week. For further details on the improvements see [64]. In the following the results obtained from the measurements of individual collagen fibrils are provided.

7.2 Diameter and swelling

The AFM images were analysed with the method described in section 6.1. Using data from the AFM images in air and PBS the air-dried diameter and the hydrated diameter of six OIM and six WT fibrils was obtained. The fibrils were imaged in air and in PBS (pH=7.4). The mean swelling ratio between the two groups showed no significant difference ($p=0.138$). From table 3 it can be seen that the swelling ratio does not correlate with the hydrated or dried diameter of the individual collagen fibrils. When observing the box-plot in figure 40 it can be seen that the swelling ratio of both groups overlap due to the interfibrillar variations within the groups. The swelling ratio resembles the water uptake of the fibril, the higher the ratio the more water is absorbed by the structure. Further correlations between the swelling ratio and the interfibrillar cross-links are stated in literature [34].
A statistical difference between the air-dried and the hydrated fibril diameters between the investigated OIM and WT fibrils was obtained ($p<0.05$). The hydrated as well as the air-dried diameter of WT collagen fibrils is found to be significantly larger than the air-dried and hydrated diameter of OIM collagen fibrils (see figure 41).

	Air-dried diameter [nm]	Hydrated diameter [nm]	Swelling	
OIM	57	92	1.61	
OIM	57	113	1.98	
OIM	106	173	1.64	
OIM	90	153	1.70	
OIM	101	121	1.19	
OIM	59	102	1.72	
		Mean- Value OIM	1.64 ±	0.25
WT	149	347	2.33	
WT	125	219	1.75	
WT	81	139	1.72	
WT	97	172	1.78	
WT	122	233	1.91	
WT	191	280	1.47	
		Mean-Value WT	1.83 ±	0.28

Table 3: Swelling ratio of OIM and WT

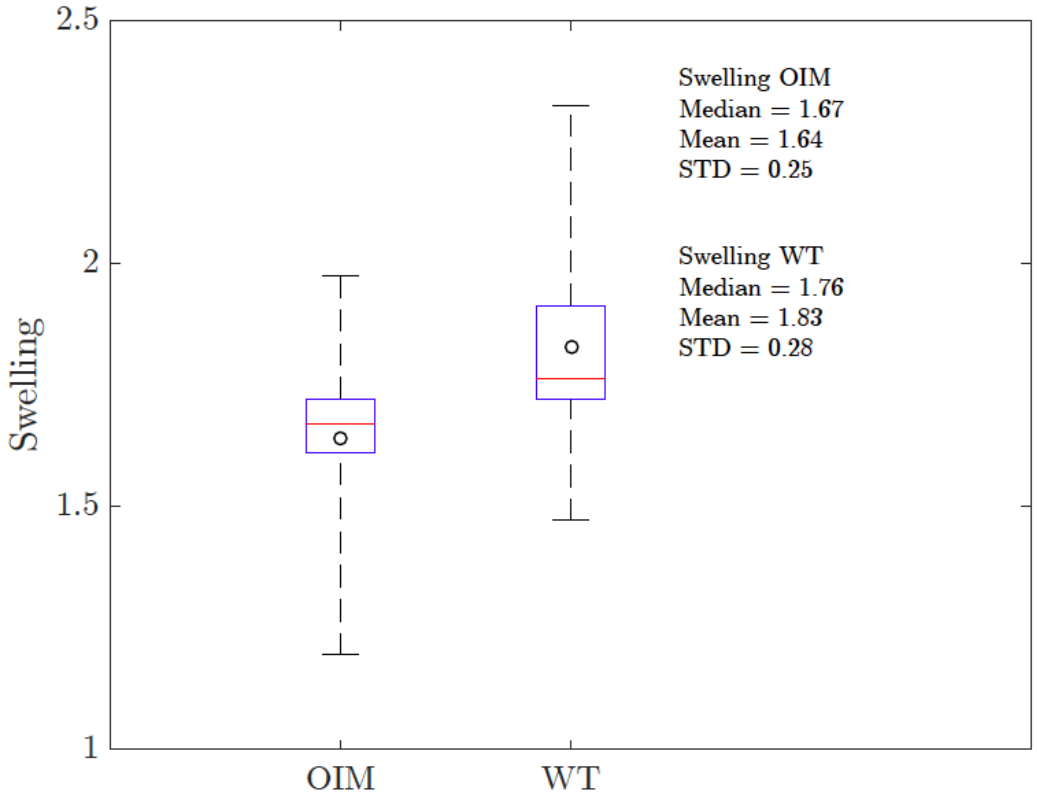

Figure 40: Swelling ratio of OIM and WT fibrils with no significant difference (p=0.138)

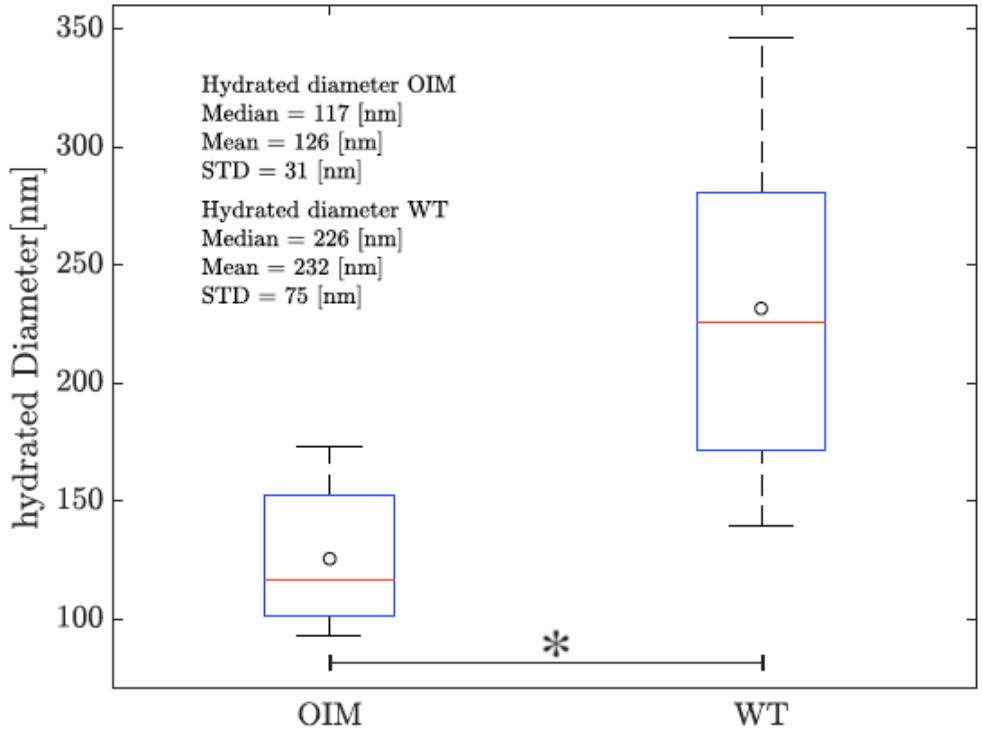

(a) Hydrated diameter

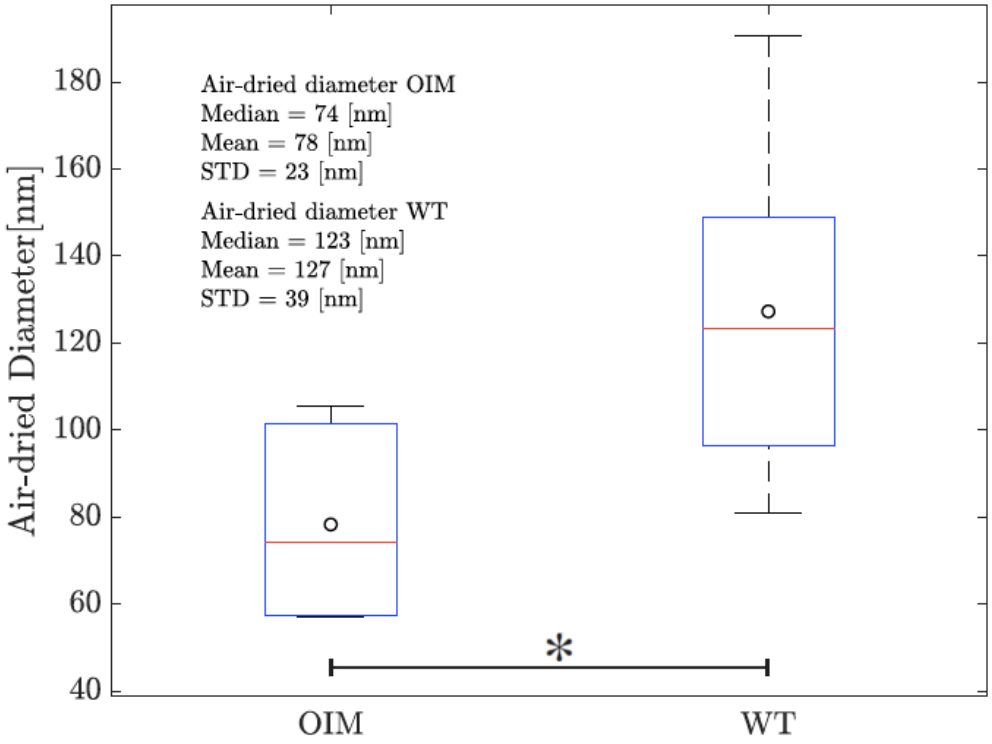

(b) Air-dried diameter

Figure 41: Air-dried and hydrated Diameter of OIM and WT fibrils both values show a significant difference($p<0.05$)

7.3 Mechanical testing of individual collagen fibrils

According to the methods described in section 5, WT and OIM collagen fibrils have been investigated. The fracture-data of five OIM and six WT fibrils was analysed. Further data of tensile tests in the physiological strain range of six OIM and five WT collagen fibrils where evaluated. The obtained data will be presented in the following sections.
According to Svensson et. al. [28] the data of the fracture curve can be separated into 3 sections. This separation allows a better comparison with literature values and was applied to the presented data.
For better discrimination the OIM data points are generally indicated with yellow coloured markers or dashed lines, whereas the WT data is generally visualized with blue coloured markers or solid lines within the figures.

7.4 Physiological range

7.4.1 Fibril stiffening

The recorded data from the tensile tests in the physiological strain range were transformed into stress-strain curves. One goal was to obtain values for fibril stiffening through rising strain rates. In figure 42 the stress-strain curves of one example collagen fibril is shown. Within this figure the viscoelastic properties of the individual collagen fibril is visible. The viscoelastic behaviour is resembled through the hysteresis loop within the stress-strain curve of extension and retraction. Further the viscoelastic behaviour is seen in the increase of the slope due to a rise of the strain rate. In figure 42 the different strain rates are visualized by different shades of blue. Bright blue marks the low strain rate and with rising strain-rate the color gets darker. The rising strain rate further is indicated in figure 42 with the black arrow.
To generate a comparable parameter the slope of the stress-strain curve is calculated at 2.5% strain. The strain value of 2.5% was determined by the geometrical properties of the collagen fibrils. The slope of the stress-strain curve is defined as the elastic modulus. Therefore the elastic modulus at 2.5% strain is observed at different strain rates.

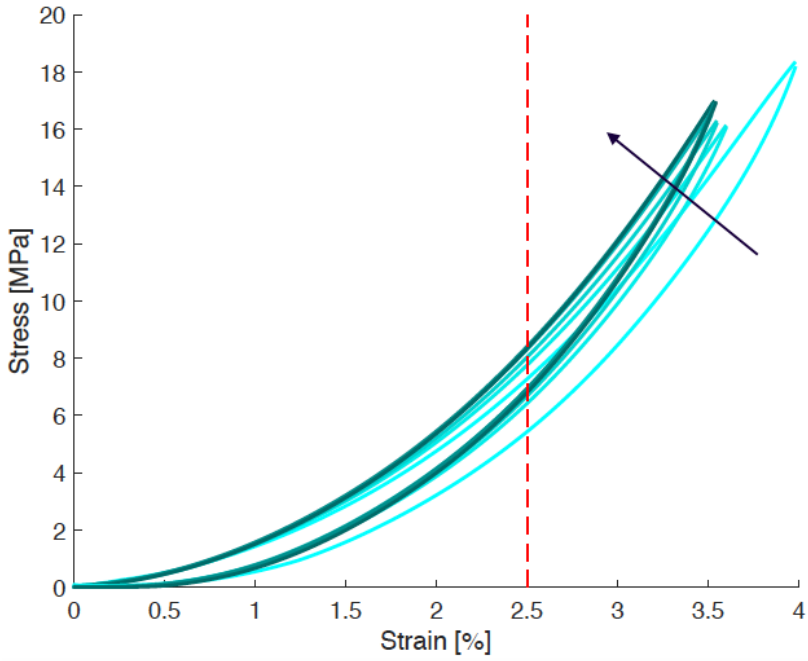

Figure 42: Stress-strain curve of one example collagen fibril. The dashed red line highlights the strain value of 2.5 % and the black arrow indicates the stiffening through the rise of the strain rate. The different colors resemble different strain rates.

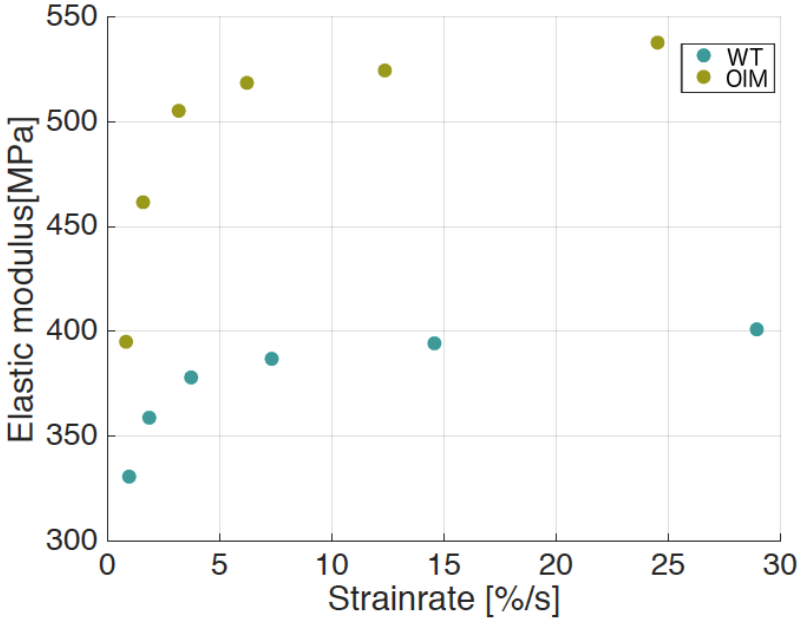

Figure 43: Stiffening of one OIM and one WT collagen fibril

Due to the different lengths of the individual collagen fibrils different strain rates where achieved during the tensile test in the physiological range. In figure 43 the rise of the elastic modulus and thereby the stiffening of the fibril due to the increasing strain rate

can be seen. The trend that the OIM collagen fibril shows higher elastic moduli than the WT collagen fibril, which can be seen in figure 43 for the two example fibrils will be discussed in more detail. The elastic modulus versus strain rate curves for all collagen fibrils WT and OIM are presented in figure 44. Due to the different magnitudes of the elastic modulus the y-axis is scaled logarithmic. The logarithmic scale visualizes the rise of the elastic modulus from the collagen fibrils, except one OIM fibril. To compare the OIM collagen fibrils with the WT fibrils the elastic modulus at 15 [%/s] strain rate is used. The value for the elastic modulus at 15 [%/s] strain rate is obtained via interpolation between the data points. The value of 15 [%/s] was chosen by geometrical properties of the fibrils and further due to the fact of flattening of the elastic modulus curve at this value.

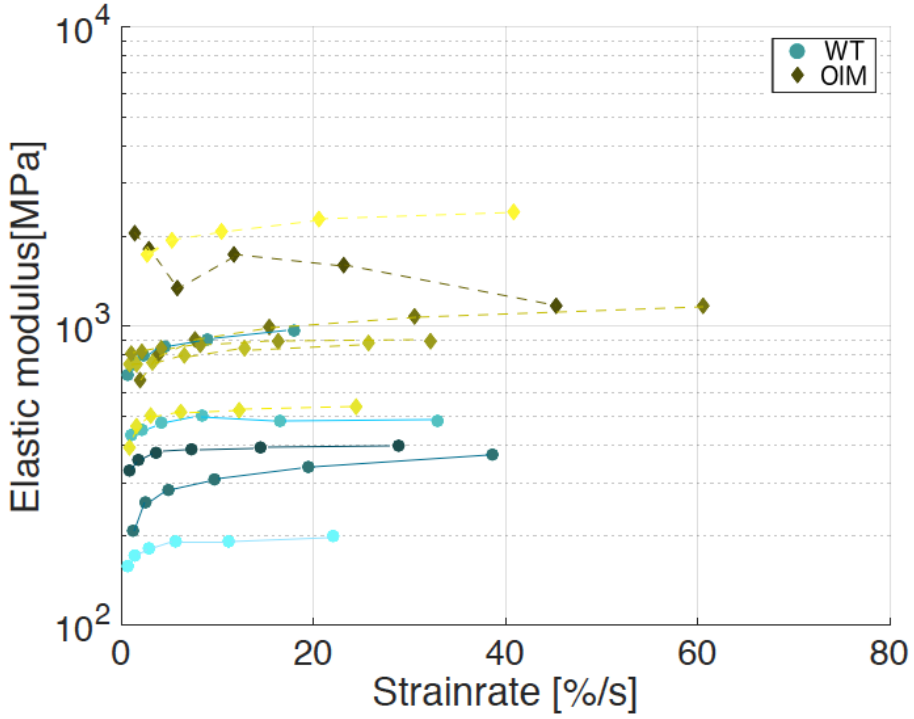

Figure 44: Elastic modulus versus strain rate of OIM and WT collagen fibrils. The axis of the elastic modulus is scaled logarithmic.

At a strain value of 2.5% and strain rate of 15[%/s] the OIM collagen fibrils show a significantly ($p<0.05$) higher elastic modulus compared to the WT collagen fibrils. Similar behaviour maybe observed in the physiological range of the tensile fracture tests. With this result it can be stated that individual OIM collagen fibrils show a higher elastic modulus within the physiological strain range. From figure 44 a clear trend of fibril stiffening is visible. The fibril stiffening is resembled by the rise of the elastic modulus. Within 44 it can be observed that all fibrils show the stiffening trend independent of

WT or OIM. The stiffening due to the strain-rate is typical for viscoelastic materials. The stress-strain curves of a viscoelastic material generally shows a hysteresis loop. The area of this loop resembles the dissipated energy during extension and retraction. The dissipated energy of the observed collagen fibrils is discussed in the following section.

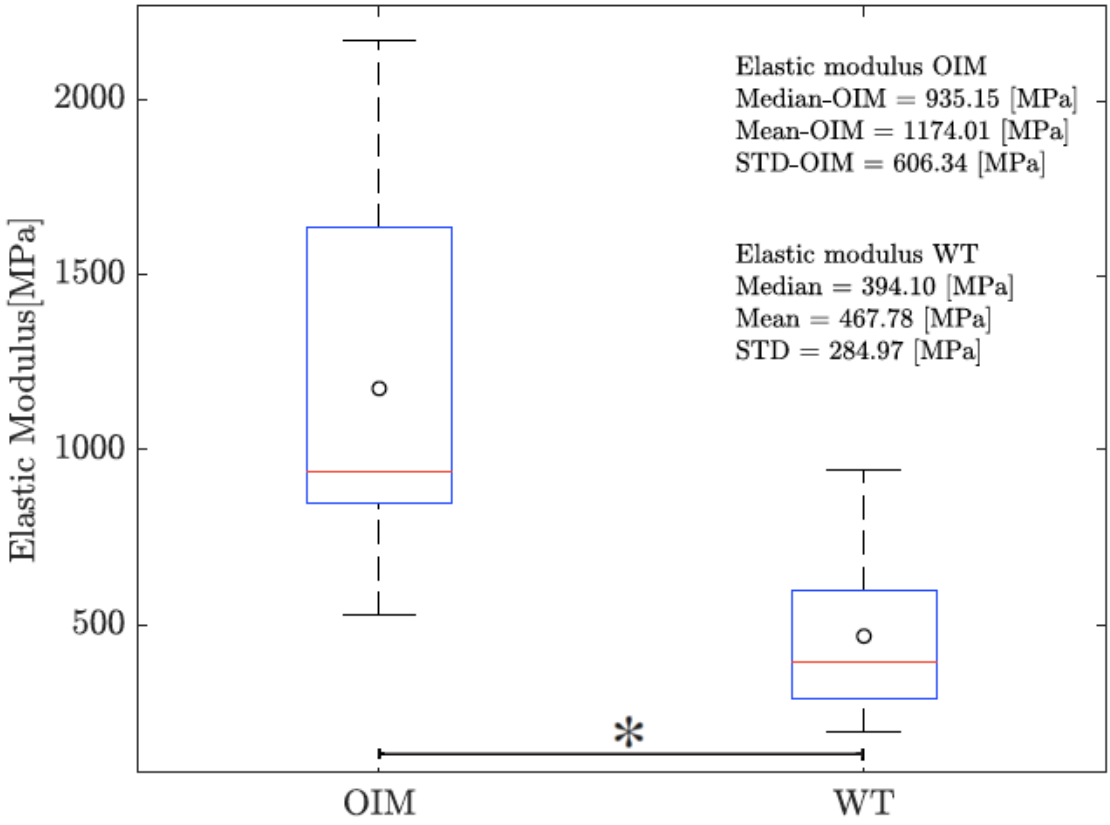

Figure 45: Elastic modulus at 2.5% strain and 15[%/s] strain rate showing a significant difference between WT and OIM collagen fibrils ($p<0.05$).

7.4.2 Energy dissipation

The energy dissipation during loading and unloading provides information on the efficiency of the observed structure. For energy-storing tendons the energy storage and release with low energy dissipation during movement is an important feature. By observing the influences of OIM on this efficiency at the fibrillar level, important insight about the mechanism of this diseases may be gained. As already mentioned in the previous section the length of the fibrils varies within both groups.

For analysing the energy dissipation this variation may have significant influence on the absolute values of the dissipated energy. For this reason mean-value and the standard-deviation of the groups where adjusted to have similar values. The longest fibril of the

WT-group and the two shortest fibril of the OIM group were excluded. Through this the mean-value for WT shifted to $123\mu m \pm 39\mu m$ and for OIM to $114\mu m \pm 27\mu m$ fibril length. The fibril lengths, the original mean value and the corrected mean value can be seen in table 4.

WT	Length [µm]	OIM	Length [µm]
1	193	1	145
2	164	2	125
3	130	3	105
4	110	4	83
5	88	5	80
		6	59
Mean-value	137±42	Mean-value	99±31
Corrected Mean-Value	123±39	Corrected Mean-value	114±27

Table 4: Length of the observed collagen fibrils. For the corrected mean-value the red marked collagen fibrils are neglected

The similar mean-values and standard deviations of the both groups allow a more accurate comparison of the obtained data. In figure 47 each shade of yellow and blue represents one fibril either WT or OIM. The y-axis is presented logarithmic scaled. The obtained data shows that the OIM collagen fibrils dissipate nearly 10 times more energy than WT fibrils.

In figure 47 the variation of the strain-rate can be seen. Although, the aforementioned adjustment of the fibril length mean-values of the groups, the variation between the individual fibrils remains. During the tensile test in the physiological range the maximum achievable displacement (5.5μm) of the piezo actuator of the AFM was performed. For this reason the strain varies according to the fibril length. To correct the error of the different strains and strain rates during the tensile tests in the physiological strain range, the energy dissipation in [%] is calculated.

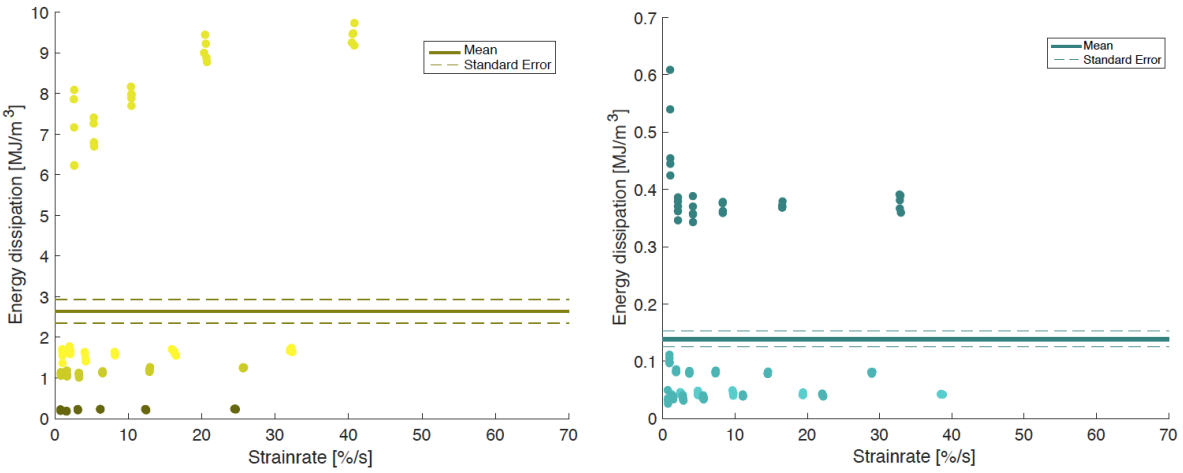

(a) OIM (b) WT

Figure 46: energy dissipation for WT and OIM including the standard-deviation error

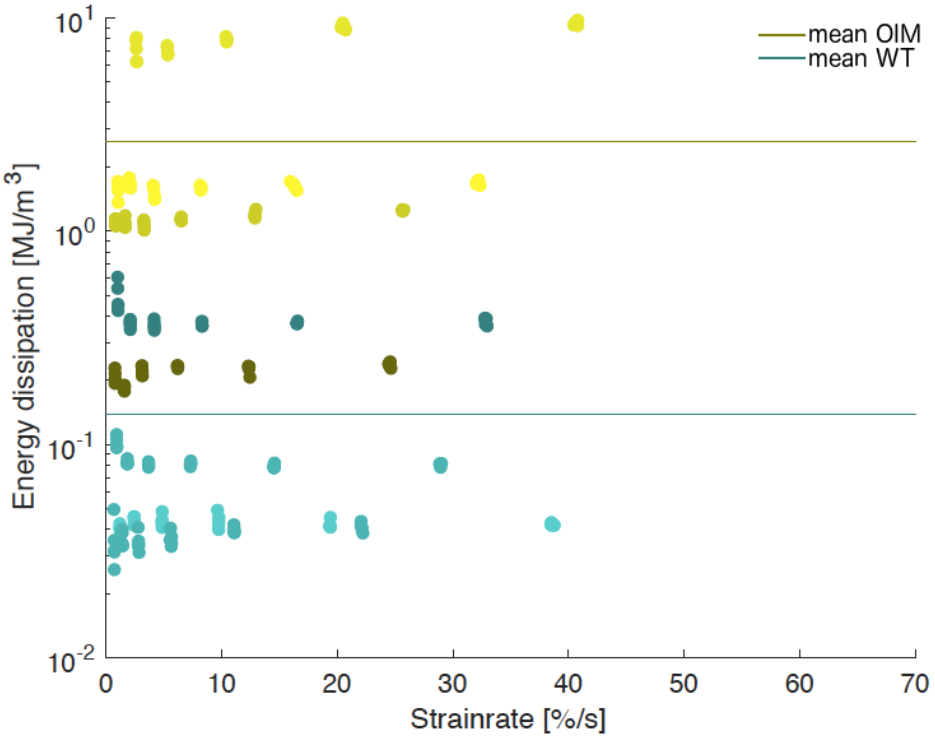

Figure 47: Energy dissipation (log-scale) per strain rate. Each dot resembles on measurement.Yellow is OIM and blue is WT

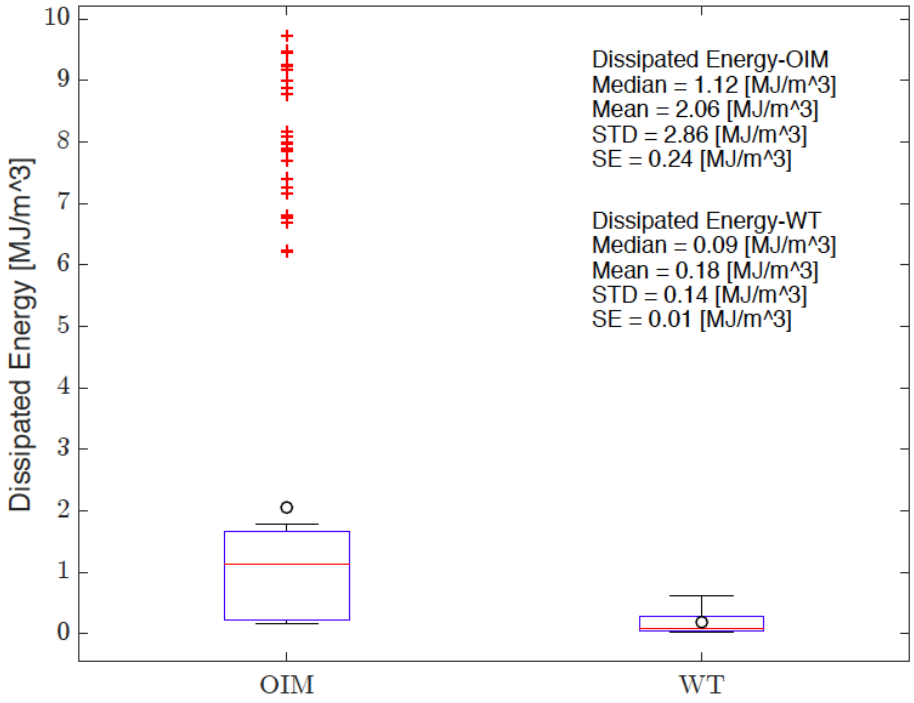

Figure 48: Absolute Energy dissipation of WT and OIM collagen fibrils. With a significant difference between the two groups ($p<0.05$)

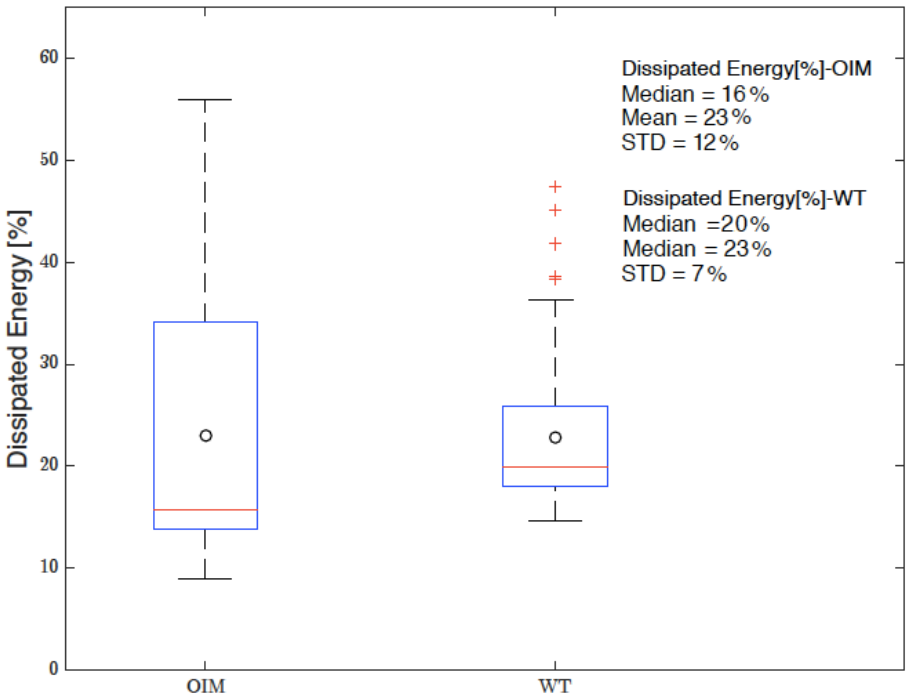

Figure 49: Percentile Energy dissipation of WT and OIM collagen fibrils with no significant difference

For the absolute energy dissipation in $[MJ/m^3]$ a statistical significant difference was found between the WT and OIM collagen fibrils ($p<0.05$) as can be seen in figure 48. However, when observing the percentile energy dissipation this observation changed and the statistical signifcant difference vanishes. The values for the percentile energy dissipation are visualized in figure 49.

7.5 Fracture tests

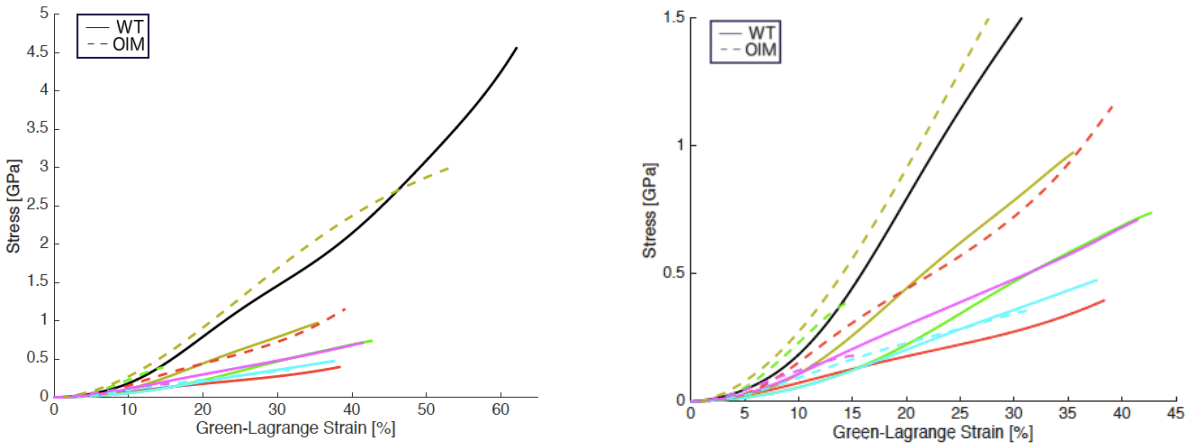

(a) Stress-Strain-Diagramm

(b) Detail of the Stress-Strain-Diagram up to 45% Strain

Figure 50: Stress-Strain-Diagram of WT and OIM collagen fibrils. The dashed lines resembles the OIM samples and the solid lines resemble the WT samples

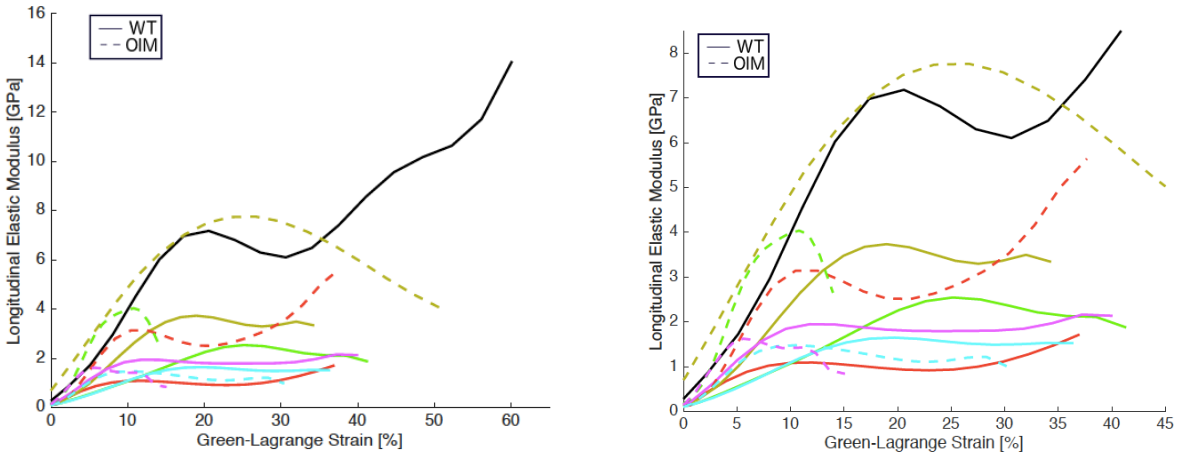

(a) Elastic modulus as a function of strain

(b) Detail of Elastic modulus versus strain

Figure 51: Elastic modulus as a function of strain for WT and OIM collagen fibrils. The dashed lines resembles the OIM collagen fibrils and the solid lines resemble WT collagen fibrils

The obtained fracture curves are evaluated according to the literature. The different groups which engaged with tensile tests on the hierarchical level of individual collagen fibrils extracted different parameters from the stress-strain curves.The two main parameters to compare with literature are the ultimate strength and the rupture strain.
Svensson et al. [28] defined four more parameters. According to their paper [28] the fracture curves can be separated into 3 parts. Svensson et al. stated that these three parts could be seen in most of the observed rat tail tendon fibrils. However, for some fibrils Svensson et al. could not determine the third part of the fracture curve.
As mentioned previously, the slope of the stress-strain curve resembles the elastic modulus of the fibril as a function of strain. When observing the elastic modulus versus Green-Lagrange strain of the individual collagen fibrils the first part of the stress-strain curve is described by a steep incline until the curve flattens, the decline of the elastic modulus marks the beginning of the second part. The third part consists of another rise of the elastic modulus.The maximum elastic moduli (saddle point) of section I and section III are observed. The maximum elastic modulus of section I is called E_1 and the maximum elastic modulus of section III is called E_2. For rat tail tendons Svensson et al. states that the first elastic modulus E_1 is commonly larger then the second E_2. Svensson et al. further defines the corresponding strain as ϵ_1 and ϵ_2 .
The obtained data during this project resembles the observation of Svensson et al. For all WT fibrils the segmentation of the stress-strain curve into three parts was visible. Within the OIM group three of the five fibrils displayed the segmentation. Through they reduction of the stress-strain curve into E_1, E_2, ϵ_{GL1} and ϵ_{GL2} better comparisons with literature can be made. Further the four parameters could help to determine influences of different geometrical and material properties on the mechanical properties of individual fibrils. Such influencing factors may be the swelling,the fibril-diameter,the fibril-length or the aspect ratio.
However, in figure 52 the ultimate strength and the fracture strain of the fibrils is presented. The results show considerable large variations within both groups, this results in a large standard deviation (compared to the mean value). When looking at figure 50(a) it appears that one WT and one OIM sample show extreme behaviour compared to the other fibrils. These two fibrils where examined in greater detail. However both fibrils do not show any exceptional geometrical properties. However, the OIM collagen fibril marked with a brown color in 50, which exihibited the largest ultimate strength and rupture strain within the OIM group, showed the lowest swelling. Due to the large standard deviation (compared to the mean value) the median-values presented in figure 52 may be more accurate for the discussion. However, the median-values only can be seen as trends since the statistical evaluation showed no significant difference neither for the

ultimate strength (p=0.429) nor for the fracture strain (p=0.247) between OIM and WT. In figure 53 and 54 the fracture side of one OIM fibril and one WT fibril are presented. After the fracture test the fibrils were rinsed with deionized water and air-dried. The ruptured air-dried fibrils then were imaged in contact mode in air.

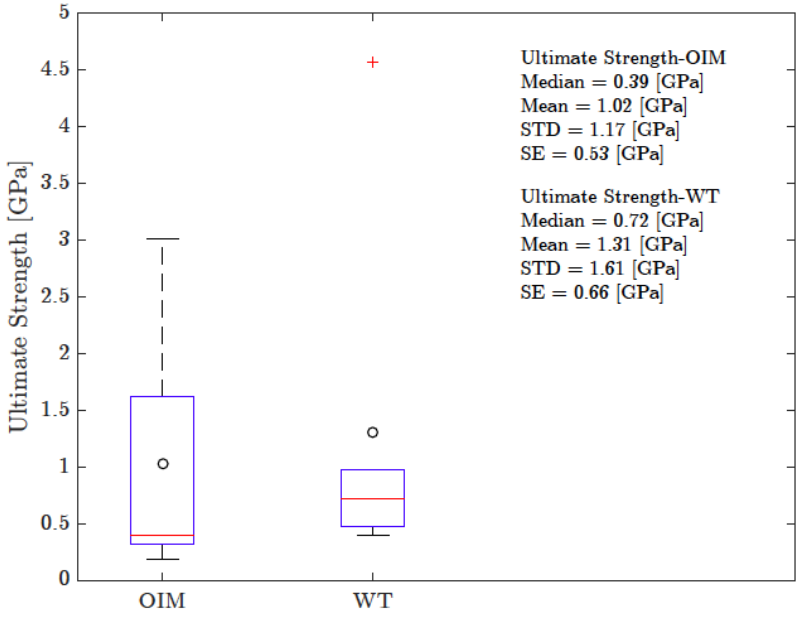

(a) Ultimate strength of the Fibrils

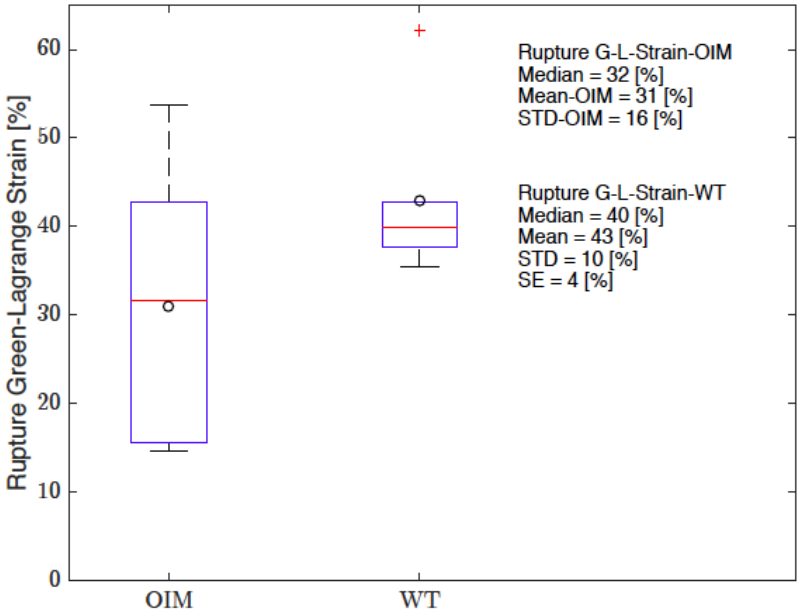

(b) Fracture Green-Lagrange Strain

Figure 52: Ultimate strength and ruptures strain of the fracture-test

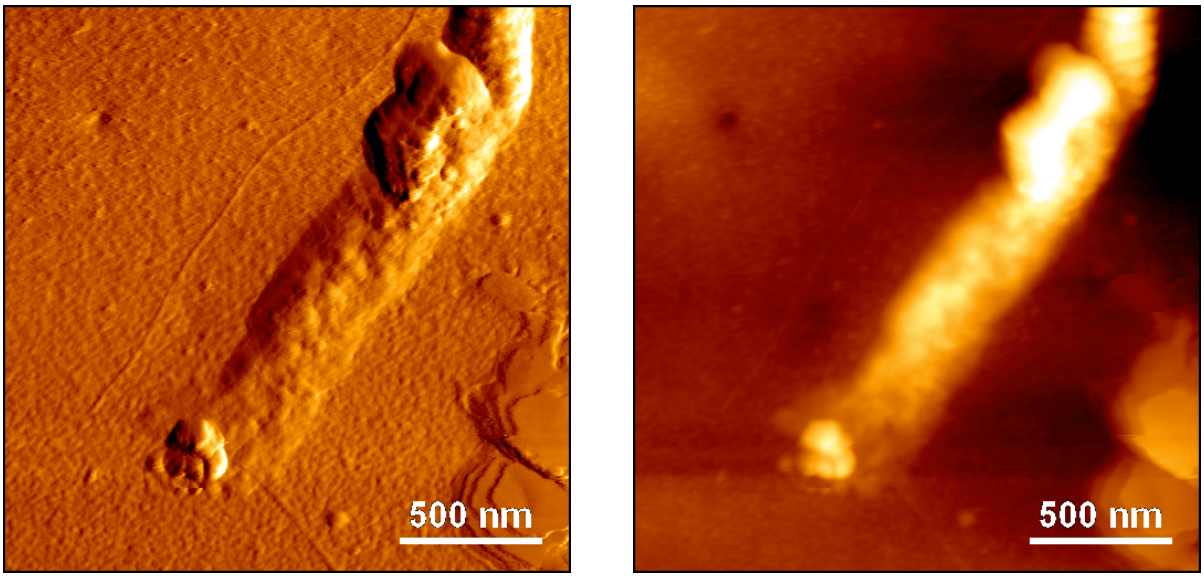

(a) Error-signal (b) Measured height

Figure 53: Contact-mode image of air dried fractured OIM-fibril

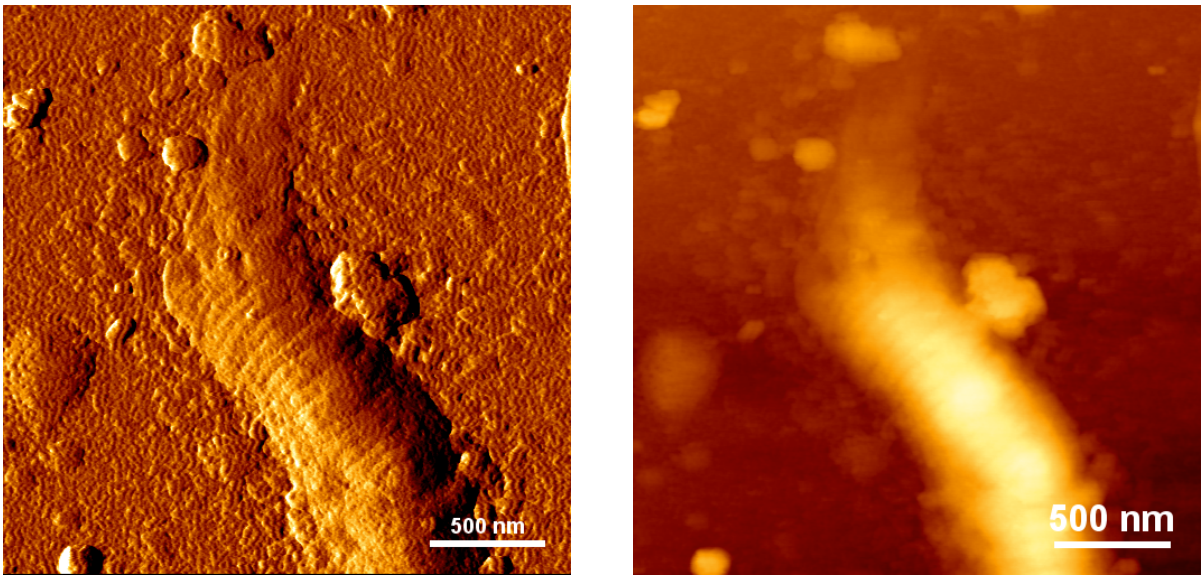

(a) Error-signal (b) Measured height

Figure 54: Contact-mode image of air dried fractured WT-fibril

7.5.1 Physiological strain within the fracture test

In section 2.4.5 the physiological strain-range of tendons and fibres is described as up to 8% strain. However, for fibrils it is likely to be less due to the hierarchical architecture. Although it is unknown if strain concentrations occur which could lead to strains within the fibrillar level in the same range as on the tissue or fibre level. For this reason a more precise focus is lead on the strain-range from 0 to 10% within the fracture curves. The value of 10% was selected due the fact that both mean-values for the strain at E_1 for WT and OIM where larger then 10%. In other words, no fibril reached the plateau within this range. From the generated stress-strain curves a mean curve from the OIM and WT fibrils was generated. In figure 55(a) the red dashed line resembles the mean-value curve of the OIM-group and in 55(b) the solid red line visualizes the mean-value curve for WT-samples. When merging the two mean curves in one figure, the stronger incline of the OIM-samples becomes evident. In the upper regions of the stress-strain curve this trend was no longer visible. Further the mean-value curves could only be created to a strain level of 15%, due to the fact that at this value the first fibrils fracture. As there exist large differences in fracture-strain, two fibrils already fractured at a level of 15% strain and others reached strains of nearly 60%. Again this result shows the large variation within biological samples.

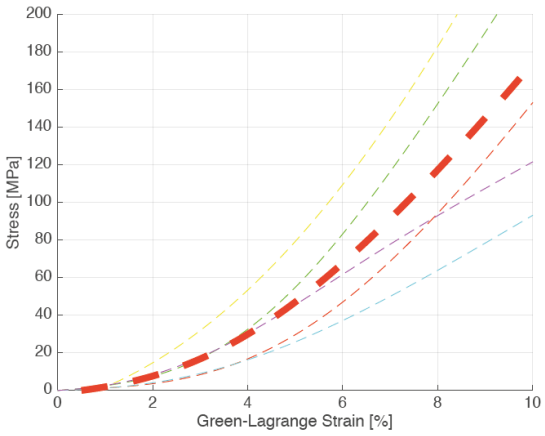

(a) Physiological part of the fracture curve of OIM fibrils including the mean value curve (red dashed line)

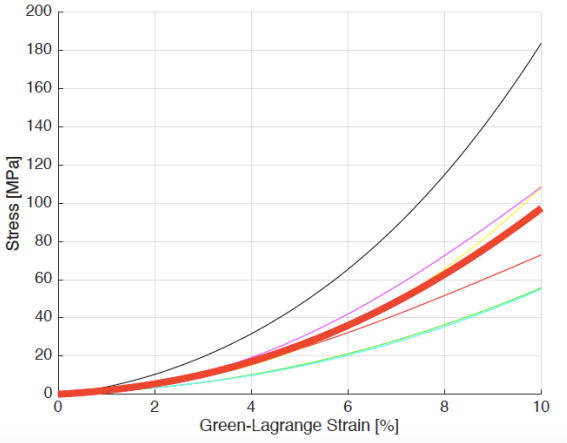

(b) Physiological part of the fracture curve of WT fibrils including the mean value curve (red line)

Figure 55: Physiological range of the fracture curves until 10% strain

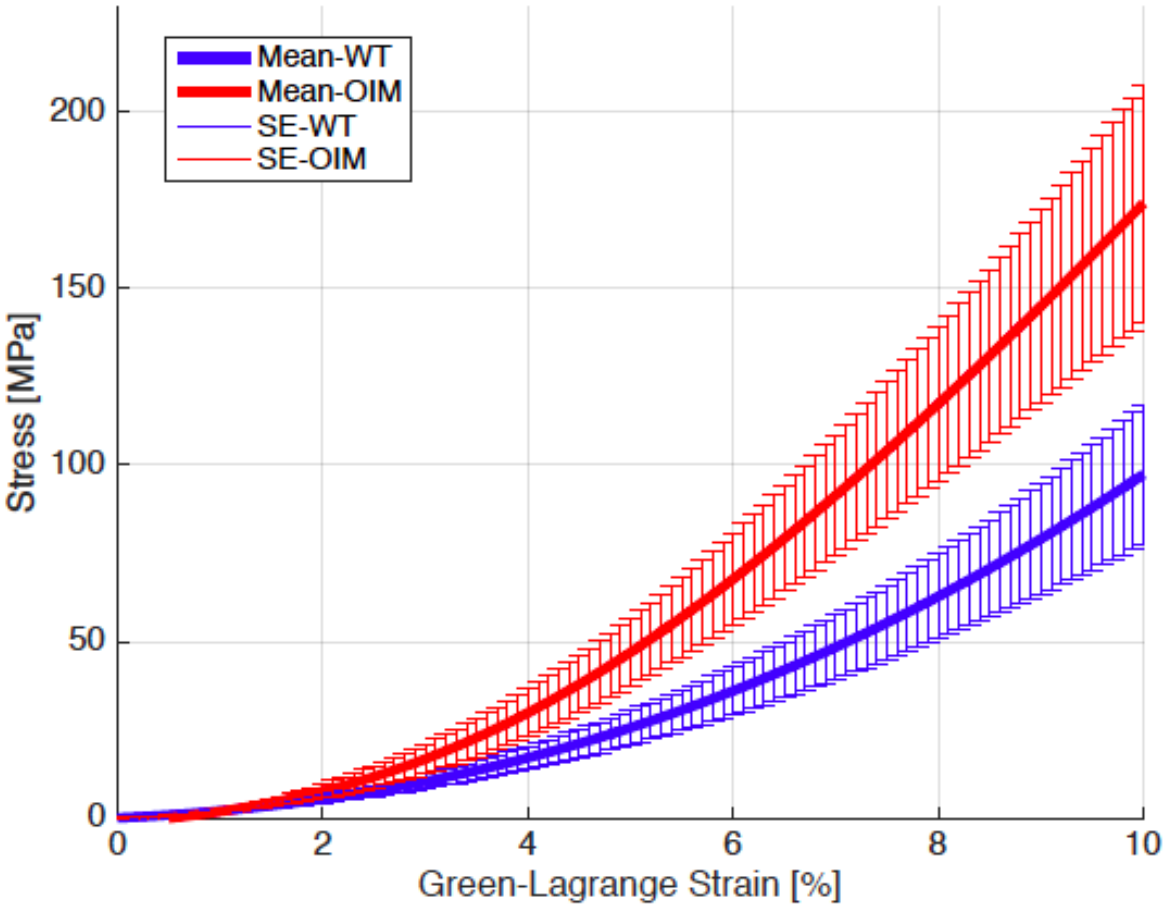

Figure 56: Mean-value curve of all OIM and WT fibrils within the physiological range including the standard error

7.5.2 Geometric influences on the mechanical properties

As mentioned above for comparative reasons the stress-strain curves were analysed in the same manner as mentioned in [28]. In figure 57 the values are presented, further the mean-values including the standard deviation are visualized.

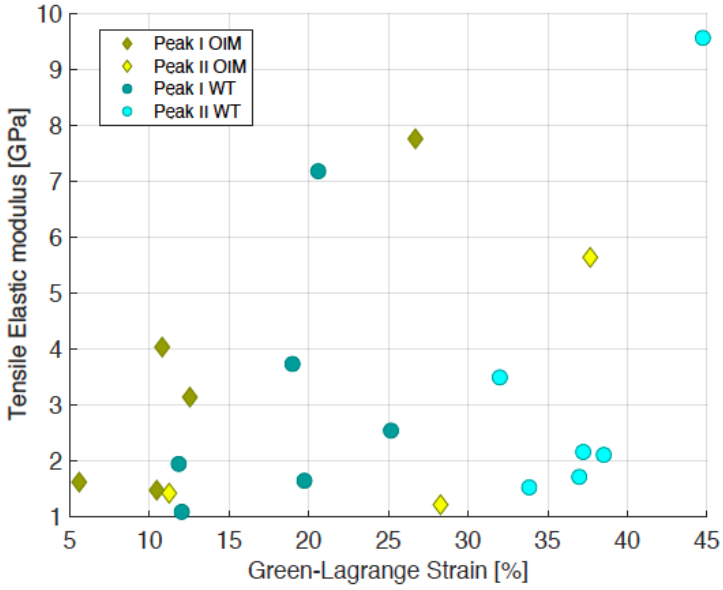

(a) WT and OIM values for each fibril

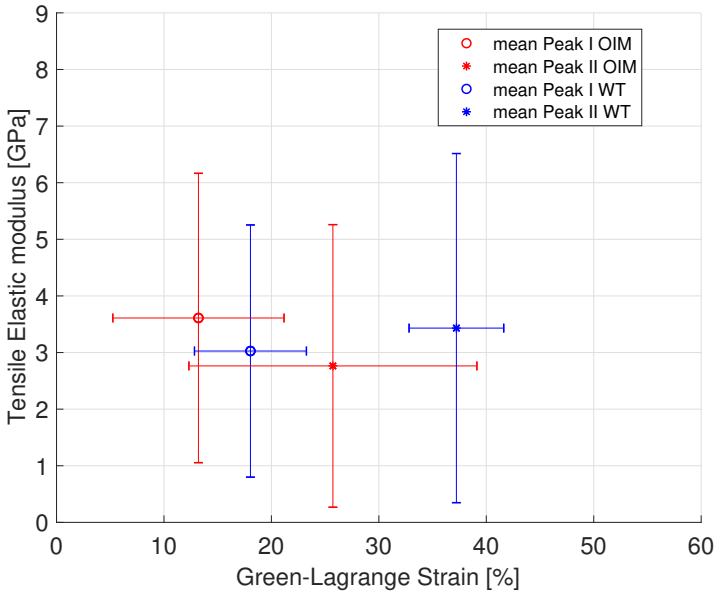

(b) Mean-values of all OIM and WT fibrils including standard deviation

Figure 57: Elastic modulus and Green-Lagrange Strain values of WT and OIM fibrils from Part I and III. In (b) no significant difference was found between the WT and OIM group

The markes in figure 57 (b) indicate the peak of the corresponding section according to Svensson et al. [28]. The obtained values for E_1(p=0.792), E_2(p=0.381), ϵ_{GL1}(p=0.247) and ϵ_{GL2}(p=0.262) showed no significant difference between OIM and WT collagen fibrils. These four parameters E_1, E_2, ϵ_{GL1} and ϵ_{GL2} are further analysed by putting them into contrast with the geometrical specimen parameters. This may lead to information about the influences of potentially different boundary conditions during the tensile tests. At the tensile test the collagen fibril is bend at the edges of the epoxy droplet. By observing the relation between the fibril length an the fracture test parameters conclusions about the influence of these bend may be obtained. During this study no significant correlations between the geometrical parameters and the mechanical properties could be determined. However, for clearer statements on the influence of the geometrical parameters more fibrils need to be tested. For E_2, of the OIM samples for example only three data points exist.

	E_1	ε_{GL1}	E_2	ε_{GL2}
WT				
1	1.1 [GPa]	12 [%]	1.7 [GPa]	37 [%]
2	2.5 [GPa]	25 [%]	2.1 [GPa]	39 [%]
3	1.6 [GPa]	20 [%]	1.5 [GPa]	34 [%]
4	7.2 [GPa]	21 [%]	9.6 [GPa]	45 [%]
5	3.7 [GPa]	19 [%]	3.5 [GPa]	32 [%]
6	2.0 [GPa]	12 [%]	2.2 [GPa]	37 [%]
Mean value	**3.0±2.2 [GPa]**	**18±5 [%]**	**3.4±3.08 [GPa]**	**37±4 [%]**
OIM				
1	3.1 [GPa]	13 [%]	5.6 [GPa]	38 [%]
2	4.0 [GPa]	11 [%]		
3	1.5 [GPa]	10 [%]	1.2 [GPa]	28 [%]
4	7.8 [GPa]	27 [%]		
5	1.6 [GPa]	6 [%]	1.4 [GPa]	11 [%]
Mean value	**3.6±2.6 [GPa]**	**13±8 [%]**	**2.8±2.5 [GPa]**	**25.7±13.4 [%]**

Table 5: Elastic modulus and Green-Lagrange Strain values of WT and OIM fibrils from Part I and III of the stress-strain curves

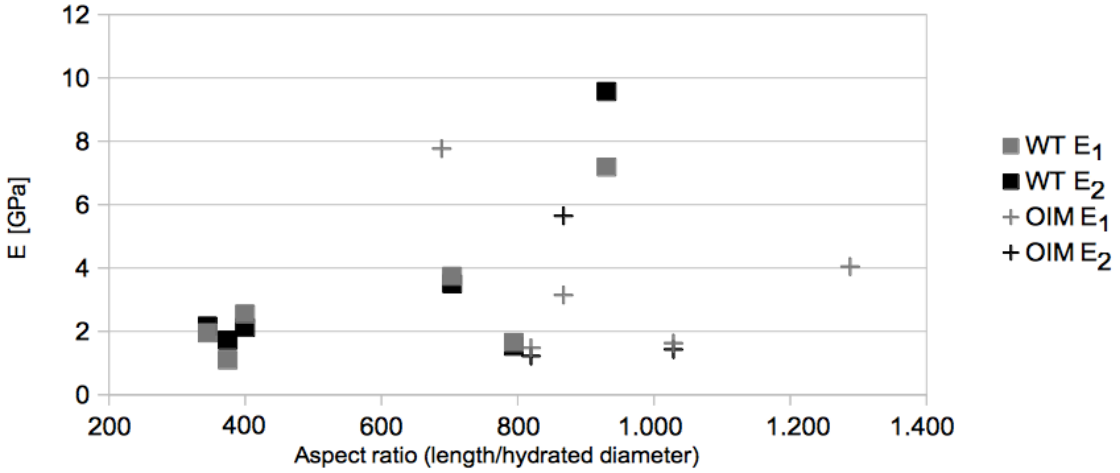

(a) Relation between Elastic modulus and aspect-ratio

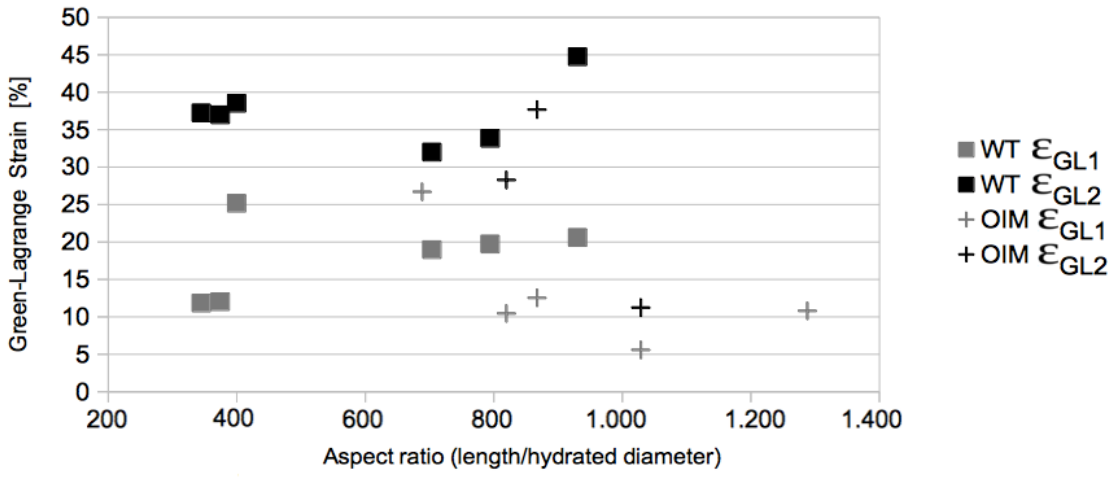

(b) Relation between Green-Lagrange Strain and aspect-ratio

Figure 58: Influence of aspect-ratio (Fibril length/hydrated fibril diameter) on the elastic modulus E_1 and E_2 and strains ϵ_{GL1} and ϵ_{GL2} at which E_1 and E_2 were determined

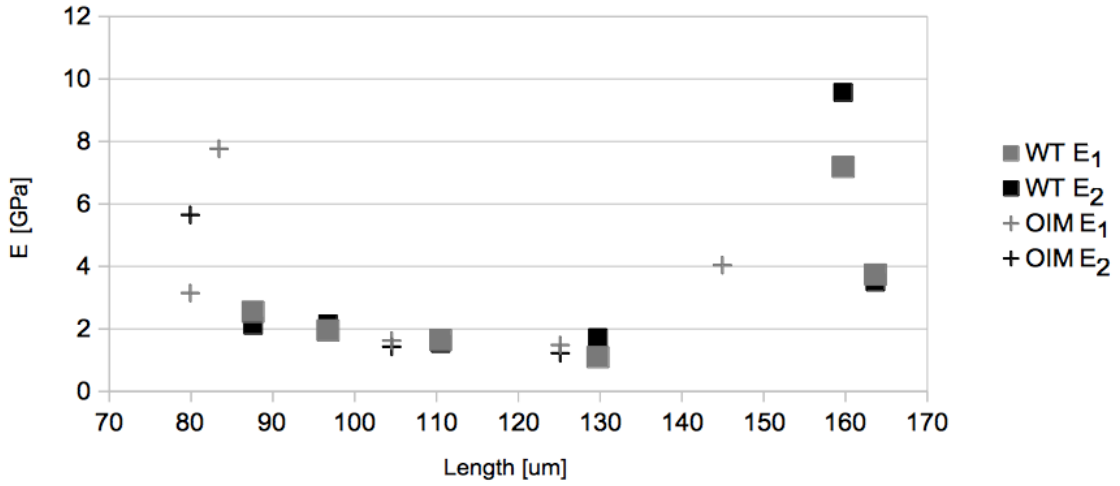

(a) Relation between Elastic modulus and fibril length

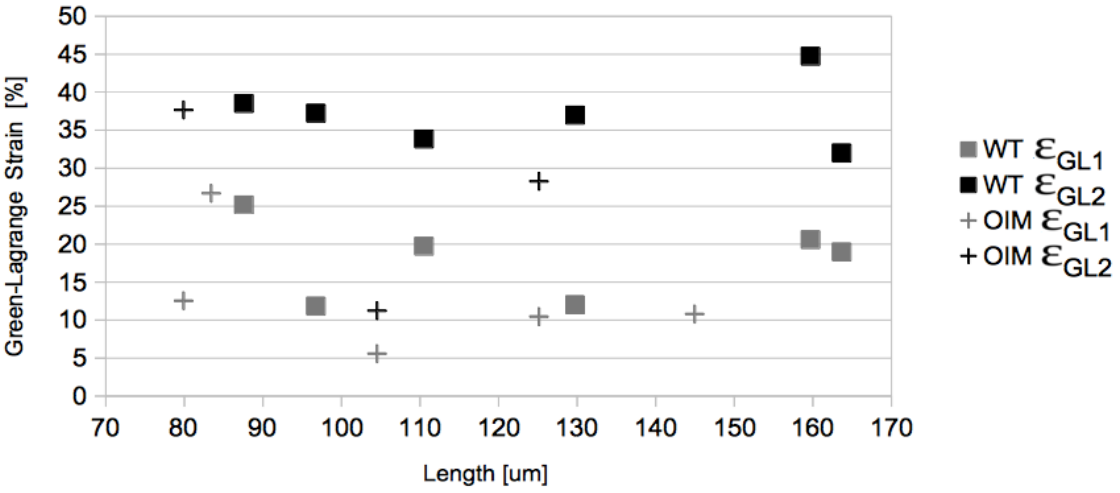

(b) Relation between strain and fibril length

Figure 59: Influence of fibril length on the elastic modulus E_1 and E_2 and strains ϵ_{GL1} and ϵ_{GL2} at which E_1 and E_2 were determined

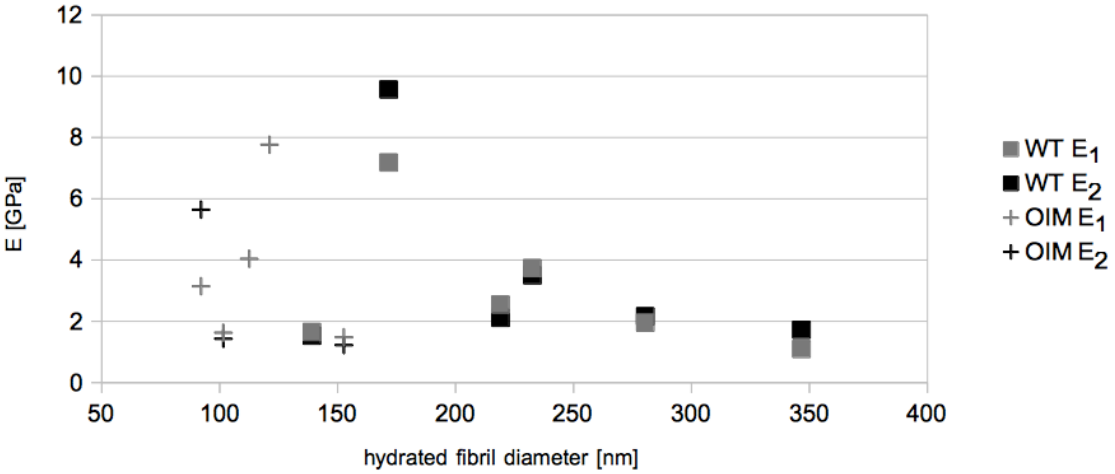

(a) Relation between Elastic modulus and hydrated fibril diameter

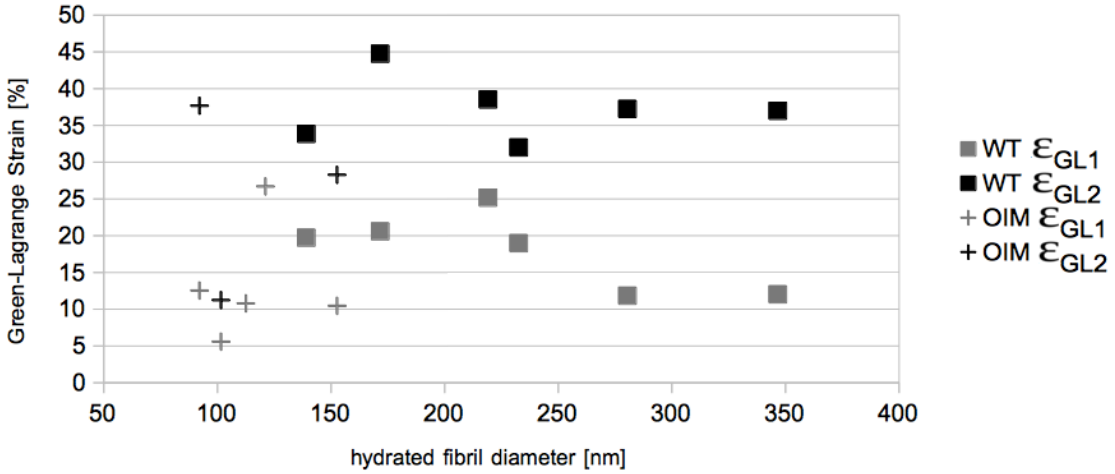

(b) Relation between strain and hydrated fibril diameter

Figure 60: Influence of hydrated diameter on the elastic modulus E_1 and E_2 and strains ϵ_{GL1} and ϵ_{GL2} at which E_1 and E_2 were determined

7.5.3 Single-molecule Stress and Strains

Hulmes et. al. [14] stated that one collagen molecule occupies the area of 10.079 $[nm^2]$ within dried collagen fibrils. As described in section 6.3 the approximated stresses for the individual collagen molecules are calculated from data of the fracture tests. The generated fracture stress-strain curves provide the basis for the individual collagen molecule approximations. According to the model of Depalle et al. [66] the collagen molecules within the fibrils extends less then the fibril. For this reason the focus is lead to lower strain values during this chapter. Although from the generated stress-strain curves the ultimate molecule strength was estimated and compared. Again as in the fibrillar stress-strain curves (fig. 50) the black curve shows extreme behaviour compared to the other fibrils. This led to a rise of the mean ultimate strength of the WT fibrils. The statistical evaluation showed no significant difference between the two groups.

However, when looking at fig. 61 there might be a trend that the WT molecules show smaller ultimate strength then the OIM molecules. As mentioned previous, the values of the ultimate strength are just approximations based on this model. Therefore the model only provides the area occupied by one collagen molecule within the dried collagen fibril. However, the model does not consider any mechanisms of deformation within the collagen fibril. The fracture mechanism at the fibrillar level are topic of ongoing researches and are not fully specified until now. The current state of knowledge is that the collagen molecule strain is lower then the fibril strain during elongation [66]. For this reason a detailed figure from 62 (a) up to a strain value of 2.5% is provided in the following. At the strain-level of 2.5% a significant difference between the individual collagen molecule approximations between the WT and OIM samples is stated ($p<0.05$). This observation corresponds to previous results from section 7.5.1 and 7.4.2.

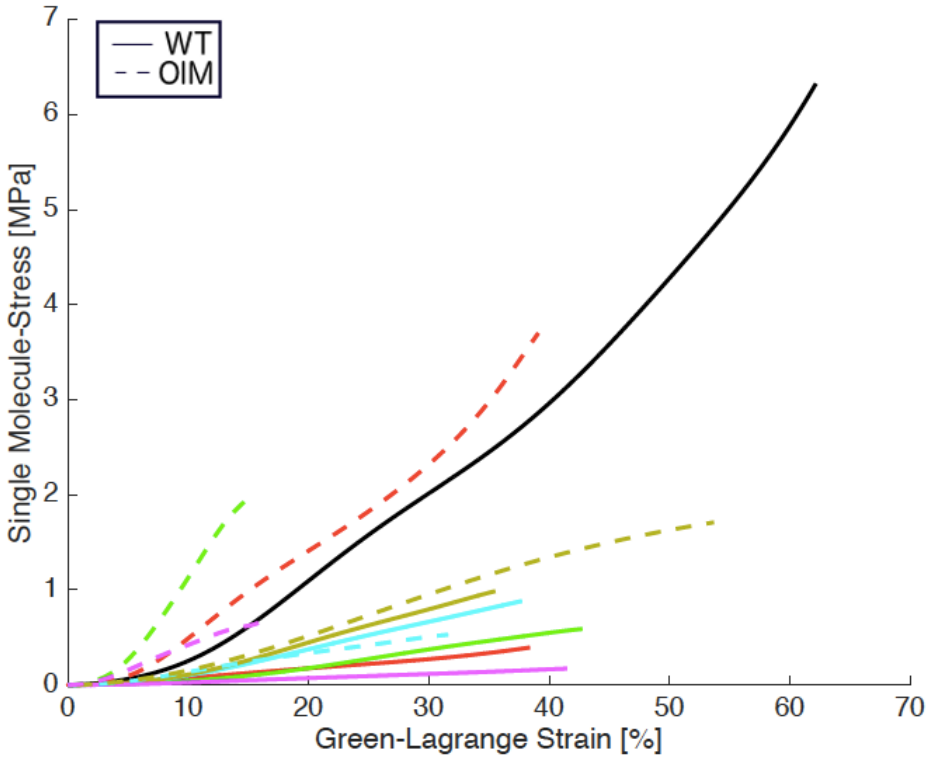

(a) Stress-strain curve for single molecule approximation

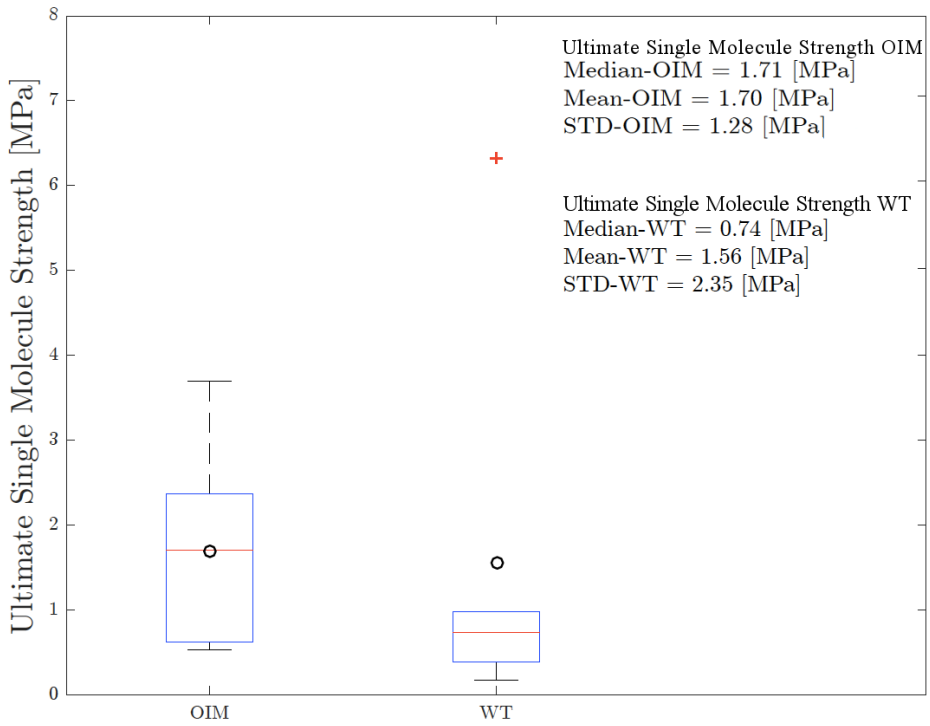

(b) ultimate strength for single molecule approximation

Figure 61: Generated data with the approximation of Hulmes et al. WT are solid lines and OIM are the dashed lines. No significant difference between WT and OIM (p=0.429)

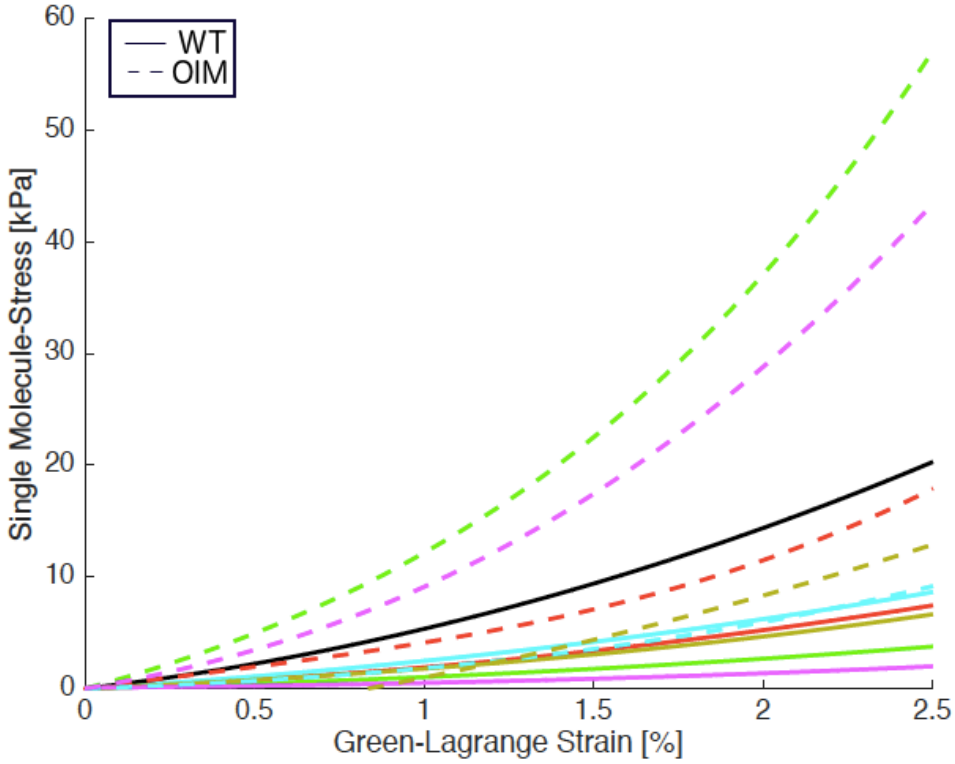

(a) Detail of the single collagen molecule stress-strain approximation up to a strain value of 2.5%

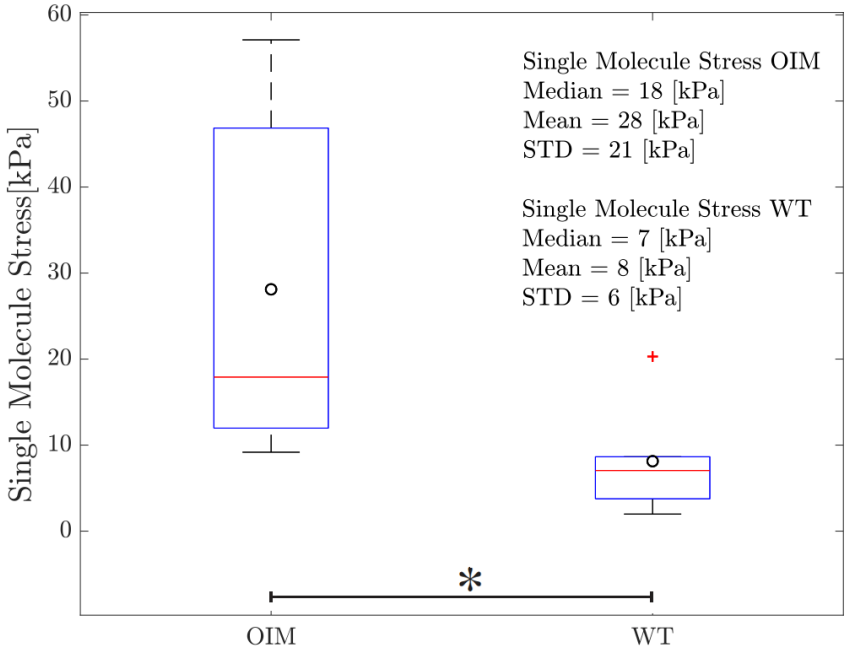

(b) Approximated collagen molecule stresses at 2.5 % strain. Significant difference between WT and OIM ($p<0.05$)

Figure 62: Detail of the approximated individual collagen molecule stresses within th physiological strain-range

7.6 Indentation tests

For the indentation test the force-maps of 12 OIM and 22 WT collagen fibrils where analysed according to section 6.5. The observed OIM and WT fibrils from the indentation test are different collagen fibrils then the collagen fibrils observed during tensile testing. However, the samples where generated from the same WT and OIM individual. Figure 63 shows a lower radial elastic modulus for OIM samples then for WT. The statistical analysis showed a significant difference between the two groups (p=0.01). This result shows that the indentation modulus of the WT group is significantly higher then for the OIM-group.

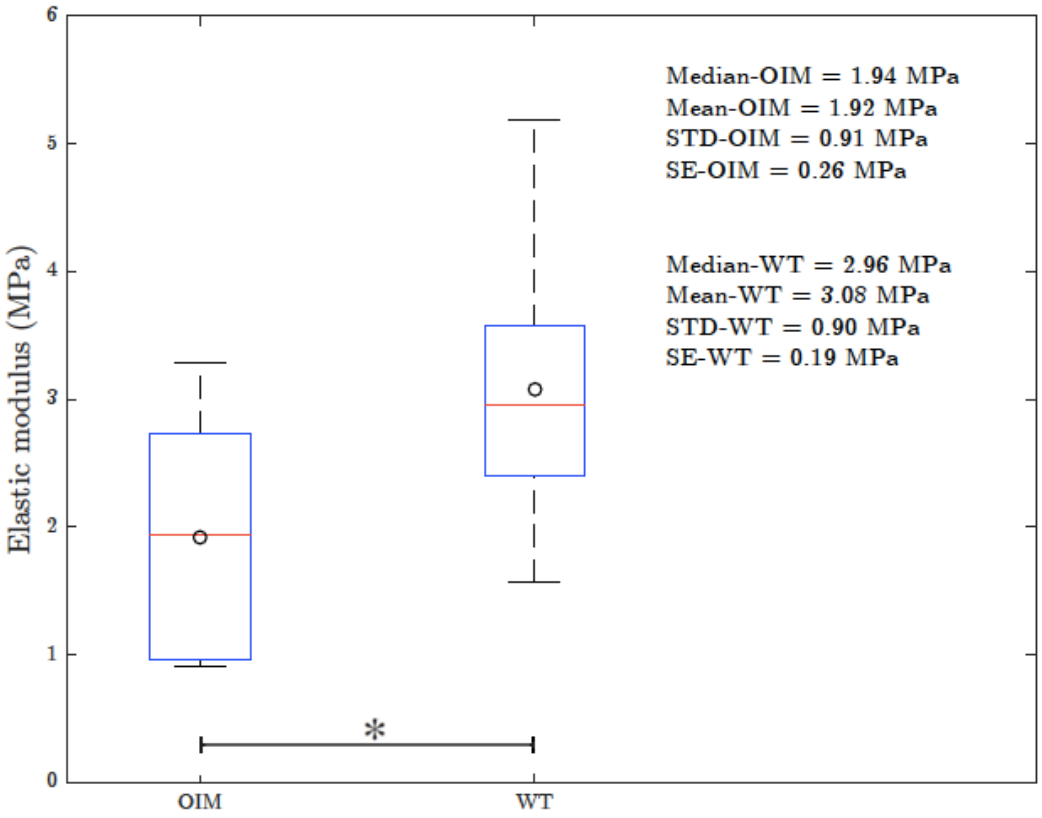

Figure 63: Radial elastic modulus of WT and OIM samples in hydrated state achieved by PBS (pH=7.4). OIM and WT samples show a significant difference (p=0.01)

8 Discussion

Biological tissues are very complex multi-level materials with a considerable variation in each individual fibril. For this thesis homotrimeric (OIM) and heterotrimeric (WT) collagen type I fibrils were tested to investigate the influence of the different collagen molecule on the fibril. Although, the most observed parameters do not show significant variation between OIM and WT collagen fibrils, the tests revealed information about the structure and function of these biological material.
As often recognized in measurements of biological materials, especially at this length-scale, the generated data may show variations on the order of 20% of the mean or median value. This was also observed during this study. The main goal of this study was to improve and enhance tensile testing on individual collagen fibrils. A significant time during this thesis was spent to achieve this goal. Therefore only a small number of samples could be tested, as the preparation for each individual collagen fibril still was limited to 4-5 samples per week. The insignificance in the obtained values may be due to overlapping region in the mechanical properties of both tested groups. The small number of tested samples could therefore lie within this region. A larger amount of samples have to be tested in further studies to obtain a conclusive result.

8.1 Optimization of tensile testing individual collagen fibrils

Although the sample preparation and the tensile test were optimized during this study, the preparation for each individual collagen fibril took around 14-15 hours and showed a high error rate (25%). Due to this circumstances and limited resources during this thesis only a small number of samples could be tested.

One goal of the thesis was to optimize the preparation protocol of individual collagen fibril samples for the tensile test. This goal was achieved under the use of an micromanipulator. By performing different steps of the preparation protocol with the micromanipulator instead of the AFM, the preparation time was reduced. Thereby the provided improvements lead to an increase in sample preparation from 1 sample to a maximum of 4-5 samples per week. However, the used epoxy resin still limits the sample preparation due to the long hardening time (12 h). One goal of further studies should be to eliminate this limitation. If the hardening time could be eliminated from the sample preparation, then the sample preparation would be reduced to 2-3 hours per sample. This would allow the testing of more samples in a shorter period of time and thereby more data on the mechanical properties of individual collagen fibrils could be gained.

8.2 Correlations between observed parameters

Previous studies by Andriotis et al.[34] show a relation between the swelling and the indentation modulus of OIM and WT collagen fibrils. Within their study a low swelling is correlated with a high indentation modulus. The lower swelling of the fibril indicates a higher amount of structural bound water. Further Miles et al.[67] revealed a relation between structural bound water and non-enzymatic cross-linking. Miles at al. therefore stated that a higher amount of structural bound water results in more non-enzymatic cross-links. These non-enzymatic cross-links create stiffer collagen fibrils which can be evaluated by indentation or tensile testing.
Andriotis et al. confirmed this relations between swelling and the mechanical properties [34]. Within their publication Andriotis et al. measured a lower swelling of OIM fibrils compared to WT. The OIM fibrils therefore exhibited a higher indentation modulus compared to the WT fibrils [34].
However, the results of this project showed no significant difference in swelling between OIM and WT fibrils (p=0.138). The obtained swelling-ratios during the project are 1.64 ± 0.25 for OIM-fibrils and 1.83 ± 0.28 for WT fibrils. These values are in the same range as swelling-ratios of the OIM-fibrils in the publication of Andriotis et. al [34] were they gained swelling ratio of 1.6 ± 0.3 for OIM fibrils. However, the larger swelling ratios for WT-fibrils of 2.6 ± 0.4 obtained by Andriotis et. al. could not be reproduced during this project. In the study of Andriotis et al. [34] the swelling ratio of OIM and WT are significantly different with a difference of 1 in the swelling ratio. The indifferent values obtained during this study indicate that the observed groups show no significant difference. Potential cause of this insignificance, could arise from only samples of one WT and one OIM mouse were investigated. Another suspicion is that there may have been an error at the genotyping of the mice. An error in genotyping could have led to heterozygote (OIM/+) mice instead of homozygote (OIM/OIM) mice. Heterozygous mice express both types of collagen molecules, the homotrimeric $[\alpha 1(I)]_3$ and the heterotrimeric $[\alpha 1(I)]_2\ \alpha 2(I)$. This could explain the similar values along all mechanical tests and the mostly non-significant differences between the obtained data.
The statistically significant difference obtained during this study may as well just represent two different animals or heterozygous (OIM/+) versus wild type instead of homozygous (OIM/OIM) versus wildtype. Further evidence for the discrepancy is visible when comparing the indentation modulus of this study with Andriotis et al. [34]. Although there is a significant difference between indentation modulus of OIM and WT fibrils in this study(OIM fibrils 1.9 MPa $\pm$0.9 MPa and WT fibrils 3.1 MPa $\pm$0.9 MPa (p=0.01)) the difference is reversed compared to the study of Andriotis et al.[34]. Further the dif-

ference between the group is much smaller compared to the study of Andriotis et al.. Andriotis et al. reported values of 3.3 MPa±0.5 MPa for the indentation modulus of WT fibrils and 16.2 MPa ±3MPa indentation modulus for OIM fibrils.

Again the observed difference of the indentation modulus of the two groups during this study seem to result either from different mice and or from heterozygous vs WT genotypes. However, the obtained samples are further researched and the producer of the genetically mutated mice is contacted. Until further clarification of the situation the samples are treated as WT and OIM during the discussion.

From the gained swelling data a weak trend is seen when observing the mean values. The OIM fibrils show a lower mean swelling ratio then the WT fibrils. The higher amount of structural unbound water may indicate a higher amount of non-enzymatic crosslinks [34]. The higher amount of non-enzymatic cross-links could explain the significant difference ($p<0.05$) of the tensile elastic modulus within physiological strain-range between the two groups. The OIM fibrils showed a larger elastic modulus then the WT fibrils. Further the lower amount of structural unbound water in OIM-fibrils could lead to an earlier rearrangement of collagen molecules during extension and therefore to an faster rise of the elastic modulus. As seen in stress-strain curves of the physiological strain range.
In the first region of elongation the collagen molecules unwind and get straightened. Further elongation of the fibril results in collagen molecule sliding[24]. However, due to the high p-value ($p=0.138$) of the insignificant difference of the swelling ratios between OIM and WT fibrils both assumptions have to be taken with care.
For more precise statements more fibrils of both groups need to be tested. Further the fibrils need to be chemically analysed to determine the amount of AGE's formed within the individual fibrils.

During this thesis the visco-elastic behaviour was observed through the tensile tests in the physiological strain range. The tensile test in the physiological range generated two results, the fibril stiffening through by rising strain-rates and the energy-dissipation. The stiffening is a typical characteristic of visco-elastic materials, it can be seen on every length-scale of the tendon from the tissue [68, 11] down to fibril level [27].On the fibrillar level water molecules play an important role for determining viscoelastic behaviour. There exist two types of interactions of fibrils with water moleces, the structural bound water molecules and unbound water molecules. During dehydration the unbound water molecules evaporate and the bound water molecules remain in the collagen fibril. In the physiological hydrated state the unbound water influences the mechanical behaviour of collagen fibrils. Shen et. al. [24] stated that the viscoelastic behaviour of single collagen

fibrils is created by the rearrangements of collagen molecules in the fibril and due to movements of the unbound water molecules.
During this thesis the percentile and the total energy dissipation were observed. The total energy dissipation showed a significant difference between OIM and WT fibrils. However, this situation could be created due to different strain values at the physiological tensile test. By observing the percentile energy dissipation this assumption is enhanced since the significance in difference vanishes for the percentile energy dissipation between OIM and WT fibrils.
However, to generate accurate data on the total as well as the percentile energy dissipation more test, where the individual fibrils are extended to the same strain value, must be performed. To obtain curves with same strain values I suggest to control the original length of the collagen fibrils during sample preparation.
I would propose a value of 100 μm for the original length, as this can be controlled during sample preparation by placing the epoxy droplets on the fibril. This standard original length would result in better comparability of the energy dissipation between different fibrils and groups. The viscoelastic behaviour is further defined by a time dependence of the stress-strain curve. Through different strain-rates the slope of the stress-strain curve changes. The slope of the stress-strain curve is defined as the current elastic modulus depending on the strain and the strain-rate. For this reason the current elastic modulus was observed at a strain value of 2.5% for the different strain-rates. The results presented in section 7.4.1 show a rise of the elastic modulus due to a increase of the strain-rate. This rise of the elastic modulus was found for 10 out of 11 fibrils independent of WT or OIM. The rise thereby indicates once more viscoelastic material properties of individual collagen fibrils.
However, the current elastic modulus was further observed at a strain value of 2.5% and a strain-rate of 15[%/s], which revealed a significant difference between the two groups. Again it is stated that the elastic modulus of OIM-fibrils is significantly ($p<0.05$) larger then the elastic modulus of WT-fibrils in the physiological range. The elastic modulus and thereby the stiffness of the individual collagen fibrils is influenced by multiple factors. According to previous studies different influencing factors where determined:

- Composition [34]
- Non-enzymatic cross-links (AGEs)[69, 29]
- Hydration and osmotic pressure [30]

Until now it is known that the osmotic pressure influences the mechanics of collagen fibrils. However, the influence of cross-linking and fibril composition is not fully established until

now. However, within this thesis a difference between the OIM and WT collagen fibrils has been observed within the physiological range. This indicates that the composition of the molecule, OIM is homotrimeric and WT is heterotrimeric, also is an influencing factor for the mechanical properties of collagen fibrils. The homotrimeric molecule thereby leads to a stiffer fibril at low strains.
Further there might be more influencing factors of the mechanical properties of individual collagen fibrils which are unknown at current date. However, future projects will engage with different tests on the level of individual collagen fibrils and thereby new information will be revealed.

During the evaluation of the hydrated and the dried diameter of the individual collagen fibrils a significant difference ($p<0.05$) for both diameters was found between the groups. The OIM samples show smaller diameters then the WT samples. On the one hand, a study on the diameter of individual collagen fibrils obtained from human bone tissue of OI and WT individuals by Cassella et al. stated the opposite relation [70] Due to the different tissues and animals from which the fibrils where gained and thereby the difference of mineralized fibrils (bone) and non-mineralized fibrils (tendon) the comparison might be inappropriate. On the other hand, on the length scale of individual collagen fibres, Misof et al. [11] made the same observations as within this study. They stated that the diameter of WT-fibrils is larger then that of OIM fibres.
This might result from different amino acids being present on the collagen molecule surface which may result in a different assembly of fibrils and fibres within the OI affected individuals. However, to state such assumptions chemical and structural analysis of the OIM collagen molecules is needed.

8.3 Fracture Test

Statistically there was no significant difference between OIM and WT fibrils for all parameters (ultimate tensile strength, rupture strain, E_1, E_2, ϵ_{GL1} and ϵ_{GL1}) obtained during the fracture tests (see figure 57) . Again this indicates the error in genotyping.

When observing the data of the fracture test (figure 50) two fibrils (brown OIM fibril and black WT fibril) show "extreme" values for ultimate strength as well as ultimate strain, compared to the other fibrils. The reason for the stronger material behaviour is unknown. However, there might be more AGE or enzymatic cross-links within these two fibrils. This is indicated through the swelling-ratio, as the brown OIM-fibril showing the lowest swelling ratio of 1.2. However, the swelling ratio of the black WT fibril is 1.75 which does not indicate a higher amount of AGE's compared to the other WT and OIM

fibrils. This shows again that chemical analysis of the fibrils is of great importance, which may help to clarify the results.

The ultimate tensile strength of the individual collagen fibrils is obtained during different studies [33, 26, 28]. When looking at the paper of Svensson et. al [28] the fracture strength of fibrils obtained from native rat-tail tendons with an age of 3 months reached a value of 200 MPa ±110 MPa, measured with the AFM-method.
Yamamoto et. al.[26] gained values of 100 MPa ±32 MPa for the ultimate strength. Yamamoto et. al. tested mice-tail tendon obtained from 4 week old mice, the test was performed with the Micromanipulator-method.
And the group around Liu et al. [33] used MEMS devices to test the fibrils thereby the generated maximum strength values are of 71 MPa ±23 MPa. Liu et. al. tested fibrils obtained from rat patellar tendons with unknown age.
All values in literature are below the obtained median and mean values of the tested fibrils (WT-fibrils: 1.31 GPa ±1.61 GPa; OIM-fibrils: 1.02 GPa ±1.17 GPa). This could result from the different tissue-types and ages of the mice. The fibrils used during this study where obtained from 5 month old female mice, which are older compared to the other studies. It is stated that the age plays an important role in the alteration of the mechanical properties of collagen based tissue [29]. With age, different types of cross-links, mainly AGE's form, within the fibrils, leading to stiffer and stronger fibrils[29]. This could explain the higher ultimate strength of the fibrils measured during this study. Again to therefore chemical analysis of the observed collagen fibrils are values for the amount of AGE's are needed.

Literature values for the rupture strain range from 34% ± 11% [26], 16% ± 4% [28] up to 63% ± 21% [33]. The obtained values for the fracture strain during this study (OIM 31% ± 16%, WT 43% ± 10%) are within this region.
All published studies on the mechanical properties on the length-scale of individual fibrils show a large standard deviation and a low sample rate. This large variation could result from the variation within the fibrils. However, also the sample geometry (gauge-length and aspect ratio), as well as the bias could have an influence on the obtained values [28]. Again therefore a standardized length of the tensile test samples would be an main advantage.
The comparison of the tensile rupture strain on the fibrillar level with higher hierarchical levels reveals interesting relations. Tensile tests on single collagen fibres from rat-tail tendons show failure strains of 7.1% ± 1.2% [9]. For whole rat-tail-tendons the failure strain is in the same range of 10.4% ± 2.6% for 4 month old rats. The difference between the hierarchical levels highlights the complex mechanism within fracture of collagen rich

tissues. The paper of Puxkandl et al. [10] further states that the extension of the collagen fibrils within the rat-tail tendon is considerably less than the total extension of the whole tendon . When combining this results it seems as if within fracture situations of tendons the collagen fibrils may not extend to fracture strain. This led to the assumption that other fracture/deformation mechanisms within the matrix between the fibrils are of greater importance during fracture[10]. However, until now it is unknown if there occur local regions with high strains where the fracture strain of individual fibrils is reached.

At the level of individual collagen fibrils the parameters defined by Svensson et al. [28] extracted from the stress-strain fracture curves can be compared with literature. Svennson et al. observed that most rat-tail tendon collagen fibrils show three segments during the fracture test. Within this study 9 out of the 11 tested fibrils showed this segmentation. Svensson stated that E_1 is in the most cases larger then E_2. When neglecting one outlier (black WT- fibril) this observation was also made during this study, again independent of WT or OIM fibrils (see figure 57).
Svensson et al. obtained values for E_1 of 2.2 GPa $\pm$0.9 GPa and for E_2 values of 1.4GPa $\pm$0.7 GPa for native-RTT's. The values obtained during this study are in the same order of magnitude (WT-fibrils: $E_1 = 3$ GPa $\pm$2.2 GPa and $E_2 = 3.4$ GPa $\pm$3.1 GPa, OIM-fibrils: $E_1 = 3.6$ GPa $\pm$2.6 GPa and $E_2 = 2.8$ GPa $\pm$2.5 GPa). The differences between the values could arise from the different sample type(Svennson: Rat-tail tendon of 4 month old rats; this project Mouse-tail-tendon of 5 month old mice) and thereby the different ages. In section 7.5.2 the influence of geometric fibril-parameters on the values of E_1 and E_2 were observed. Through the very low sample rate here could no statements on a possible influence be made.

The results of the approximations of single molecule forces based on the model of Hulmes et al. [14] have to be taken with care. Due to the fact that the stated occupied area of one molecule is modeled for heterotrimeric collagen type I molecules (WT) [14]. Different models [66, 71] suggest that the homotrimeric collagen type I molecules (OIM) show kinks. Further these models [66, 71] suggest that the helical structures of homotrimeric OIM collagen molecules are further apart through changes within the amino acid sequences of the molecules. Therefore, the individual homotrimeric OIM molecule should occupy a larger area then the heterotrimeric WT molecule. When looking at the paper published by Depalle et al. [66] the model suggests that the molecular strains are below the fibrillar strains similar to the circumstances within tendons and fibres [10]. For this reason it is difficult, to approximate single molecule forces and stresses from data obtained via tests on collagen fibrils. Since the intermolecular relations within the fibrils are not known to full extend until now. To obtain data on the real behaviour of individual collagen

molecules within the fibrils, different methods need to be established. This methods have to measure the collagen molecule elongation and force during fibril elongation.

9 Conclusion

The goal of improving and thereby optimizing the preparation protocol for tensile testing samples was successfully established. The time needed to prepare one sample was reduced to one third of the original time. Further the rupture test of individual collagen fibrils was established. This already where major achievements due to the fact that this enables fracture test with a higher amount of samples being tested in a shorter period of time (max. 4-5 samples/week) compared to the previous study (1 samples/week)[30]. The time needed for optimization and improvement of the tensile test limited the time available for testing individual collagen fibrils. Therefore only a low sample number could be tested. Further, the obtained values of the tensile test have to be taken with care due to possible error in genotyping and due to the fact that the samples where obtained from one animal per group. Further tests such as chemical analysis of the fibrils are needed to determine the amount of cross-links. The amount of cross-links present in the fibrils would clarify the claims made based on the swelling ratio. During the study the large variations within biological tissues could be seen. For this reason it is essential to test more fibrils to generate a significant amount of data to define the mechanical properties of individual collagen fibrils more expressive. During this study only six samples per group could be measured due to the still large time exposure per tensile test and limited time as 50% of this thesis was method development. However, there also might be an overlapping region between the two groups and the observed OIM fibrils could be within this region and therefore no significant difference could be found. The only way to state such assertions is to contact the mouse producer and to clarify if the tested samples are OIM samples. Within the sample preparation for the tensile testing I would suggest to keep the controllable geometrical parameters as constant as possible. The geometrical parameter of fibril length can be determined during sample preparation and therefore i would suggest a length of 100 μm. Further, if possible, I would search for individual collagen fibrils with similar diameters. Further I would suggest to test collagen fibrils of different animals to obtain more expressive data.

10 Outlook

Observing biological tissue can be challenging, due to the mentioned variation within the observed parameters. To generate more relevant data on the mechanical behaviour in general, more fibrils need to be tested. Currently a PhD. position at the ILSB institute (TU-Vienna), engages with the development of a different method or device for performing tensile tests on individual collagen fibrils. This device would allow a higher sample rate and thereby more data.

In future projects different types of mechanical tests should be performed. Interesting results could be generated via force clamp tests or cyclic loading tests. These tests could help to explain the origin of the energy dissipation. How much of the dissipated energy results from structural changes of the tertiary structure of the molecule and to what extend the interactions of the collagen-molecules with water molecules participate in the dissipation.

The molecular dynamics during extension and retraction could be examined through this type of experiment. Information about force dependence of the unfolding and refolding process within the fibril may be obtained. Further threshold forces or time dependent likelihoods of refolding and unfolding events might be found.

Another important step is to obtain information about composition of the fibril via chemical analysis. The revealed composition of the fibrils would determine the amount of cross-links within OIM and WT fibrils and the distribution of amino acids along the collagen molecule. To generate data on the influence of cross-links on the mechanical behaviour of the fibrils, samples from different animals at same ages and also with different ages should be observed.

Further cyclic tensile tests would be of great interest. This test generate information about time dependent processes during retraction and extension of the molecules. There are many more exciting measurements to perform which will reveal interesting information about collagen fibrils and the interaction between the molecules in the fibrils.

By generating more knowledge on the hierarchical level of fibrils interesting connections between macroscopic and nanoscopic tissue properties can and will be obtained.

11 Appendix

11.1 JPK-script

```
# Stepper motor movement
from com.jpk.util.jyspmutils import ZPiezoControl
from com.jpk.inst.lib import JPKScript
from com.jpk.inst.lib.hw.dsprpc import API

# definition of a class to control the stepper motors
# independently of the current system state
class StepperControl:
    @staticmethod
    def __moveStepperGroup(distance):
        instrument = JPKScript.getInstrument()
        dspManager = instrument.getDSPManager()

        encoder = instrument.getScannerGeometry().
            getStepperMotorAverageEncoder()
        dspManager.moveStepperMotorsEvenly(0, encoder.encode(distance))
        dspManager.getDSPStatus().waitUntilClear(
                                                API.Stat.movingStepperMotor |
                                                    API.Stat.aborting )

    @staticmethod
    def moveDown(distance):
        StepperControl.__moveStepperGroup(distance)

    @staticmethod
    def moveUp(distance):
        StepperControl.__moveStepperGroup(-distance)


# controlling the piezo
zpc = ZPiezoControl()
# move piezo to 1µm = 1e-6m absolute position
zpc.moveToAbsolutePosition(0.3e-6)
# move piezo relative
zpc.moveUp(0e-6)
#zpc.moveDown(1e-6)

# move the stepper motors 100µm = 100e-6m
StepperControl.moveUp(0.3e-6)
#StepperControl.moveDown(1e-6)
```

List of Tables

List of Figures

References

[1] C. Ross Ethier and Craig A. Simmons. *Introductory Biomechanics: From Cells to Organisms*. Cambridge University Press, 2007.

[2] Bruce Alberts et al. *Molecular Biology of the Cell*. Garland Science, fifth edition edition, 2008.

[3] Philipp J. Thurner. *Lecture: 317.026 Tissue biomechanics SS16*. TU Wien, 2016. Lecture 2: Nano- and ultrastructure of biological tissues and nanomechanics- entropic elasticity.

[4] Malfait F., Wenstrup RJ, and De Paepe A. Clinical and genetic aspects of ehlers–danlos syndrome, classic type. *Genet. Med.*, 2010.

[5] David F. Barker, Sirkka Lissa Hostikka, Jing Zhou, Louise T. Chow, Arnold R. Oliphant, Steven C. Gerken, Martin C. Gregory, Mark H. Skolnick, Curtis L Atkin, and Karl Tryggvason. Identification of mutations in the col4a5 collagen gene in aport syndrome. *Science*, 1990.

[6] Aline Brequou Bourgeois. Osteogenesis imperfecta: From diagnosis and multidisciplinary treatment to future perspectives. *Swiss Medical Weekly*, 2016.

[7] Antonella Forlino, Wayne A. Cabral, Aileen M. Barnes, and Joan C. Marini1. New perspectives on osteogenesis imperfecta. *Nat Rev Endocrinol*, 2011.

[8] Shapiro JR, McBride DJ, and Fedarko NS. Oim and related animal models of osteogenesis imperfecta. . *Connect. Tissue Res.*, 1995.

[9] Y. Pedro Kato, David L. Christiansen, Rita A. Hahn, Sheu-Jane Shieh, Jack D. Goldstein, and FrederickH . Silve. Mechanical properties of collagenfibres: a comparison of reconstitutedand rat tail tendon fibres. *Biomaterials Vol 10*, 1989.

[10] R. Puxkandl, I. Zizak, O. Paris, J. Keckes, W. Tesch, S. Bernstorff, P. Purslow, and P. Fratzl. Viscoelastic properties of collagen: synchrotron radiation investigations and structural model. *The Royal Society*, 2002.

[11] K. Misof, W.J. Landis, K. Klaushofer, and P. Fratzl. Collagen from the osteogenesis imperfecta mouse model (oim) shows reduced resistance against tensile stress. *The American Society for Clinical Investigation, Inc.*, 1997.

[12] Birgitte Hansen and Gregor B. E. Jemec. The mechanical properties of skin in osteogenesis imperfecta. *Arch Dermatologie*, 2002.

[13] Laurianne Imbert, Jean-Charles Aurégan, Kélig Pernelle, and Thierry Hoc. Mechanical and mineral properties of osteogenesis imperfecta human bones at the tissue level. *Bone, Volume 65*, 2014.

[14] David J. S. Hulmes, Tim J. Wess, Darwin J. Prockop, and Peter Fratzl. Radial packing, order, and disorder in collagen fibrils. *Biophysical Journal Volume 68*, 1995.

[15] Peter Fratzl, editor. *Collagen - Structure and Mechanics*. Springer, 2008.

[16] Abraham J. Domb, Neeraj Kumar, and Aviva Ezra, editors. *Biodegradable polymers in clinical use and clinical development*. Wiley, 2011.

[17] R. Bruce Martin, David B. Burr, and Neil A. Sharkey. *Skeletal Tissue Mechanics*. Springer, 1998.

[18] Jürgen Brinckmann. Collagens at a glans. *Topics in Current Chemistry*, 2005.

[19] Philipp J. Thurner. *Lecture: 317.026 Tissue biomechanics SS16*. TU Wien, 2016. Lecture 10: Ligaments and Tendons.

[20] N.C. Avery and A.J. Bailey. *Collagen*, chapter Chapter 4, pages 81–110. Springer, 2008.

[21] Nicholas C. Avery, Trevor J. Sims, and Allen J. Bailey. *Extracellular Matrix Protocols*, chapter Quantitative Determination of Collagen Cross-links, page 103. Humana Press, 2009.

[22] Stephen C. Cowin and Stephen B. Doty. *Tissue Mechanics*. Springer, 2007.

[23] Frederick H. Silver, Joseph W. Freeman, and Gurinder P. Seehra. Collagen self-assembly and the development of tendon mechanical properties. *Journal of Biomechanics*, 2003.

[24] Zhilei Liu Shen, Harold Kahn, Roberto Ballarini, and Steven J. Eppell. Viscoelastic properties of isolated collagen fibrils. *Biophysical Journal*, 2011.

[25] Gerhard A. Holzapfel. *Nonlinear Solid Mechanics: A continuum Approach for Engineering*. John Wiley & Sons, LTD, 2000.

[26] Noritaka Yamamoto. Tensile strength of single collagen fibrils isolated from tendons. *European Journal of Biophysics*, 2017.

[27] René B. Svensson, Tue Hassenkam, Philip Hansen, and S. Peter Magnusson. Viscoelastic behavior of discrete human collagen fibrils. *Journal if the mechanical behavior of biomedical materials*, 2010.

[28] Rene B. Svensson, Hindrik Mulder, Vuokko Kovanen, and S. Peter Magnusson. Fracture mechanics of collagen fibrils: Influence of natural cross-links. *Biophysical Journal 104*, 2013.

[29] Rene B. Svensson, Stuart T. Smith, Patrick J. Moyer, and S. Peter Magnusson. Effects of maturation and advanced glycation on tensile mechanics of collagen fibrils from rat tail and achilles tendons. *Acta Biomaterialia*, 2018.

[30] Sylvia Desissaire. The effect of osmotic pressure on the mechanical and structural properties of individual collagen fibrils. Master's thesis, Vienna University of Technology, 2016.

[31] Philip Hansen. Glutaraldehyde cross-linking of tendon—mechanical effects at the level of the tendon fascicle and fibril. *Connective Tissue Research*, 2009.

[32] Zhilei Liu Shen, Mohammad Reza Dodge, Harold Kahn, Roberto Ballarini, , and Steven J. Eppell. In vitro fracture testing of submicron diameter collagen fibril specimens. *Biophysical Journal Volume 99*, 2010.

[33] Yehe Liu, Roberto Ballarini, and Steven J. Eppell. Tension tests on mammalian collagen fibrils. *The Royal Society*, 2015.

[34] O. G. Andriotis, S. W. Chang, M. Vanleene, P. H. Howarth, D. E. Davies, S. J. Shefelbine, M. J. Buehler, and P. J. Thurner. Structure–mechanics relationships of collagen fibrils in the osteogenesis imperfecta mouse model. *The Royal Society*, 2015.

[35] Marco P. E. Wenger, Laurent Bozec, Michael A. Horton, and Patrick Mesquida. Mechanical properties of collagen fibrils. *Biophysical Journal*, 2007.

[36] August J. Heim and William G. Matthews. Determination of the elastic modulus of native collagen fibrilsvia radial indentation. *Applied Physics Letters*, 2006.

[37] Stefan Strasser, Albert Zink, Marek Janko, Wolfgang M. Heckl, and Stefan Thalhammer. Structural investigations on native collagen type i fibrils using afm. *Biochemical and Biophysical Research Communications*, 2006.

[38] Colin A. Grant, David J. Brockwell, Sheena E. Radford, and Neil H. Thomson. Tuning the elastic modulus of hydrated collagen fibrils. *Biophysical Journal*, 2009.

[39] Tetsuo Fukunaga, Keitaro Kubo, Yasuo Kawakami, Senshi Fukashiro, Hiroaki Kanehisa, and Contantinos N. Maganaris. In vivo behavior of human muscle tendon during walking. *The Royal Society*, 2001.

[40] Y. Kawakami, T. Muraoka, S., H. Kanehisa, and T. Fukunaga. In vivo muscle fibre behaviour during counter-movement exercise in humans reveals a significant role for tendon elasticity. *Journal of Physiology*, 2002.

[41] G.A. Lichtwark, K. Bougoulias, and A.M. Wilsona. Muscle fascicle and series elastic element length changes along the length of the human gastrocnemius during walking and running. *Journal of Biomechanics 40*, 2007.

[42] SP Magnusson, P Hansen, P Aagaard, J Brønd, Poul Dyhre-Poulsen, J Bojsen-Moller, and M Kjaer. Differential strain patterns of the human gastrocnemius aponeurosis and free tendon, in vivo. *Acta Physiologica*, 2003.

[43] Joan C. Marini. *Bone and Extracellular Matrix Branch*, chapter Osteogenesis imperfecta, page 597. Wiley, 2010.

[44] Frank Rauch and Francis H Glorieux. Osteogenesis imperfecta. *The Lancet*, 2004.

[45] S. D. Chipman and et al. Defective pro alpha 2(i) collagen synthesis in a recessive mutation in mice: a model of human osteogenesis imperfecta. *PNAS*, 1993.

[46] Daniel Rugar and Paul Hansma. Atomic forche microscopy. *Physic Today*, 1990.

[47] T. R. Albrecht, S. Akamine, T. E. Carver, and C. F. Quate. Microfabrication of cantilever styli for the atomic force microscope. *Journal of Vacuum Science and Technology A*, 1990.

[48] Pier Carlo Braga and Davide Ricci. *Atomic Force Microscopy - Biomedical Methods and Applications*. Human Press, 2004.

[49] Victor J. Morris, Andrew R. Kirby, and A. Patrick Gunning. *Atomic Force Microscopy for Biologists*. Imperial College Press, 2010.

[50] Paul A. Tipler and Gene Mosca. *Physik 7. Auflage*. Springer, 2015.

[51] JPK Instruments. *NanoWizard - User Manual*. JPK Instruments, 2010.

[52] Jeffrey L. Hutter and John Bechhoefer. Calibration of atomicforce microscope tips. *AIP Review of Scientific Instruments*, 1993.

[53] Hans-Jurgen Butt and Manfred Jaschke. Calculation of thermal noise in atomic i force microscopy. *Nanotechnology*, 1995.

[54] Richard M. Martin. Piezoelectricity. *Physical Review*, 1972.

[55] Victor Bellitto, editor. *Atomic Force Microscopy - Imaging, Measuring and Manipulating Surfaces at the Atomic Scale*. INTECH, 2012.

[56] Lukas Kain. Structural and mechanical evaluation of collagen fibrils from equine tendon: The effect of age, tendon zone and type. Master's thesis, Technical University Vienna, 2017.

[57] JPK Instruments. Determining the elastic modulus of biological samples using atomic force microscopy. *JPK Technotes*.

[58] W. C. Oliver and G. M. Pharr. An improved technique for determining hardness and elastic modulus using load and displacement sensing indentation experiments. *Materials Research Society*, 1992.

[59] Marko Loparic, Dieter Wirz, A.U. Daniels, Roberto Raiteri, Mark R.Van Landingham, Geraldine Guex, Ivan Martin, Ueli Aebi, and Martin Stolz. Micro- and nanomechanical analysis of articular cartilage by indentation-type atomic force microscopy: Validation with a gel-microfiber composite. *Biophysical Journal*, 2010.

[60] D.P. Pioletti, L.R. Rakotomanana, and P.-F. Leyvraz. Strain rate effect on the mechanical behavior of the anterior cruciate ligament–bone complex. *Medical Engineering & Physics*, 1999.

[61] Wolfgang Demtröder. *Experimentalphysik 2*. Springer, 2004.

[62] D.J. Keller and F. S. Franke. Envelope reconstruction of probe microscope images. *Surface Science*, 1993.

[63] Orestis G. Andriotis, Wiparat Manuyakorn, Jurgita Zekonyte, Orestis L. Katsamenis, Sebastien Fabri, Peter H. Howarth, Donna E. Davies, and Philipp J. Thurner. Nanomechanical assessment of human and murine collagen fibrils via atomic force microscopy cantilever-based nanoindentation. *journal of the mechanical behavior of biomedical materials 39*, 2014.

[64] Jakob Scherübl. Optimization of tensile tests on single collagen b. Technical report, ILSB TU Vienna, 2017.

[65] W. Oliver and G. Pharr. Measurement of hardness and elastic modulus by instrumented indentation: advances in understanding and refinements to methodology. *J. Mater. Res. 19*, 2004.

[66] Baptiste Depalle, Zhao Qin, Sandra J. Shefelbine, and MarkusJ.Buehler. Influence of cross-link structure,density and mechanical properties in the mesoscale deformation mechanisms of collagen fibrils. *Journal of the mechanical behavior of biomedical materials 52*, 2015.

[67] Miles CA, Avery NC, Rodin VV, and Bailey AJ. The increase in denaturation temperature followingcross-linking of collagen is caused by dehydration ofthe fibres. *Journal of Molecular Biology*, 2005.

[68] R. C. Haut. Age-dependent influence of strainrate on the tensile failure of rat-tail tendon. *Journal of Biomechanical Engineering, Volume 105*, 1983.

[69] Markus J. Buehler. Nanomechanics of collagen fibrils under varying cross-link densities: Atomistic and continuum studies. *Journal of the mechanical behaviour of biomedical materials*, 2008.

[70] J. P. Cassella, P. Barber, A. C. Catterall, and S. Yousuf Ali. A morphometric analysis of osteoid collagen fibril diameter in osteogenesis imperfecta. *Bone Volume 15*, 1994.

[71] Shu-Wei Chang, Sandra J. Shefelbine, and Markus J. Buehler. Structural and mechanical differences between collagen homo- and heterotrimers: Relevance for the molecular origin of brittle bone disease. *Biophysical Journal Volume 102*, 2012.